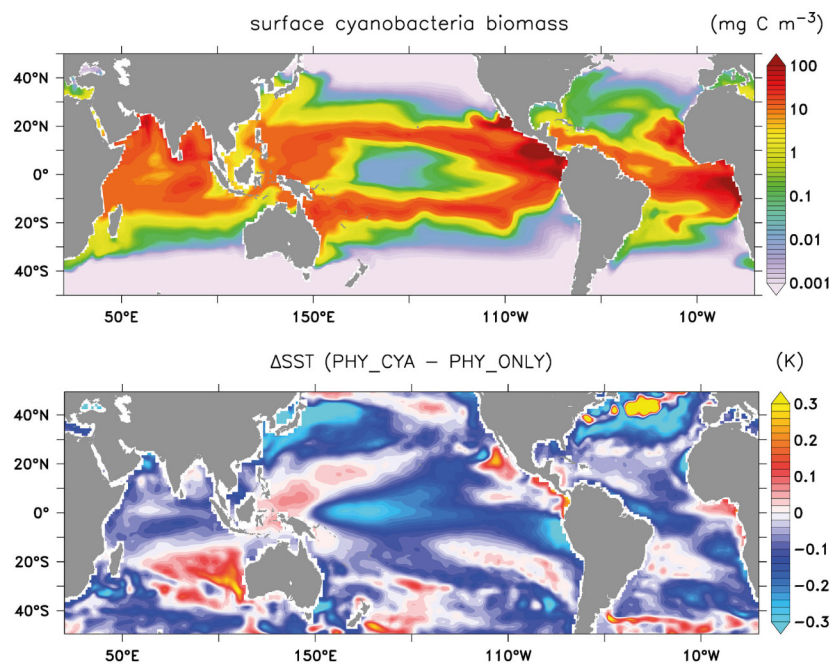




The effects of marine nitrogen-fixing cyanobacteria on ocean biogeochemistry and climate – an Earth system model perspective



Hanna Paulsen

Hamburg 2018

Hinweis

Die Berichte zur Erdsystemforschung werden vom Max-Planck-Institut für Meteorologie in Hamburg in unregelmäßiger Abfolge herausgegeben.

Sie enthalten wissenschaftliche und technische Beiträge, inklusive Dissertationen.

Die Beiträge geben nicht notwendigerweise die Auffassung des Instituts wieder.

Die "Berichte zur Erdsystemforschung" führen die vorherigen Reihen "Reports" und "Examensarbeiten" weiter.

Anschrift / Address

Max-Planck-Institut für Meteorologie
Bundesstrasse 53
20146 Hamburg
Deutschland

Tel./Phone: +49 (0)40 4 11 73 - 0
Fax: +49 (0)40 4 11 73 - 298

name.surname@mpimet.mpg.de
www.mpimet.mpg.de

Notice

The Reports on Earth System Science are published by the Max Planck Institute for Meteorology in Hamburg. They appear in irregular intervals.

They contain scientific and technical contributions, including Ph. D. theses.

The Reports do not necessarily reflect the opinion of the Institute.

The "Reports on Earth System Science" continue the former "Reports" and "Examensarbeiten" of the Max Planck Institute.

Layout

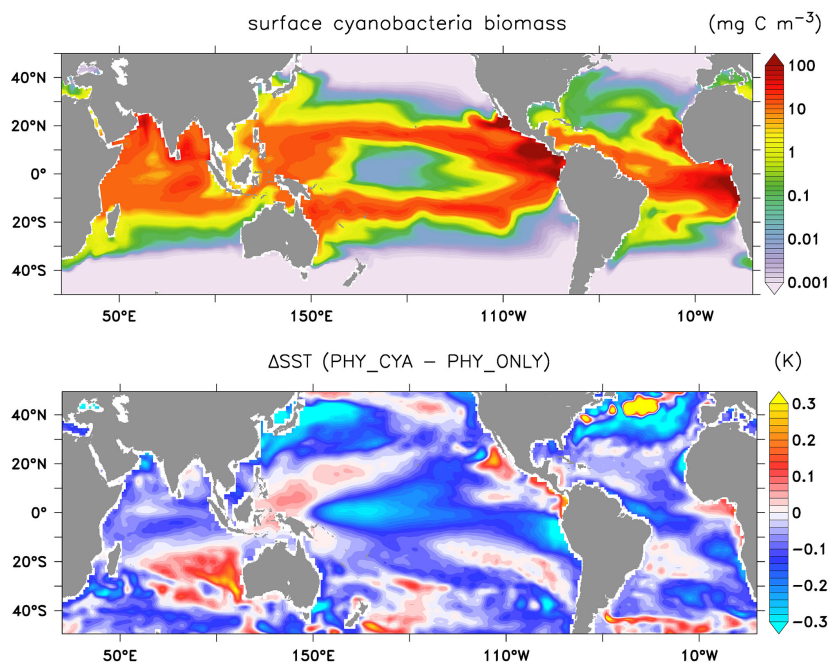
Bettina Diallo and Norbert P. Noreiks
Communication

Copyright

Photos below: ©MPI-M
Photos on the back from left to right:
Christian Klepp, Jochem Marotzke,
Christian Klepp, Clotilde Dubois,
Christian Klepp, Katsumasa Tanaka



The effects of marine nitrogen-fixing cyanobacteria on ocean biogeochemistry and climate – an Earth system model perspective



Dissertation with the aim of achieving a doctoral degree
at the Faculty of Mathematics, Informatics and Natural Sciences
Department of Earth Sciences of Universität Hamburg
submitted by

Hanna Paulsen

Hamburg 2018

Hanna Paulsen

Max-Planck-Institut für Meteorologie
Bundesstrasse 53
20146 Hamburg

Tag der Disputation: 15.12.2017

Folgende Gutachter empfehlen die Annahme der Dissertation:

Dr. Tatiana Ilyina
Prof. Dr. Inga Hense

Abstract

Marine nitrogen (N_2) fixing cyanobacteria provide a major supply of bioavailable nitrogen to the ocean's euphotic zone. Furthermore, cyanobacteria organisms, largely positively buoyant, absorb light at the ocean surface and thereby modify the distribution of radiative heating in the water column. In this thesis, I investigate the role of marine cyanobacteria in the Earth system – both with respect to ocean biogeochemistry and with respect to the biogeophysical feedback by light absorption – in present and high CO_2 climate conditions by using the comprehensive Earth system model of the Max Planck Institute for Meteorology (MPI-ESM).

To this end, I develop and implement a parameterization of prognostic N_2 -fixing cyanobacteria into the HAMburg Ocean Carbon Cycle model (HAMOCC), the global ocean biogeochemistry component of MPI-ESM. Including cyanobacteria as additional phytoplankton group considerably improves the representation of N_2 fixation compared to the diagnostic approach used hitherto. Cyanobacteria growth (contributing $\sim 7\%$ to the global primary production) and N_2 fixation (with a global value of $\sim 135 \text{ Tg N yr}^{-1}$) are confined to the tropical and subtropical ocean. Temperature, phosphate and iron limitation, which in addition to fixed nitrogen deficits determine N_2 fixers' growth, lead to a decoupling of N_2 fixation from the upwelling areas of nitrogen-depleted water masses. Large-scale patterns of the relative abundance of surface phosphate to nitrate are improved in the new parameterization. The prognostic growth dynamics is capable of reproducing a reasonable seasonal variability of N_2 fixation and furthermore enables the consideration of the potential response of N_2 fixation to changing environmental conditions, such as seawater temperature, seawater pH and changes in atmospheric dust deposition.

I furthermore include the prognostic cyanobacteria in the dynamic feedback from biological light absorption on the ocean heat budget in MPI-ESM. The simulations reveal that cyanobacteria shade and hence cool the subsurface water that feeds the shallow meridional overturning cells and that is upwelled at the equator and in the eastern boundary upwelling systems. This advective process outweighs the direct local heating by cyanobacteria light absorption and results in a net surface cooling effect in large parts of the tropical and subtropical ocean by up to 0.5 K. The regional surface cooling has implications for the climate mean state, such as a strengthening ($\sim 6\%$) and westward shift ($\sim 3^\circ$ longitude) of the Walker circulation, as well as for climate variability, such as an increase in El Niño–Southern Oscillation variability ($\sim 16\%$). Including the dynamic feedback from bulk phytoplankton and cyanobacteria light absorption on the ocean heat budget in MPI-ESM reduces the tropical sea surface temperature bias and improves tropical Pacific variability compared to the standard model version which applies a globally constant light attenuation depth.

Under rising CO_2 , i.e. in a scenario in which atmospheric CO_2 increases by 1% per year, both phytoplankton groups (bulk phytoplankton and cyanobacteria) are projected to decrease in the tropical and subtropical ocean. The related increase in the penetration depth of light leads to upwelling of warmer subsurface water, which amplifies tropical surface warming regionally by up to 20% under quadrupling atmospheric CO_2 . In an additional scenario, in which potential physiological advantages of cyanobacteria under high CO_2 are considered (such as a pH-dependent growth rate, temperature adaptation, and the uptake of dissolved organic phosphorus), cyanobacteria only regionally increase their abundance. This increase

counteracts the decline in water turbidity in the eastern tropical Pacific and dampens the additional warming signal of the Pacific cold tongue.

This thesis indicates the relevance of including N₂-fixing cyanobacteria as phytoplankton functional type in Earth system models. First, cyanobacteria growth dynamics are needed to simulate N₂ fixation and its potential future evolution. Second, cyanobacteria – and changes in cyanobacteria abundance – have a regulative effect on the tropical climate system via light absorption. Cyanobacteria hence introduce additional variability in the Earth system, especially in the tropical regions, which should indeed be accounted for.

Zusammenfassung

Marine stickstofffixierende Cyanobakterien liefern einen entscheidenden Beitrag zur Zufuhr von bioverfügbarem Stickstoff in die euphotische Zone des Ozeans. Hinzu kommt, dass Cyanobakterien zum Grossteil mit positivem Auftrieb behaftet sind und somit durch Lichtabsorption an der Oberfläche die Verteilung der Strahlungswärme in der Wassersäule beeinflussen. In dieser Arbeit untersuche ich die Rolle von Cyanobakterien im Erdsystem – zum einen im Hinblick auf Ozeanbiogeochemie, und zum Anderen im Hinblick auf den biogeophysikalischen Feedback durch Lichtabsorption – unter heutigen und unter hohen CO₂ Klimabedingungen. Ich wende hierfür das Erdsystemmodell des Max Planck Instituts für Meteorologie (MPI-ESM) an.

Zu diesem Zweck entwickle und implementiere ich eine Parameterisierung der prognostischen Wachstumsdynamik von stickstofffixierenden Cyanobakterien mit positivem Auftrieb in HAMOCC (HAMBURG Ocean Carbon Cycle model), der globalen Ozean-Biogeochemie Komponente des MPI-ESM's. Die Implementierung von prognostischen Cyanobakterien als weitere Phytoplanktongruppe in HAMOCC verbessert die Repräsentation der Stickstofffixierung erheblich im Vergleich zum diagnostischen, geochemischen Ansatz, der bisher verwendet wurde. Wachstum von Cyanobakterien (mit einem Beitrag von ~7% zur globalen Primärproduktion) und Stickstofffixierung (mit einem globalen Wert von ~135 Tg N yr⁻¹) sind auf den tropischen und subtropischen Ozean beschränkt. Durch die Temperatur-, Phosphat- und Eisenlimitierung, die neben Nitratdefiziten das Wachstum von Cyanobakterien im Modell bestimmen, ist die Stickstofffixierung teilweise von den Auftriebsgebieten nitratarmen Wassers entkoppelt. Die grossskalige Verteilung von relativen Phosphat- und Nitratvorkommen an der Oberfläche wird verbessert. Die prognostische Wachstumsdynamik, die durch saisonale Änderungen der physikalischen Bedingungen beeinflusst wird und auf einen variablen Cyanobakterien-Bestand wirkt, produziert eine sinnvolle saisonale Variabilität der Stickstofffixierungsraten. Ausserdem ermöglicht die prognostische Formulierung die Untersuchung der potentiellen Reaktion von Stickstofffixierung auf sich verändernde Umgebungsbedingungen, wie Wassertemperaturen, pH Werte und Änderungen in der atmosphärischen Staubdeposition.

Ich beziehe die prognostischen Cyanobakterien als Ergänzung zu gewöhnlichem Phytoplankton in der Eindringtiefe von kurzwelliger Strahlung im Ozean mit ein im MPI-ESM. Simulationen zeigen, dass Cyanobakterien das unter ihnen liegende Wasser abschatten und somit abkühlen. Dieses kältere Wasser speist die flachen meridionalen Umwälzzellen, und gelangt am Äquator und den östlichen Auftriebsgebieten an die Oberfläche. Dieser advective Prozess wirkt der direkten lokalen Erwärmung durch die Lichtabsorption der Cyanobakterien entgegen und führt zu einer Netto-Abkühlung bis zu 0.5 K in grossen Teilen des tropischen und subtropischen Ozeans. Diese regionale Abkühlung der Ozeanoberfläche hat Effekte auf den mittleren Zustand des Klimas, wie z.B. eine Verstärkung (~6%) und Verschiebung (~3° Länge) der Walker-Zirkulation westwärts, als auch Effekte auf die Klimavariabilität, wie z.B. eine Erhöhung der "El Niño – Southern Oscillation" (ENSO) Variabilität (~16%). Die Betrachtung des dynamischen Feedbacks von Lichtabsorption durch Phytoplankton (nicht-diazotrophes Phytoplankton und Cyanobakterien) auf den Wärmehaushalt des Ozeans reduziert den Bias in den tropischen Oberflächentemperaturen und verbessert die tropische Variabilität im Pazifik im MPI-ESM im Vergleich zur Standard-

Modellversion, die global eine konstante Lichtdämpfung vorschreibt.

Unter ansteigendem CO₂ (1% Anstieg von atmosphärischem CO₂ pro Jahr) wird in grossen Teilen eine Abnahme von nicht-diazotrophen Phytoplankton und Cyanobakterien simuliert. Die damit einhergehende tiefere Eindringtiefe der kurzwelligeren Strahlung führt zu einem Auftrieb von wärmeren Wasser. Dies verstärkt die Oberflächenerwärmung in den Tropen, regional um bis zu 20% bei einer Vervierfachung der atmosphärischen CO₂ Konzentrationen. In einem zusätzlichen Szenario, in dem potentielle physiologische Vorteile und Adaptationsmechanismen von Cyanobakterien berücksichtigt werden (darunter eine pH-abhängige Wachstumsrate, eine Temperatur-Adaptation und die Aufnahme von gelöstem organischem Phosphor), führt nur regional zu einer Zunahme von Cyanobakterien. Dies wirkt der Abnahme der Trübheit des Wasser entgegen und dämpft dadurch die zusätzliche Erwärmung im östlichen equatorialen Pazifik ab.

Diese Arbeit zeigt zwei Aspekte auf, warum es relevant ist stickstofffixierende Cyanobakterien mit positivem Auftrieb als funktionelle Phytoplanktongruppe in Erdsystemmodellen aufzunehmen. Zum einen ist die Wachstumsdynamik von Cyanobakterien notwendig, um Stickstofffixierung und dessen potentielle zukünftige Entwicklung abzubilden. Zum anderen haben Cyanobakterien – und Änderungen im Vorkommen von Cyanobakterien – eine regulierende Wirkung auf das tropische Klimasystem. Cyanobakterien sorgen damit für eine zusätzliche Variabilität im Erdsystem, insbesondere in den tropischen Regionen, die in der Tat berücksichtigt werden sollte.

Contents

Abstract	i
Zusammenfassung	iii
1 Introduction and thesis objectives	1
1.1 Role of cyanobacteria in global ocean biogeochemistry	1
1.2 Role of cyanobacteria in the biogeophysical feedback of light absorption	3
1.3 Role of cyanobacteria in a high CO ₂ world	4
1.4 Thesis outline	6
2 Incorporating a prognostic representation of marine nitrogen fixers into the global ocean biogeochemical model HAMOCC	7
2.1 Introduction	7
2.2 Model description	10
2.2.1 The ocean biogeochemical model HAMOCC	10
2.2.2 Prognostic parameterization of N ₂ fixers	11
2.2.3 Model setup and experimental design	15
2.3 Evaluation of the model results with respect to diazotrophic biomass and N ₂ fixation rates	16
2.3.1 Observational basis	16
2.3.2 Mean state of diazotrophic biomass and N ₂ fixation rates . . .	17
2.3.3 Seasonal variability of diazotrophic biomass and N ₂ fixation rates	28
2.4 Effects of N ₂ fixers on the mean biogeochemical model state	31

2.4.1	Effects on organic matter fluxes and inventories within the euphotic zone	31
2.5	Sensitivity of prognostic N ₂ fixers to selected parameters	36
2.5.1	Sensitivity to the half saturation constant of phosphate and iron	37
2.5.2	Sensitivity to the buoyancy velocity	39
2.6	Summary and Conclusions	42
3	Sensitivity of the tropical climate system to light absorption by marine cyanobacteria	45
3.1	Introduction	45
3.2	Model description and experimental setup	47
3.2.1	The MPI-ESM	47
3.2.2	Parameterization of radiative heating in the water column and experimental setup	48
3.3	Global distribution of cyanobacteria and chlorophyll	50
3.4	Effects of cyanobacteria light absorption on the mean tropical climate state	52
3.4.1	Effects on ocean temperature and mixed layer depth	54
3.4.2	Effects on wind patterns and precipitation	56
3.4.3	Effects on ocean circulation	58
3.4.4	Feedback on phytoplankton abundance	59
3.4.5	Synthesis and discussion of the mean state changes	60
3.5	Effects on temporal variability	62
3.5.1	Effects on seasonal dynamics of SST and cyanobacteria concentrations	62
3.5.2	Effects on the tropical Pacific interannual variability	65
3.6	Sensitivity of the results to the strength of cyanobacteria light absorption	66
3.7	Implications for the Earth system model	69
3.8	Summary and Conclusions	71
4	Impacts of phytoplankton light absorption on climate under rising CO₂	75
4.1	Introduction	75

4.2	Model description and experimental setup	78
4.2.1	The MPI-ESM	78
4.2.2	Parameterizations of radiative heating in the ocean and experiment description	79
4.3	Comparison of the preindustrial control climate states with globally uniform light absorption and with phytoplankton-dependent light absorption	85
4.4	Change in the phytoplankton and chlorophyll distributions under rising atmospheric CO ₂ concentrations	87
4.5	Impact of the light-absorption feedback on climate under increasing CO ₂ forcing	92
4.5.1	Ocean temperature and mixed layer depth	92
4.5.2	Surface air temperature, wind patterns and precipitation . . .	95
4.5.3	Ocean circulation and feedback on phytoplankton growth . .	98
4.6	Effects of potential physiological adaptation mechanisms of cyanobacteria in an increasing CO ₂ ocean	99
4.6.1	Modified evolution of phytoplankton and chlorophyll	101
4.6.2	Impacts of the modified evolution of phytoplankton and chlorophyll on climate	105
4.7	Summary and discussion	107
4.8	Conclusions	110
5	Conclusions and outlook	113
5.1	Conclusions	113
5.2	Outlook	116
	References	xxiv
	Acknowledgements	xxv

Chapter 1

Introduction and thesis objectives

Marine nitrogen (N₂) fixing cyanobacteria play a crucial role in ocean biogeochemical cycling due to their major supply of bioavailable nitrogen to the ocean's euphotic zone. Furthermore, cyanobacteria, largely positively buoyant, absorb light at the ocean surface and thereby modify the vertical distribution of heat in the water column. Under climate change, cyanobacteria are assumed to benefit and to become more abundant in the ocean. In this thesis, a comprehensive Earth system model is applied to investigate the different aspects of marine cyanobacteria within the Earth system: (1) the role of cyanobacteria with respect to N₂ fixation and ocean biogeochemistry, (2) the role of cyanobacteria with respect to the biogeophysical feedback of light absorption in the climate system, and (3) the role of cyanobacteria in a high CO₂ world and its implications for the first two aspects. The goal is to better understand the interactions and feedbacks between marine biota and the climate system and explore their role in the future evolution of Earth's climate.

1.1 Role of cyanobacteria in global ocean biogeochemistry

Nitrogen is essential for living organisms. The availability of bioavailable nitrogen (such as nitrate and ammonium) limits biological production throughout large parts of the world's ocean (e.g., *Moore et al.*, 2013). Besides upwelling and mixing of bioavailable nitrogen from depth to the surface, N₂-fixing organisms provide a major source of bioavailable nitrogen to the euphotic zone (e.g., *Gruber and Galloway*, 2008). Recent estimates of global N₂ fixation rates span a large range of about 80 to 200 Tg N yr⁻¹ (e.g., *Karl et al.*, 2002; *Großkopf et al.*, 2012), assigning biological N₂ fixation a considerable supply of 'new' nitrogen on the global scale (*Galloway et al.*, 2004; *Gruber*, 2004). N₂ fixation therefore plays a key role in controlling the oceanic nitrogen inventory (e.g., *Karl and Letelier*, 2008), and – by affecting the strength of the biological pump – also the carbon cycle. Marine N₂ fixation is proposed to be

a potential driver of partial pressure of atmospheric carbon dioxide ($p\text{CO}_2$) and climate regulation, even on geological timescales (e.g., *Falkowski, 1997; Michaels et al., 2001*).

Only specific marine organisms, called diazotrophs, are capable of utilizing N_2 to meet their nitrogen requirements for growth. The best studied and considered as most important open ocean diazotroph is the large filamentous cyanobacterium of the genus *Trichodesmium* (e.g., *Capone et al., 1997*). The relevance of other diazotrophic groups, such as unicellular cyanobacteria (e.g., *Zehr et al., 2001*) and diazotrophs associated with diatoms (DDA) (*Carpenter et al., 1999; Foster and Zehr, 2006*) has been recently suggested (*Carpenter et al., 1999; Zehr et al., 2001*). On the basis of current knowledge, the characteristics of *Trichodesmium*, however, to a large extent represent the ecological niche of diazotrophs in general (*Monteiro et al., 2010, 2011*). The ability to fix N_2 together with the high optimum temperature for growth ensure the ecological success of diazotrophic cyanobacteria throughout vast areas of the tropical and subtropical ocean (*Luo et al., 2012*).

In the future, the ecological niche of N_2 -fixing cyanobacteria is expected to increase (*Hutchins and Fu, 2017*). Higher temperatures and stratification favour cyanobacteria compared to ordinary phytoplankton and might lead to a shift in the community composition (*Boyd and Doney, 2002; Doney, 2006; Paerl and Huisman, 2008*). Due to the close coupling of the nitrogen to the carbon cycle, changes in cyanobacteria abundance and related N_2 fixation might impact on the ocean's carbon sequestration capacity (e.g., *Capone, 2001*), which, in turn, affects climate. Understanding the process of N_2 fixation and realistically representing it in climate models is hence a prerequisite to reduce uncertainties in projections of future climate.

The process of N_2 fixation is often only poorly represented in ocean biogeochemistry components of state-of-the-art Earth system models used for climate projections. Only two models of the Coupled Model Intercomparison Project 5 (CMIP5) include N_2 fixers explicitly (*Moore et al., 2004; Dunne et al., 2013*). The other biogeochemical models either neglect the process of N_2 fixation or represent it diagnostically based on stoichiometric considerations. The latter is also the case for the Hamburg Ocean Carbon Cycle Model (HAMOCC), the ocean biogeochemical component of the Max Planck Institute Earth System Model (MPI-ESM) (*Ilyina et al., 2013*). Biological production is represented by one bulk phytoplankton functional type in the model. N_2 fixation is calculated diagnostically from the relative abundance of surface nitrate to phosphate, based on the Redfield ratio. The input of 'new' N into the system via N_2 fixation is thus solely driven by nitrate depletion and neglects the biological growth dynamics of diazotrophic organisms that actually underly this process in the real ocean. In this respect, I am posing the question:

- **What are the effects of N_2 -fixing cyanobacteria on ocean biogeochemistry?**

To this end, the first part of the thesis is dedicated to the development and implementation of N₂-fixing cyanobacteria as an additional prognostic phytoplankton group in HAMOCC. The growth parameterization is thereby largely based on physiological knowledge about the cyanobacterium *Trichodesmium*. The resulting patterns and dynamics of N₂ fixation are evaluated against the previous (diagnostic) model version as well against observations, and changes in the mean biogeochemical state are assessed. Furthermore, the sensitivity of the new model component to certain parameters is tested.

1.2 Role of cyanobacteria in the biogeophysical feedback of light absorption

Besides affecting ocean biogeochemistry and the carbon cycle as elaborated above, cyanobacteria affect the climate system in a more direct way – namely by absorbing light. All phytoplankton contain photosynthetic pigments like chlorophyll which absorb light in the process of converting inorganic material into organic biomass. Most of the absorbed light is dissipated as heat (*Lewis et al.*, 1983, and references therein). Hence, the presence of phytoplankton redistributes the heating of incoming shortwave radiation in the water column (e.g. *Sathyendranath et al.*, 1991). The resulting temperature changes affect ocean and atmosphere dynamics, which in turn feed back on phytoplankton growth itself. Several model studies have demonstrated the relevance of this biogeophysical feedback of phytoplankton light absorption for the climate mean state and variability (e.g., *Wetzel et al.*, 2006; *Anderson et al.*, 2007; *Patara et al.*, 2012).

Previous studies, however, only considered the effect of phytoplankton in general. Cyanobacteria may play indeed a special role in this feedback (*Hense et al.*, 2017). The ability of cyanobacteria to generate gas vacuoles makes their cells positively buoyant, which, together with their N₂-fixing ability, leads to dense surface accumulations of biomass extending over up to several millions of square kilometres in the tropical and subtropical ocean (e.g., *Capone et al.*, 1998). Observations show a local heating effect of 1.5–5.0 K caused by cyanobacteria surface blooms (*Kahru et al.*, 1993; *Capone et al.*, 1998). Idealized one-dimensional and regional model studies support the view that cyanobacteria have an impact on surface temperature and mixed layer dynamics locally (*Hense*, 2007; *Sonntag and Hense*, 2011; *Sonntag*, 2013). Cyanobacteria are abundant throughout large parts of the tropical and subtropical ocean, exactly the areas where climate is particularly sensitive to the strength of biological light absorption (*Anderson et al.*, 2007, 2009; *Gnanadesikan and Anderson*, 2009). This leads to the hypothesis that cyanobacteria play a role on a larger scale than indicated by observations and idealized ocean-only model studies. The impact

of cyanobacteria on ocean temperature on the global scale, and the consequential implications for climate, have, however, not been studied yet. In this context I state the following research question:

- **What are the effects of light absorption by N₂-fixing cyanobacteria on the climate system?**

The implementation of prognostic cyanobacteria into HAMOCC (the scope of the first part of the thesis), allows me to use the comprehensive Earth system model MPI-ESM to study the effects of this phytoplankton group on the climate system. Therefore, I include cyanobacteria in the dynamic feedback from biological light absorption on ocean temperature, and study resulting implications for ocean and atmosphere dynamics as well as for ocean biogeochemistry itself.

1.3 Role of cyanobacteria in a high CO₂ world

With a changing climate, phytoplankton abundance and biogeography (e.g., *Hutchins and Fu, 2017*), and consequently the patterns of light absorption and feedback strengths, will change. How a changing phytoplankton distribution could alter future evolution of climate due to the biogeophysical feedback remains unknown. Nearly all previous model studies dealing with the biogeophysical feedback from phytoplankton radiative heating on climate applied a constant forcing and did not consider the effects of long-term changes in the phytoplankton distribution (e.g., *Patara et al., 2012*, and references therein). The only exception is the study of *Park et al. (2015)* who showed in transient simulations that in the Arctic a positive feedback between sea ice and phytoplankton could amplify Arctic warming. Thereby, a decline in sea ice promotes phytoplankton growth and hence surface light absorption, which, in turn, promotes warming and sea ice melting. Apart from the Arctic, the effects of changes in phytoplankton on other regions of the Earth are unexplored.

Particularly in the tropical and subtropical ocean, the habitat of N₂-fixing cyanobacteria, substantial long-term changes in phytoplankton abundance and primary production are expected. Increased stratification and reduced ventilation decrease the supply of nutrients to the surface and impair the growth conditions of ordinary phytoplankton (*Behrenfeld et al., 2006; Falkowski and Oliver, 2007*). Model studies simulate a decline in net primary production in the tropical and subtropical ocean (*Bopp et al., 2013; Laufkötter et al., 2015*). Cyanobacteria, in contrast to non-diazotrophic phytoplankton, however, may benefit from climate change and expand their range in the future (*Hutchins and Fu, 2017*). Cyanobacteria are not limited by nitrate and hence are not affected by the increase in nitrate limitation. Furthermore, the ability to utilize dissolved organic phosphorus in addition to phosphate (*Dyhrman et al., 2006*;

Sohm and Capone, 2006) might help cyanobacteria to cope with the intensified phosphate limitation under global warming. Moreover, increasing temperatures might lead to a poleward expansion of cyanobacteria's habitat (*Breitbarth et al., 2007*). In addition, there is evidence that higher seawater CO₂ concentrations will further stimulate the growth of *Trichodesmium* (*Barcelos e Ramos et al., 2007; Hutchins et al., 2007; Levitan et al., 2007; Kranz et al., 2009*). If these proposed physiological characteristics and adaptation mechanisms are, however, sufficient to lead to an overall increase in the abundance of cyanobacteria is uncertain (*Hutchins and Fu, 2017*). Moreover, to what extent cyanobacteria might counteract the decline in overall phytoplankton remains unknown.

Both factors, the overall evolution of phytoplankton under rising CO₂, as well as the consequential feedback on climate via changes in light absorption, are unresolved. It is speculated that a decline in phytoplankton in the tropical and subtropical ocean would cool the surface ocean due to decreased surface light absorption, and thus counteract the warming associated with climate change (*Patara et al., 2012*). Other model studies, on the other hand, would rather suggest the opposite effect, that means an amplified surface heating, due to advective processes (*Anderson et al., 2007, 2009; Gnanadesikan and Anderson, 2009; Jochum et al., 2010*). Until now, these are only speculations inferred from simulations with constant forcing. No transient simulations have been done so far to further investigate this open issue. Therefore, I address the following question:

- **How do changes in phytoplankton alter climate's response to rising CO₂, and what is the role of cyanobacteria?**

I conduct transient atmospheric CO₂ increase scenarios with MPI-ESM, a state-of-the-art Earth system model applied for climate projections such as in CMIP5 (*Jungclaus et al., 2013; Ilyina et al., 2013; Giorgetta et al., 2013*). I compare simulations with and without including the dynamic biogeophysical feedback of biological light absorption on temperature. I investigate how phytoplankton, in particular cyanobacteria, respond to changing environmental conditions under transient forcing, and how these changes feed back on climate. By additionally including proposed physiological characteristics and adaptation mechanisms of cyanobacteria in their growth parameterization, I explore the potential success of cyanobacteria in a high CO₂ world, and further assess how sensitive climate responds to a modified evolution of phytoplankton.

1.4 Thesis outline

Each of the three main chapters of this thesis is written in the style of journal publications, containing its own introduction and summary/conclusions. The individual chapters can thus be read largely independently from each other. Chapter 2 describes the newly developed growth parameterization as well as evaluation of the prognostic N_2 fixers in HAMOCC. This part has been published in *Journal of Advances in Modeling Earth systems* (Paulsen *et al.*, 2017). Including cyanobacteria as prognostic tracer in HAMOCC as part of MPI-ESM allows me to assess the impact of this phytoplankton group on the climate system via affecting radiative heating (Chapter 3). After investigating the involved processes under constant atmospheric CO_2 forcing, the impacts of changes in the phytoplankton distribution on climate under rising CO_2 are studied (Chapter 4). Emphasize is hereby on the projected evolution of cyanobacteria and the sensitivity of climate to it. In Chapter 5, I summarize the findings of the work and draw the main conclusions. Furthermore, I give an outlook on possible future research.

Technical remark

This introduction (Chapter 1) and Conclusions (Chapter 5) are written in the first person singular, whereas the main Chapters 2, 3, and 4 are written in the first person plural.

Further, it has to be noted that in Chapter 2, which is focusing on ocean biogeochemistry, the term " N_2 fixers" or "diazotrophs" is used (referring to their functional role of fixing N_2). In Chapters 3 and 4, which are focusing on the biogeophysical feedback, the term "cyanobacteria" is used, which refers the same tracer in the model but stresses the trait of positive buoyancy.

Chapter 2

Incorporating a prognostic representation of marine nitrogen fixers into the global ocean biogeochemical model HAMOCC¹

2.1 Introduction

Nitrogen (N₂) fixation is a major source of 'new' nitrogen to the euphotic zone that is thought to mostly compensate the loss through denitrification, therefore playing a key role in controlling the oceanic nitrogen inventory (e.g., *Karl and Letelier, 2008*). Since nitrogen limits primary production in large parts of the world's ocean (e.g., *Gruber and Sarmiento, 1997; Falkowski, 1997*), the input of 'new' nitrogen by means of N₂ fixation affects the efficiency of the biological pump, and hence the carbon cycle. The process of N₂ fixation, however, is often either neglected, or only poorly represented in the ocean biogeochemistry components of state-of-the-art Earth system models used for climate projections. This is also the case for the Hamburg Ocean Carbon Cycle Model (HAMOCC), the ocean biogeochemical component of the Max Planck Institute Earth System Model (MPI-ESM). Here, we present the incorporation of prognostic N₂ fixers into HAMOCC, aiming at improving the representation of present-day N₂ fixation in the model.

Only specific heterotrophic and autotrophic marine organisms, called diazotrophs, have the capacity to utilize N₂ for metabolic processes. In our study, we focus on

¹**Paulsen H.**, T. Ilyina, K.D. Six, and I. Stemmler (2017): Incorporating a prognostic representation of marine nitrogen fixers into the global ocean biogeochemical model HAMOCC. *Journal of Advances in Modeling Earth Systems.*, 9(1), 438–464.

the autotrophic types since heterotrophic diazotrophs are still poorly understood and their contribution to global N₂ fixation is unclear (Zehr *et al.*, 2001; Langlois *et al.*, 2005). There are three main groups of marine autotrophic diazotrophs, (1) the large, non-heterocystous cyanobacterium *Trichodesmium* (Carpenter and Romans, 1991; Capone *et al.*, 1997; Karl *et al.*, 2002; LaRoche and Breitbarth, 2005), (2) small-sized unicellular cyanobacteria (Zehr *et al.*, 2001), and (3) symbiont heterocystous diazotrophs associated with diatoms (DDA) (Carpenter *et al.*, 1999; Foster and Zehr, 2006). The ability to fix N₂ ensures diazotrophs their ecological success throughout vast areas of the tropical and subtropical oceans (Luo *et al.*, 2012). Recent estimates of global N₂ fixation rates span a large range of about 80 to 200 Tg N yr⁻¹ (e.g., Karl *et al.*, 2002; Großkopf *et al.*, 2012), assigning diazotrophy a considerable supply of fixed nitrogen to the euphotic zone on the global scale (Galloway *et al.*, 2004; Gruber, 2004).

In the future, the ecological niche of N₂ fixers may increase. Model studies project warmer sea surface temperatures, associated with intensified vertical stratification and reduced supply of nutrients from depth (e.g., Behrenfeld *et al.*, 2006; Falkowski and Oliver, 2007). While these conditions are unfavorable for non-diazotrophic phytoplankton (e.g., Doney, 2006; Boyce *et al.*, 2010; Bopp *et al.*, 2013), they could favor the growth of N₂ fixers (Boyd and Doney, 2002; Doney, 2006; Paerl and Huisman, 2008). In addition, there is evidence that higher oceanic carbon dioxide (CO₂) concentrations will further stimulate the growth of *Trichodesmium* (Barcelos e Ramos *et al.*, 2007; Hutchins *et al.*, 2007; Levitan *et al.*, 2007). Due to the coupling of the nitrogen to the carbon cycle, these climatic induced changes in N₂ fixation might impact on the ocean's carbon sequestration capacity (e.g., Capone, 2001), which, in turn, affects climate.

The majority of the current generation of global climate-biogeochemical models in the 5th phase of the Coupled Model Intercomparison Project (CMIP5, <http://cmip-pcmdi.llnl.gov/>) do not account for N₂ fixation nor the loss through denitrification at all (e.g., Palmer and Totterdell, 2001; Vichi *et al.*, 2007; Collins *et al.*, 2011; Watanabe *et al.*, 2011). Only a few CMIP5 models include an explicit representation of N₂ fixers (Moore *et al.*, 2004; Dunne *et al.*, 2013). The respective parameterizations consider the main relevant characteristics of diazotrophs, such as a relatively slow growth rate and no growth limitation by nitrogen. Still, these models have deficiencies in either reproducing a reasonable global N₂ fixation (Moore *et al.*, 2004), or the spatial distribution of N₂ fixation (Dunne *et al.*, 2013). Several one-dimensional (e.g., Hood *et al.*, 2001; Fennel *et al.*, 2002), as well as regional and global models (e.g., Hood *et al.*, 2004; Moore and Doney, 2007; Sonntag, 2013; Landolfi *et al.*, 2015), take into account additional distinct physiological characteristics of N₂ fixers, such as a specific temperature dependence of diazotrophic growth, or buoyancy. These parameterizations are mostly based on the physiology of the best studied, surface bloom form-

ing marine nitrogen fixer *Trichodesmium* (e.g., Capone *et al.*, 1997, 2005). The models succeed in simulating regional spatial and temporal patterns of N_2 fixation. The studies of Monteiro *et al.* (2010, 2011) include all three main diazotroph types (*Trichodesmium*, unicellular cyanobacteria, and symbiotic diazotrophs) by means of a "self-assembling" phytoplankton community. In their global model, the three diazotroph types largely co-exist. The authors state that N_2 fixation in the ocean can possibly be represented to a great extent by a model based solely on *Trichodesmium*.

In HAMOCC, the global ocean biogeochemistry model of the MPI-ESM, N_2 fixation has hitherto been represented by a diagnostic formulation. Thereby, the nitrate influx into the surface layer is a function of the nitrate deficit relative to phosphate (derived theoretically based on phosphate concentrations and the Redfield ratio), multiplied by a constant fixation rate (Ilyina *et al.*, 2013). Although this simplified approach yields a reasonable global N_2 fixation, the observed spatial patterns are not captured. The areas of N_2 fixation are rather coupled to the upwelling areas of nitrate-depleted waters, similar to what can be found in the geochemical model approach of Deutsch *et al.* (2007). Large fixation rates in HAMOCC occur in high latitudes, which is in contradiction with observations. Furthermore, the whole influx due to N_2 fixation is prescribed to take place in the first model layer (12 m), in contrast to observations which rather indicate considerable fixation rates down to greater depth levels (e.g., Davis and McGillicuddy, 2006; Luo *et al.*, 2012). Besides the deficiencies in simulating the spatial distribution (horizontally and vertically), the temporal variability is also not captured. The diagnostic formulation is not able to simulate a realistic seasonal cycle due to its tight coupling to upwelling and due to the lacking explicit growth dynamics of N_2 fixers.

Here, we replace the diagnostic formulation of N_2 fixation in HAMOCC by including a prognostic representation of diazotrophs. As the ecological niche of diazotrophs is thought to be to a large extent represented by physiological characteristics of *Trichodesmium* (Monteiro *et al.*, 2010, 2011), we base the formulation of growth dynamics on the physiology of this most abundant and widely studied open ocean diazotroph. The aim of this comprehensive approach is to realistically represent the process of N_2 fixation and its effects on biogeochemical cycles in the global biogeochemical model. This chapter provides a detailed description of the parameterization of prognostic N_2 fixers, as well as an analysis and evaluation of the model performance on the basis of observations and previous model studies. Successfully reproducing today's state of N_2 fixation is a prerequisite for capturing its response to future climate. Moreover, the new model component in HAMOCC provides the basis for further studies on the role of diazotrophs in ocean biogeochemical cycles, and on the response of N_2 fixation to different environmental factors.

The remaining chapter is organized as follows: Section 3.2 gives a short overview of the main aspects of the global biogeochemical model HAMOCC, followed by a de-

tailed description of the parameterization of the newly implemented N_2 fixers. The section includes the model setup and experimental design. Section 2.3 provides an evaluation of modeled N_2 fixers and N_2 fixation against observations and results from biogeochemical models. Differences in biogeochemistry between two model runs, one with and one without prognostic N_2 fixers, are discussed in Section 2.4. The sensitivity of N_2 fixers to selected model parameters is assessed in additional experiments (Section 2.5). The paper closes with a summary and conclusions, discussing the strengths and constraints of the new model component (Section 2.6).

2.2 Model description

2.2.1 The ocean biogeochemical model HAMOCC

The global ocean biogeochemistry model HAMOCC, as part of MPI-ESM, serves to quantify the uptake and storage of CO_2 in the ocean. HAMOCC includes biogeochemical processes in the water column, the sediment, and at the air-sea interface. The present study extends the version HAMOCC 5.2, which was used as part of the MPI-ESM in the CMIP5 experiments (*Ilyina et al.*, 2013).

Biogeochemical tracers in the water column are fully advected, mixed and diffused by the flow field of the physical model. Biogeochemistry dynamics, which are premised on an extended NPZD (nutrients, phytoplankton, zooplankton, detritus) model approach (*Six and Maier-Reimer*, 1996), include the compartments nutrients (phosphate, nitrate, and iron), oxygen, silicate, phytoplankton, zooplankton, dissolved organic matter, and detritus. Organic material is composed following a constant Redfield ratio of carbon ($C:N:P:O_2 = 122:16:1:-172$) based on *Takahashi et al.* (1985) and of the micronutrient iron ($Fe:P = 366E10^{-6}:1$) (*Johnson et al.*, 1997). The sinking speed of organic matter increases linearly with depth after *Martin et al.* (1987). Atmospheric deposition of iron is accounted for by applying the present-day climatology of monthly atmospheric dust deposition from *Mahowald et al.* (2006). It is assumed that a fixed fraction of the dust deposition (3.5 %) is iron, of which 1 % is biologically available.

Denitrification, the reduction of nitrate (NO_3) to N_2 which occurs in suboxic zones, is represented by means of a first order approach with a time constant of $0.00125 d^{-1}$ in the water column, and $0.01 d^{-1}$ in the sediment, respectively. This process takes place when oxygen falls below a threshold value of $O_{2_{crit}} = 0.5 \mu mol L^{-1}$ in the water column, and $O_{2_{crit}} = 1 \mu mol L^{-1}$ in the sediment. In the previous model version (*Ilyina et al.*, 2013), N_2 fixation, the conversion of N_2 into bioavailable nitrogen, was realized as a direct input of nitrate to the surface layer with a rate of $0.05 d^{-1}$ in case of a nitrate to phosphate ratio below the Redfield value of 16 N to 1 P. In this

study, the implementation of prognostic diazotrophic growth and related N₂ fixation replaces the diagnostic formulation. The applied parameterization is described in detail in the next subsection (Section 2.2.2).

2.2.2 Prognostic parameterization of N₂ fixers

The parameterization of bulk diazotrophic growth is based on observed physiological responses of *Trichodesmium* to environmental conditions. Unicellular cyanobacteria have similar characteristics in many aspects, and thus are not explicitly accounted for. The knowledge about symbiotic diazotrophs is so limited due to the complex relationship with diatoms that we do not consider them in the parameterization.

Analogous to bulk phytoplankton, N₂ fixers are included as a three dimensional prognostic tracer, advected and mixed by the oceanic flow field of the general circulation model. The governing differential equation describing the dynamics of the N₂ fixers concentration (Diaz) is given by

$$\frac{\partial \text{Diaz}}{\partial t} + \mathbf{V} \cdot \nabla \text{Diaz} - D \text{Diaz} = \sum_k \Psi_{BGC}. \quad (2.1)$$

Hereby, \mathbf{V} is the 3D advection vector, D the diffusion operator (both computed in the ocean general circulation model), and Ψ includes the source and sink terms of biogeochemical processes,

$$\Psi_{BGC} = G - M - w_{Diaz} \frac{\partial \text{Diaz}}{\partial z}, \quad (2.2)$$

where G is growth, and M mortality of N₂ fixers. The last factor in Equation 2.2 describes changes in the distribution due to vertical movement with the constant buoyancy velocity w_{Diaz} . This natural motility, provided by the presence of gas vesicles (Walsby, 1978; Villareal and Carpenter, 2003; Rodier and Le Borgne, 2008, 2010), gives *Trichodesmium* an advantage compared to bulk phytoplankton in competition for light. Following Sonntag (2013), we set the buoyancy velocity to 1 m d⁻¹.

Growth is limited by the physical conditions light (L) (Karl and Letelier, 2008; Luo et al., 2014) and temperature (T) (Breitbarth et al., 2007), and by the nutrients iron (Fe) (e.g., Moore et al., 2009) and phosphate (PO₄) (e.g., Sañudo-Wilhelmy et al., 2001). The resulting growth rate is given by multiplying the maximum growth rate μ_{max} with the respective limiting functions l_L , l_T , l_{Fe} , and l_P :

$$g = \mu_{max} \cdot l_L \cdot l_T \cdot l_{Fe} \cdot l_P. \quad (2.3)$$

The maximum growth rate of N_2 fixers (both for *Trichodesmium* and unicellular cyanobacteria) is lower compared to bulk phytoplankton due to the energetically costly process of N_2 fixation. In our model, the maximum growth rate is set to 0.2 d^{-1} , a value in the middle of the observed range for *Trichodesmium* (doubling time 3–5 days, Capone *et al.* (1997)). The actual growth of N_2 fixers biomass per time step is then given by

$$G = g \cdot \text{Diaz}. \quad (2.4)$$

Light limitation, as for bulk phytoplankton, is calculated following the photosynthetic irradiance curve formulation by Smith (1936):

$$l_L(I_{PAR}) = \frac{\alpha \cdot I_{PAR}(z)}{\sqrt{\mu_{max}^2 + \alpha \cdot I_{PAR}(z)^2}}, \quad (2.5)$$

with α as the initial slope of the photosynthesis versus irradiance curve, and $I_{PAR}(z)$ the vertical field of photosynthetically active radiation (PAR) in the water column. $I_{PAR}(z)$ is parameterized by a bimodal approach based on Zielinski *et al.* (2002):

$$I_{PAR}(z) = I_{oPAR} \left[\sigma \cdot \exp(-z \cdot k_r) + (1 - \sigma) \cdot \exp\left(-z \cdot k_w - k_{Chl} \cdot \int_0^z (1/R_{C:Chl} \cdot (\text{Diaz}(z') + \text{Phy}(z')) dz')\right) \right]. \quad (2.6)$$

Here, I_{oPAR} is the incoming photosynthetically active radiation at the sea surface, covering the wavelength range of 400–700 nm. The spectrum is divided at 580 nm (prescribed by σ) into two domains: Whereas for longer wavelengths (red domain) attenuation is dominated by sea water with the attenuation coefficient k_r , for shorter wavelengths (blue/green domain) the absorption by chlorophyll (Chl) with the absorption coefficient k_{Chl} is considered in addition to clear water with the absorption coefficient k_w . The carbon to chlorophyll ratio ($R_{C:Chl}$) of N_2 fixers in the model is the same as for bulk phytoplankton, namely $60:1 \text{ g C (g Chl)}^{-1}$ (Ilyina *et al.*, 2013).

The temperature limitation of growth l_T is described by a modified Gaussian function as used by Sonntag (2013), based on observational evidence gained by Breitbarth *et al.* (2007):

$$l_T(T) = \exp\left[-\frac{(T - T_{opt})^4}{(T_1 - T_2 \cdot \Gamma)^4}\right], \quad \text{with } \Gamma = \begin{cases} -1 & \text{for } T < T_{opt} \\ 0 & \text{for } T = T_{opt} \\ 1 & \text{for } T > T_{opt} \end{cases} \quad (2.7)$$

T_{opt} is hereby the optimal temperature for N_2 fixers growth, and T_1 and T_2 describe the distribution around this optimum. The parameter values are chosen as $T_1 = 5.5$ °C and $T_2 = 1$ °C with an optimum temperature $T_{opt} = 28.0$ °C, reproducing the observed curve for *Trichodesmium* (Breitbarth et al., 2007). Not only *Trichodesmium*, but also unicellular cyanobacteria and diazotrophs in general, are thought to favor warm temperatures (e.g., Falcón et al., 2005; Langlois et al., 2005; Needoba et al., 2007).

The growth dependency on the macro nutrient phosphate and micro nutrient iron is formulated explicitly as a multiplicative limiting approach following Michaelis-Menten kinetics:

$$l_{Fe}(Fe) = \frac{Fe}{K_{Fe} + Fe} \quad (2.8)$$

$$l_P(PO_4) = \frac{PO_4}{K_P + PO_4} \quad (2.9)$$

The iron demand for the process of N_2 fixation is reported to be nearly 10–100 times higher than for any other nitrogen assimilation (e.g., Falkowski et al., 1998; Berman-Frank et al., 2001; Kustka et al., 2003). In the parameterization, we account for this by a high half-saturation constant K_{Fe} of $0.32 \text{ nmol Fe m}^{-3}$. For phosphate a half saturation constant K_P of $1 \cdot 10^{-8} \text{ kmol P m}^{-3}$ is applied.

The fundamental difference of *our Trichodesmium* based N_2 fixers compared to bulk phytoplankton in the model is, that their growth is not limited by nitrate due to their capability to utilize N_2 . However, it is known, that not all of the cells within a colony or along a filament of *Trichodesmium* contain *nifH*, the necessary gene for N_2 fixation (Lin et al., 1998; Mulholland and Capone, 2000; Berman-Frank et al., 2001; Eichner et al., 2014). In preference to the energetic costly process of breaking the N_2 triple bond, *Trichodesmium* rather can obtain significant amounts of nitrogen through uptake of nitrate and ammonium (Holl and Montoya, 2005). In the model, we account for a potential nitrate uptake of diazotrophs by:

$$G_{NO_3}(NO_3) = \min(NO_3 - NO_{3min}, G \cdot l_{NO_3}) \quad (2.10)$$

with

$$l_{NO_3}(NO_3) = \frac{NO_3^2}{K_N^2 + NO_3^2} \quad (2.11)$$

Nitrate is taken up by the diazotrophs following Michaelis Menten kinetics with quadratic terms. The first term in the minimum expression in Equation 2.10 prevents nitrate from getting negative ($NO_{3min} = 1 \cdot 10^{-11} \text{ kmol N m}^{-3}$). For nitrate

uptake, a half-saturation constant of $K_N = 1.6 \cdot 10^{-7} \text{ kmol N m}^{-3}$ is applied. The residual nitrogen demand required to maintain the prescribed Redfield ratio of 16 N to 1 P is then supplied by N_2 , representing the process of N_2 fixation (G_{N_2}):

$$G_{N_2} = G - G_{NO_3} \quad (2.12)$$

Hence, the ratio of N_2 fixation and nitrate consumption is not prescribed, but evolves dynamically in the model: If no nitrate is available, N_2 fixation is stimulated, whereas it is reduced with increasing nitrate concentration.

As observations indicate that the grazing pressure on *Trichodesmium* is small (O'Neil and Roman, 1994; Hood et al., 2001; Hewson et al., 2004), consumption by zooplankton has been omitted. The sink term of N_2 fixers is given by its natural mortality M :

$$M = \min(\text{Diaz} - \text{Diaz}_{\min}, m_{\text{Diaz}} \cdot \text{Diaz}). \quad (2.13)$$

The dimensional coefficient m_{Diaz} represents the decay rate. The decay rate is not well constrained by observations and is set to a value of 0.1 d^{-1} as a result of the tuning process. This value is within the range of values applied by other model studies (e.g. 0.05 d^{-1} , Sonntag (2013); 0.18 d^{-1} , Moore et al. (2004)). In order to guarantee growth at any location, N_2 fixers concentration can not fall below a threshold Diaz_{\min} of $1 \cdot 10^{-11} \text{ kmol P m}^{-3}$, mimicing spores floating around in the water column.

The resulting linear loss is partitioned between the detritus pool ($f_{\text{DET}} = 0.9$), accounting for the sinking part of the organic matter which is reported to be potentially triggered by programmed cell death of *Trichodesmium* blooms (Bar-Zeev et al., 2013), and the dissolved organic matter (DOM_{Diaz}) pool ($f_{\text{DOM}_{\text{Diaz}}} = 0.1$). Nitrate is released into the system via remineralization of detritus and DOM. The contribution of N_2 fixers (and phytoplankton in general) to DOM is largely unknown. There is evidence that part of the DOM in the oligotrophic ocean is transformed into recalcitrant DOM (Jiao et al., 2010). However, the remineralization rate of DOM is in general not well constrained, and we used it as a tuning parameter to achieve a better distribution of surface nitrate in the system. As a result of model tuning, we set the bacterial degradation rate of DOM produced by N_2 fixers ($rem_{\text{DOM}_{\text{Diaz}}}$) to $4 \cdot 10^{-5} \text{ d}^{-1}$.

The organic composition of N_2 fixers in the model is analogous to bulk phytoplankton (C:N:P:O₂ = 122:16:1:172). With respect to the change of total alkalinity (TA) due to N_2 fixers growth, this means an increase in TA in case of the usage of nitrate, and no change of TA in case of the usage of N_2 (Wolf-Gladrow et al., 2007; Ilyina et al., 2013).

As *Trichodesmium* photosynthetically produces oxygen while fixing N_2 (Capone *et al.*, 1997), oxygen is released during the process of N_2 fixers production in the model. With the assumption of a constant Redfield ratio for all organic material, the amount of released oxygen depends on the source of nitrogen: If N_2 is used for growth the change in oxygen is 148 kmol O_2 per production of 1 kmol P, and for nitrate, it is 172 kmol O_2 , respectively.

2.2.3 Model setup and experimental design

HAMOCC runs as part of the Max Planck Institute Ocean Model (MPIOM), and both are components of the MPI-ESM. MPIOM is a z-coordinate global general circulation model solving the primitive equations under the hydrostatic and Boussinesq approximation on a C-grid with a free surface (Marsland *et al.*, 2003; Jungclaus *et al.*, 2013). Details on the coupling of HAMOCC and MPIOM are given in Maier-Reimer *et al.* (2005).

The spatial and temporal resolution of HAMOCC is prescribed by MPIOM. In the current study, a configuration referred to as LR (GR15) is applied (Jungclaus *et al.*, 2013). The bipolar grid, with poles over Antarctica and Greenland, has a horizontal resolution of about 1.5° , gradually varying between 15 km in the Arctic and about 184 km in the tropics. In the vertical, there are 40 unevenly spaced layers with level thicknesses increasing towards the bottom, whereby eight layers are located within the upper 90 m. The time step is 72 minutes.

For our simulations, MPIOM and HAMOCC are forced daily by the surface boundary condition dataset based on the second ECMWF Re-Analysis project (ERA-40, Simmons and Gibson (2000), also referred to as OMIP-Forcing (Röske, 2005)). In this forcing dataset, the surface conditions are based on bulk formulae, applied on the ERA-40 data covering the time period from 1958-2001. From this data, a mean annual cycle on a daily basis for relevant parameters like windstress, heat- and freshwater fluxes was calculated (Röske, 2005). Continental runoff is determined by means of a runoff model.

Two model simulations were performed, each starting from model state in equilibrium which was achieved in a preindustrial control simulation performed for CMIP5 (Ilyina *et al.*, 2013). In the first simulation, we included the prognostic N_2 fixers and run the model to a new quasi-stationary state reached after 2000 years (in the following referenced as PROG). The second simulation serves as control experiment and uses the diagnostic formation of N_2 fixation (in the following referenced as REF). For all analyses, the mean of the last 100 years is employed.

2.3 Evaluation of the model results with respect to diazotrophic biomass and N₂ fixation rates

In this section, a description of the mean model state with respect to diazotrophic biomass and N₂ fixation rates is given. After presenting the observational basis for evaluation, the general global patterns are described, followed by a detailed description and evaluation of the individual ocean basins. Furthermore, the vertical distribution, as well as seasonal dynamics of modeled N₂ fixation are discussed in the context of available observations.

2.3.1 Observational basis

We use the global compilation of observations of cyanobacterial diazotrophic biomass and N₂ fixation rates by *Luo et al.* (2012) (stored in the information system PANGAEA, doi:10.1594/PANGAEA.774851, accessed in May 2016) for model evaluation. The database provides both volumetric, as well as depth-integrated values of biomass and N₂ fixation rates. The biomass data are based on direct measurements of microscopic colony- and trichome-counts of *Trichodesmium*, and cell-counts of heterocystous cyanobacteria. Limited data is also available based on *nifH* gene abundances. However, as the usage of the latter method is accompanied by a high uncertainty (*Luo et al.*, 2012), we focus on the data based on cell-, colony-, and trichome-counts. Most data are based on the dominant cyanobacterium *Trichodesmium*. As the measurements do not cover the full diazotrophic community, the values can be seen as the lower limits of diazotrophic biomass (*Luo et al.*, 2012).

The N₂ fixation rates in the database are mostly corresponding to whole seawater samples. In some cases the rates are measured for specific organisms, i.e. *Trichodesmium*, unicellular cyanobacteria, or heterocystous cyanobacteria, which are then summed up. Due to a bias in one of the commonly applied measurement methods (¹⁵N₂ tracer addition), a large number of N₂ fixation rates within the database might be underestimated to a certain degree (*Mohr et al.*, 2010; *Luo et al.*, 2012, 2014). On the other hand, some individual N₂ fixation rates might be overestimated due to the contamination of some commercial 15-nitrogen (¹⁵N) gas stocks used to estimate N₂ fixation rates in the past (*Dabundo et al.*, 2014). Since our purpose is to evaluate the general patterns of the simulated N₂ fixation, rather than to compare exact numbers with observations, the database can nevertheless be used for our study. However, the methodological uncertainty has to be kept in mind. For our model evaluation, we binned the observational data of biomass and N₂ fixation rates onto a 3° x 3° grid and calculated the geometric means of the data in each bin. For surface values, we averaged the available data from the upper 10 m.

Timeseries of monthly values of N₂ fixation rates exist for the monitoring stations

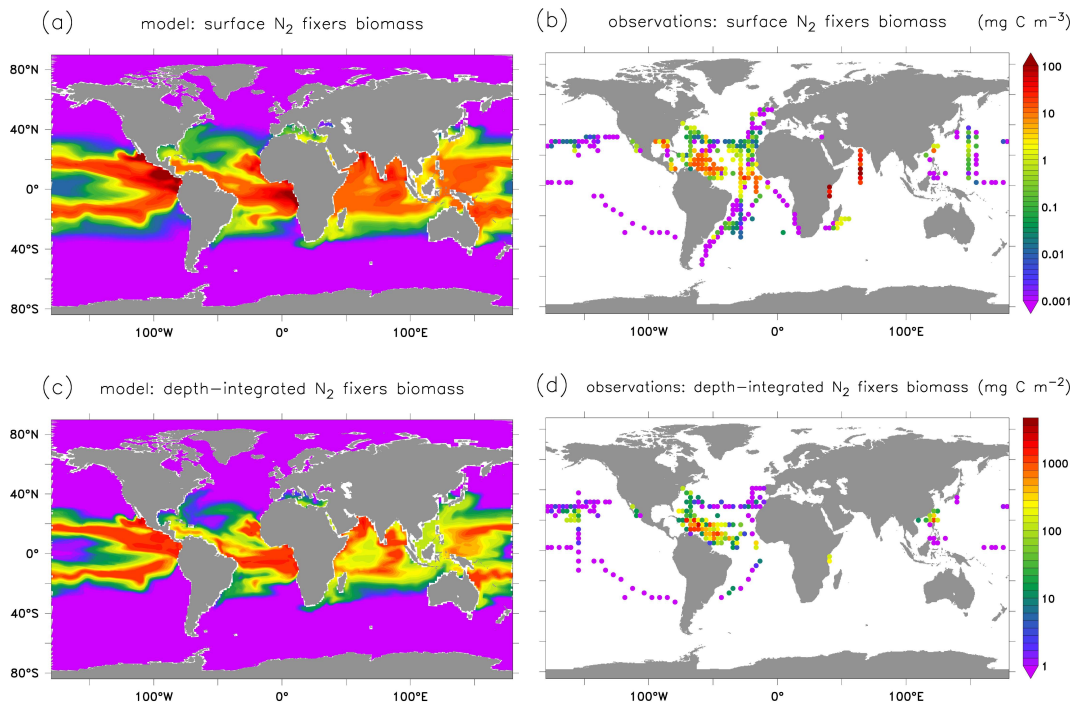


Figure 2.1: Top: Surface concentration of N₂ fixers biomass (mg C m⁻³) (a) in the model (PROG, 100 year mean), and (b) in observations (0–10 m). Bottom: depth-integrated biomass (mg C m⁻²) of N₂ fixers (c) in the model (PROG, 100 year mean) and (d) in observations. Observational data is taken from the database described in Luo et al. (2012), binned on a 3° x 3° grid. The geometric mean of each bin is shown.

ALOHA (A Long-term Oligotrophic Habitat Assessment) in the North Pacific from 2005 to 2010 (Church et al., 2009; Luo et al., 2012), and for BATS (Bermuda Atlantic Time series Study) in the North Atlantic from 1995 to 1997 (Orcutt et al., 2001; Luo et al., 2012). These timeseries are applied to evaluate the modeled seasonal dynamics of N₂ fixation.

In addition to in situ measurements, geographical information about *Trichodesmium* derived from remote sensing are used in this study for model evaluation (Gower and Carpenter, 1992; Dupouy et al., 2000; Sarangi et al., 2005; Westberry and Siegel, 2006).

2.3.2 Mean state of diazotrophic biomass and N₂ fixation rates

Global distribution

Simulated large scale patterns of N₂ fixers biomass (Figures 2.1a and 2.1c) and N₂ fixation (Figures 2.2a and 2.2c) in PROG are generally consistent with in situ measurements (Figures 2.1b and 2.1d, and Figures 2.2b and 2.2d, respectively). Surface concentrations reach values of up to ~ 400 mg C m⁻³, and depth-integrated

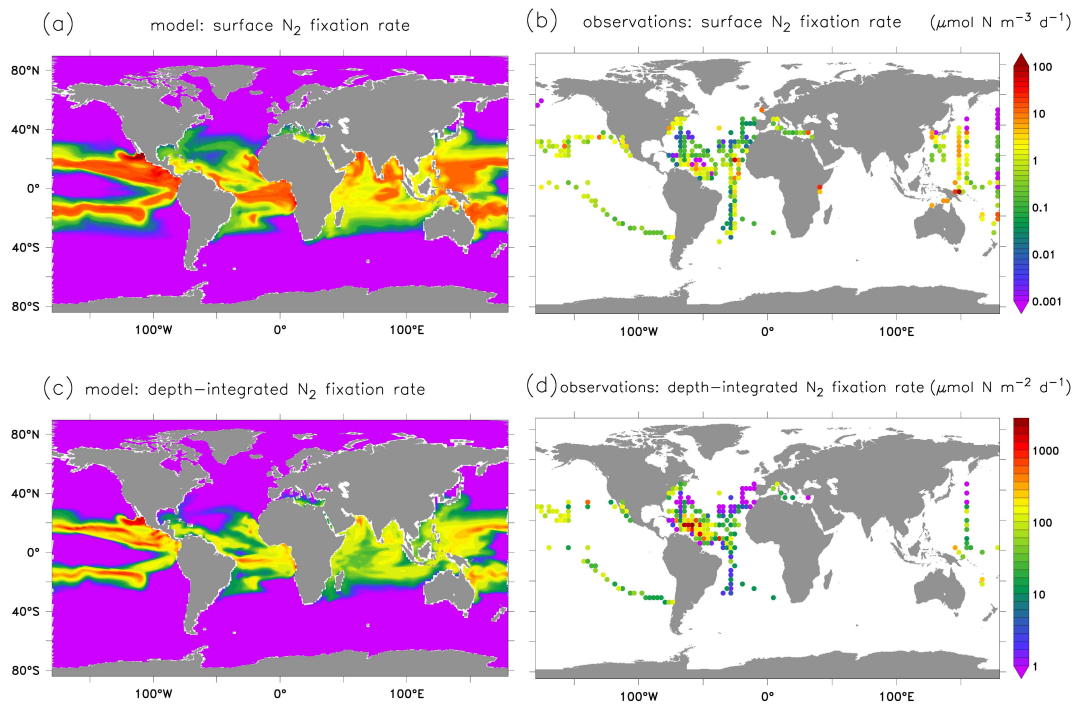


Figure 2.2: Top: Surface N_2 fixation rates ($\mu\text{mol N m}^{-3} \text{d}^{-1}$) (a) in the model (PROG, 100 year mean), and (b) in observations (0–10 m). Bottom: depth-integrated N_2 fixation rates ($\mu\text{mol N m}^{-2} \text{d}^{-1}$) (c) in the model (PROG, 100 year mean) and (d) in observations. Observational data is taken from the database described in Luo et al. (2012), binned on a $3^\circ \times 3^\circ$ grid. The geometric mean of each bin is shown.

values up to $\sim 7000 \text{ mg C m}^{-2}$. Surface N_2 fixation rates show values up to $\sim 300 \mu\text{mol N m}^{-3} \text{d}^{-1}$, and depth-integrated values up to $\sim 5000 \mu\text{mol N m}^{-2} \text{d}^{-1}$. The modeled habitat of diazotrophs is confined to tropical and subtropical waters approximately between 40°S – 40°N . The meridional extent and gradient is mainly determined by surface temperature (Figure 2.4c) and solar radiation (not shown), which are the physical factors directly affecting growth of N_2 fixers in the model (Equation 2.3). In situ (Luo et al., 2012) and remote sensing observations (Westberry and Siegel, 2006) support the view that N_2 fixers' main ecological niche is confined to the tropical and subtropical ocean. Also in model studies which include a higher level of diazotrophic diversity (Monteiro et al., 2010, 2011), the diazotroph habitat is restricted to tropical and subtropical waters, whereby not temperature but nutrient availability seems to be the dominant factor here.

The modeled global depth-integrated N_2 fixation rate in the PROG experiment yields $135.6 \text{ Tg N yr}^{-1}$ (Table 2.2). This value falls into the range of reported estimates of ~ 80 – 200 Tg N yr^{-1} . In general, the estimates based on extrapolations of direct measurements are markedly smaller ($< 100 \text{ Tg N yr}^{-1}$, e.g., Capone et al. (1997); Luo et al. (2012)) than the geochemical estimates derived from stoichiometric ratios

Table 2.1: Model parameters related to the parameterization of prognostic N₂ fixers in experiment PROG.

Symbol	Variable	Value	Units
μ_{max}	Maximum growth rate	0.2	d ⁻¹
m_{Diaz}	Decay rate	0.1	d ⁻¹
$Diaz_{min}$	Minimum concentration	$1 \cdot 10^{-11}$	kmol P m ⁻³
w_{Diaz}	Buoyancy velocity	1.0	m d ⁻¹
K_P	Half saturation constant for phosphate uptake	$1 \cdot 10^{-8}$	kmol P m ⁻³
K_{Fe}	Half saturation constant for iron uptake	0.32	nmol Fe m ⁻³
K_N	Half saturation constant for nitrate uptake	$1.6 \cdot 10^{-7}$	kmol N m ⁻³
$f_{DOM_{Diaz}}$	Fraction of DOM _{Diaz}	0.1	
f_{DET}	Fraction of detritus	0.9	
$rem_{DOM_{Diaz}}$	Remineralization rate of DOM _{Diaz}	$4 \cdot 10^{-5}$	d ⁻¹
T_{opt}	Optimum temperature of growth	28.0	°C
T_1	Temperature window parameter 1	5.5	°C
T_2	Temperature window parameter 2	1.0	°C
α	Initial slope of P versus I curve	0.03	d ⁻¹ (Wm ⁻²) ⁻¹
k_r	Mean light attenuation coefficient of water for $\nu < 580$ nm	0.35	m ⁻¹
k_w	Mean light attenuation coefficient of water for $\nu \geq 580$ nm	0.03	m ⁻¹
k_{Chl}	Light attenuation coefficient of chlorophyll	0.04	m ² (mg Chl) ⁻¹
σ	Dividing PAR domain at 580 nm	0.4	
$R_{C:Chl}$	C:Chl ratio of N ₂ fixers	60	g C (g Chl) ⁻¹

(> 100 Tg N yr⁻¹, e.g., *Gruber and Sarmiento (1997); Deutsch et al. (2007)*). Overall, the global N₂ fixation rate in our model is consistent with the value of 140 Tg N yr⁻¹ which has become widely accepted based on recent literature (e.g., *Gruber and Galloway, 2008; Voss et al., 2013*).

With regard to the standing stock of diazotrophs, *Luo et al. (2012)* give different estimates ranging from about 2 Tg C (based on cell counts) to 590 Tg C (based on *nifH*-based abundances). However, the assumptions to derive biomass from cell counts and abundances introduce high uncertainties, which can affect the global estimates up to $\pm 70\%$ (*Luo et al., 2012*). In our model, N₂ fixers develop a total biomass of 100 Tg C, which is within the range of the estimates by *Luo et al. (2012)*.

Global denitrification (water column and sediment, 141.9 Tg N yr⁻¹) is approximately balanced by global N₂ fixation (135.6 Tg N yr⁻¹). Water column denitrification is restricted to the eastern parts of the Pacific and Atlantic Ocean, and the northern part of the Indian Ocean (Figure 2.3b). This pattern is in qualitative agreement with in situ studies (*Codispoti et al 2001*). However, the extents of the denitrification areas are too large due to the overestimated size of the oxygen minimum zones (OMZs), which is a typical issue of global ocean biogeochemistry models (e.g., *Andrews et al., 2013; Cocco et al., 2013*).

Experiment REF also yields a reasonable global N₂ fixation rate of 132.6 Tg N yr⁻¹.

Table 2.2: Globally integrated 100 year mean fluxes and inventories within the euphotic zone (except for N₂ fixation which is integrated over the whole depth range, and denitrification which includes the sediment) for the experiments REF and PROG.

Parameter	REF	PROG	Units
N ₂ fixation	132.6	135.6	Tg N yr ⁻¹
Denitrification (water column and sediment)	135.0	141.9	Tg N yr ⁻¹
Primary production of bulk phytoplankton	61.01	45.53	Gt C yr ⁻¹
Primary production of N ₂ fixers		3.23	Gt C yr ⁻¹
Export production at 90 m	7.24	7.46	Gt C yr ⁻¹
Bulk phytoplankton biomass	0.62	0.61	Gt C
N ₂ fixers biomass		0.10	Gt C
Zooplankton biomass	0.51	0.39	Gt C
Detritus biomass	1.62	1.57	Gt C
DOM inventory	5.88	4.64	Gt C
DOM _{Diaz} inventory		0.82	Gt C

However, the spatial patterns of N₂ fixation are not correct (Figure 2.3a). N₂ fixation is solely determined by the surface nitrate to phosphate ratio. Thus, highest rates mainly occur in areas of denitrification (which in REF has a similar pattern as in PROG, Figure 2.3b), as well as in high latitudes, where nitrate-depleted water masses are upwelled to the surface. The major fraction of N₂ fixation is concentrated in the Pacific Ocean, similar to what has been found in the model study of *Deutsch et al.* (2007), in which N₂ fixation is diagnosed by the observed depletion of excess of P relative to the Redfield N quota ($P^* = PO_4 - NO_3/16$). Observations indicate that the upwelling areas are not the major N₂ fixation sites (Figures 2.2b and 2.2d). Furthermore, the high fixation rates in high latitudes in REF (e.g. up to 300 $\mu\text{mol N m}^{-2} \text{d}^{-1}$ in the North Pacific), are not supported by observations. It is known that the majority of N₂ fixers rather inhabit warm waters (*Luo et al.* (2012), Figure 2.2b and 2.2d). Replacing the diagnostic formulation by the prognostic growth dynamics leads to a decoupling of N₂ fixation from upwelling patterns. Thereby, the high iron limitation plays a crucial role (Figure 2.4a) since it restricts diazotrophic growth and N₂ fixation to regions of sufficient dust deposition. The impact of iron on modulating the spatial distribution of N₂ fixation is in accordance with previous model studies (*Somes et al.*, 2010; *Weber and Deutsch*, 2014). Furthermore, physical conditions, such as light and temperature, which were not accounted for in the diagnostic formulation, now influence diazotrophic activity (Figure 2.4c). The supply of cold, as well as iron-depleted water masses to the surface in the eastern upwelling regions of the South Pacific and South Atlantic leads to strong growth limitation and thus to the absence of N₂ fixers in the major denitrification sites.

In the following, the results of PROG for the individual ocean basins are discussed in more detail. Since, due to the temperature limitation, N₂ fixers growth is limited

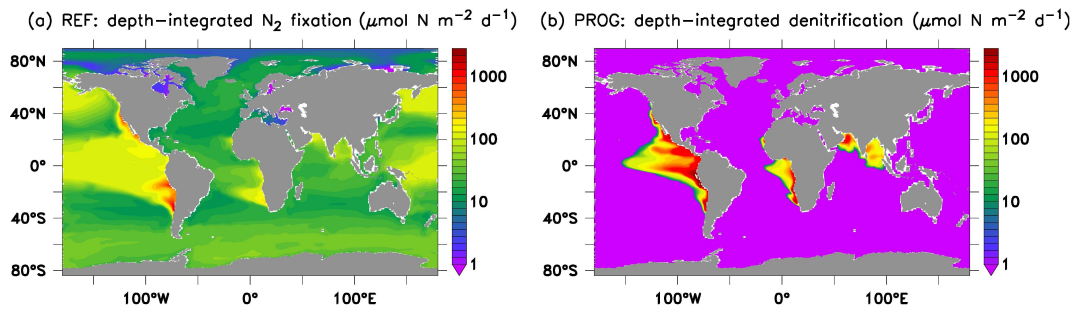


Figure 2.3: (a) 100 year mean depth-integrated N₂ fixation ($\mu\text{mol N m}^{-2} \text{d}^{-1}$) in REF. (b) 100 year mean depth-integrated denitrification rate ($\mu\text{mol N m}^{-2} \text{d}^{-1}$) in PROG.

to latitudes between 40°S–40°N, the descriptions refer to these respective regions in the Atlantic, Pacific and Indian Ocean.

Atlantic Ocean

In the Atlantic Ocean, diazotrophic growth in the model is mainly limited by phosphate (Figure 2.4b). Iron concentrations are overall high due to the high dust deposition (Mahowald *et al.*, 2006), and hence do not considerably restrict growth of N₂ fixers (Figure 2.4a). Observational studies support the controlling role of phosphate for N₂ fixers' growth in the Atlantic Ocean (e.g., Sañudo-Wilhelmy *et al.*, 2001; Ammerman *et al.*, 2003).

In the North Atlantic, high modeled values of diazotrophic biomass and N₂ fixation rates are arranged like a band along the northern coast of South America, extending into the Caribbean Sea and the Gulf of Mexico. The North Brazil Current transports phosphate rich surface water from the equatorial upwelling region northward, resulting in low growth limitation along the boundary (Figure 2.4b). The magnitudes of concentrations and fixation rates here are overall consistent with observations (surface concentrations $\sim 10 \text{ mg C m}^{-3}$; depth-integrated concentrations $\sim 100\text{--}1000 \text{ mg C m}^{-2}$, surface fixation rates $\sim 10 \mu\text{mol N m}^{-3} \text{d}^{-1}$, depth-integrated fixation rates $\sim 700 \mu\text{mol N m}^{-2} \text{d}^{-1}$). Also other models are in line with the pattern of high abundances of N₂ fixers along the northern South American coast (Hood *et al.*, 2004; Moore *et al.*, 2004; Dunne *et al.*, 2013).

At the western side of the North Atlantic basin, high modeled surface concentrations and fixation rates reach latitudes of $> 40^\circ\text{N}$ due to the drift of diazotrophs with the warm water of the Gulf Stream (Figure 2.4c). This extension to high latitudes along the western boundary agrees with observations (Figures 2.1b and 2.2b).

In the downwelling region of the North Atlantic subtropical gyre, modeled values of diazotrophic biomass and fixation rates approach zero due to the strong P-limitation

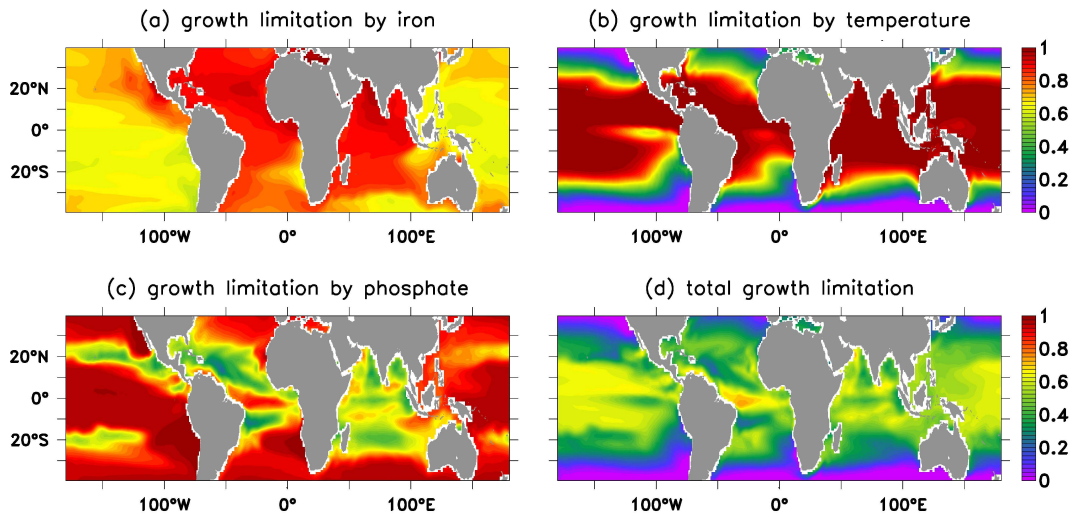


Figure 2.4: Growth limitation factors (100 year mean) of N_2 fixers in PROG: **(a)** iron (I_{Fe}), **(b)** phosphate (I_P), **(c)** temperature (I_T). **(d)** displays the total growth limitation (see Equation 3). Note that the limitation by light is not explicitly shown here.

(Figure 2.4b). Observations, on the contrary, show overall high values of biomass (up to $\sim 300 \text{ mg C m}^{-2}$) and fixation rates ($\sim 100 \mu\text{mol N m}^{-2} \text{ d}^{-1}$) here. The underestimation of simulated N_2 fixation associated with a too strong P depletion was similarly found in the model study of *Moore et al.* (2004). It indicates that the parameterizations, which in both models include phosphate limitation, lack a process with respect to the phosphorus source for N_2 fixers growth. There is observational evidence that the utilization of dissolved organic phosphorus (DOP) could provide diazotrophs with sufficient phosphorus to grow in phosphate depleted regions (*Sohm and Capone, 2006; Dyhrman et al., 2006*). Model studies support this hypothesis and showed that including the access of diazotrophs to DOP expands their simulated ecological niche into the North Atlantic subtropical gyre (*Somes et al., 2010; Landolfi et al., 2015; Somes and Oschlies, 2015*). Another proposed mechanism, based on observations, is that N_2 fixers vertically migrate to levels of higher phosphate concentrations in order to meet their phosphorus requirement (*Karl et al., 1992*). Furthermore, diazotrophs are known to have a higher N:P ratio than bulk phytoplankton (*Letelier and Karl, 1998; Krauk et al., 2006; White et al., 2006*). The assumption of a uniform Redfield ratio for all organic material in our model (see Section 2.2.2) overestimates the phosphorus requirement for diazotrophic growth. This could contribute to the phosphate depletion, and the too strong growth limitation we find in our study.

Among the highest concentrations and fixation rates in the Atlantic basin are found off the westcoast of Africa within the latitudinal range of 20°S to about 20°N . Besides the overall good growth conditions in the equatorial region (high temperatures, high iron and phosphate availability, see Figure 2.4), the overestimation of

the extent of the OMZ and hence denitrification in the eastern equatorial Atlantic leads to upwelling of strongly nitrogen-depleted water masses. This enables diazotrophs to outcompete bulk phytoplankton, which results in high diazotroph concentrations and N₂ fixation rates. North of the equator, the simulated biomass is overestimated compared to observations. Modeled and observed fixation rates accord better. South of the equator, in the Gulf of Guinea, evaluation is restricted due to sparse measurements. The few direct observations give evidence for the abundance of N₂ fixing species in this region (Dandonneau, 1971). Model studies support the picture of the eastern tropical Atlantic being an important habitat for diazotrophs. In the simulation of *Hood et al.* (2004), the Gulf of Guinea is a hotspot of *Trichodesmium* abundance, mainly controlled by light and MLD. The model of *Moore et al.* (2004), which explicitly accounts for phosphate and iron limitation, also shows high values of N₂ fixation here. In the model study of *Monteiro et al.* (2010), which simulates various diazotrophic groups, all three main types are highly abundant in the equatorial Atlantic, especially in the Gulf of Guinea.

Further to the south, our results show a sharp east-west gradient in concentrations and fixation rates. High abundances in the west are due to the drift of N₂ fixers with the surface current southward along the South American Coast. Whereas the simulated N₂ fixation rates ($\sim 10 \mu\text{mol N m}^{-2} \text{d}^{-1}$) agree with observations, the biomass concentrations ($\sim 10 \text{ mg C m}^{-3}$) seem to be overestimated by the model. However, since the biomass measurements are mostly restricted to *Trichodesmium*, the actual values for bulk diazotrophs are probably larger. In the east, low temperatures and iron concentrations in the Benguela Upwelling region prevent growth in our model. Measurements of surface concentrations support the absence of diazotrophs in the coastal upwelling area. Data on N₂ fixation, albeit sparse, indicate non-negligible fixation rates in the eastern part of the South Atlantic ($\sim 10 \mu\text{mol N m}^{-2} \text{d}^{-1}$), about 1000 km away from the coast (Figures 2.2b and 2.2d). The simulation of *Monteiro et al.* (2010), which includes various diazotrophic groups, better represents the presence of N₂ fixers in the waters off Southern Africa. However, looking at their pattern of N₂ fixers abundance, this is probably not due to the higher level of diazotrophic diversity in their model, but due to a stronger transport of diazotrophs and warm water from the Indian into the Atlantic Ocean.

Pacific Ocean

Diazotrophic growth in the Pacific Ocean is mainly limited by iron (Figure 2.4a) and regionally by phosphate (Figure 2.4b) in our model. An exception with regard to iron limitation is the eastern tropical Pacific north of the equator, where a high atmospheric dust deposition at about 20°N (*Mahowald et al.*, 2006) results in high oceanic surface iron concentrations. The implied low iron limitation (Figure 2.4a)

leads to intense growth ($> 100 \text{ mg C m}^{-2}$) and N_2 fixation ($> 1000 \text{ } \mu\text{mol N m}^{-2} \text{ d}^{-1}$) off the coast of North and Central America. In comparison to other dust deposition climatologies (e.g., *Mahowald et al.*, 2003; *Luo et al.*, 2003), the applied climatology of *Mahowald et al.* (2006) shows rather high values in the eastern tropical Pacific, which might cause an overestimation of N_2 fixers' activity in this region. Additionally, the overestimated extent of the OMZ and related denitrification might further support the high diazotroph abundance due to the upwelling of P^* enriched water masses. Satellite data support the picture of high concentrations of *Trichodesmium* in the eastern equatorial Pacific (*Westberry and Siegel*, 2006). Also in situ observations confirm the presence of N_2 fixers, but the observed concentrations and N_2 fixation rates are considerably lower (Figures 2.1 and 2.2). However, the only sparse observational data, which in many cases do not represent the full diazotrophic community, can be considered as the lower limit of diazotrophic biomass and N_2 fixation rates (*Luo et al.*, 2012). Model studies show equivocal results with respect to this region. In the geochemical, diagnostic model of *Deutsch et al.* (2007), the eastern Pacific is a dominant location of N_2 fixation due to the upwelling of nitrogen-deficient waters from the denitrification zone. Also a number of models which include explicit N_2 fixers show a high abundance of diazotrophs in the eastern equatorial Pacific (*Moore and Doney*, 2007; *Dunne et al.*, 2013; *Somes et al.*, 2010; *Landolfi et al.*, 2015). Other studies rather indicate low values or even the absence of diazotrophs in this region (*Moore et al.*, 2004; *Monteiro et al.*, 2010). Discrepancies between the models are probably due to differences in the applied dust deposition climatologies, which vary greatly with respect to the amount of dust deposition over the eastern Pacific Ocean.

In our model, the N_2 fixers' habitat extends like two zonal bands through the North and South Pacific Ocean at a latitudinal range of about $15\text{--}25^\circ\text{N}$ and $15\text{--}25^\circ\text{S}$. The ability to fix N_2 allows diazotrophs to outcompete bulk phytoplankton within the nitrate-depleted subtropical gyres. Also observations show significant N_2 fixation rates at $20^\circ\text{N}\text{--}30^\circ\text{N}$ in the central North Pacific (*Luo et al.* (2012); Figures 2.2b and 2.2d).

In the South Pacific, N_2 fixation in our model is shifted away from the coast. Cold temperatures and low iron concentrations of the water in the upwelling region limit diazotrophic growth, whereby temperature is the dominant factor (Figures 2.4a and 2.4c). The fact that considerable N_2 fixation rates were measured here (Figure 2.2b), might indicate that our parameterization misses diazotrophs which are adapted to colder temperatures. In general, more research is needed on the physiology and the importance of the more uncharacterized N_2 fixing groups (e.g. unicellular cyanobacteria) that grow in cooler water (e.g., *Moisander et al.*, 2010).

In the western Pacific, our model shows a large area of overall high concentrations on an order of $100\text{--}1000 \text{ mg C m}^{-2}$ and fixation rates of $100\text{--}1000 \text{ } \mu\text{mol N m}^{-2} \text{ d}^{-1}$. Low nitrate, and sufficient iron and phosphate concentrations promote growth

of diazotrophs here. Whereas the high fixation rates fit well to observations, the biomass concentrations, for which only very limited observations are available, seem to be overestimated. However, in the southwestern tropical Pacific off the coast of Australia (at about 20°S), in situ data based on *nifH*-gene measurements support this high biomass (Luo *et al.*, 2012). Also satellite measurements have detected *Trichodesmium* blooms in this region (Dupouy *et al.*, 2000). Moreover, modeling studies agree on the overall high abundance of N₂ fixers in the western part of the Pacific Ocean (e.g., Moore *et al.*, 2004; Monteiro *et al.*, 2010; Landolfi *et al.*, 2015).

The central equatorial Pacific is not inhabited by diazotrophs in our simulation. The upwelling of cold and iron-depleted deep waters limits diazotrophic growth (Figures 2.4a and 2.4c) and the concurrent availability of nitrate enables non-fixing phytoplankton to outcompete N₂ fixers. Although the absence of diazotrophs along the equator agrees with measurements of negligible biomass (based on *Trichodesmium* and DDA) (Luo *et al.* (2012), Figure 2.2b) as well as with the resource-ratio theory of Ward *et al.* (2013), observations of N₂ fixation rather indicate considerable fixation rates of up to a few hundred $\mu\text{mol N m}^{-2} \text{d}^{-1}$ at this location (Figure 2.2d). Again, this discrepancy between the model and observations indicates that the model does not capture the full diazotrophic community. However, also a higher level of diazotrophic diversity as applied in the model study of Monteiro *et al.* (2010) does not reproduce the presence of N₂ fixers in the central equatorial Pacific.

Indian Ocean

In the Indian Ocean, the model produces high surface values of biomass (up to $\sim 100 \text{ mg C m}^{-3}$) and N₂ fixation (up to $\sim 10 \mu\text{mol N m}^{-3} \text{d}^{-1}$) throughout the whole ocean basin (Figures 2.1a and 2.2a). High dust deposition and hence iron availability (Figure 2.4a) in combination with upwelling of nitrogen-depleted water from the underlying OMZ result in overall good growth conditions. Phosphate is the main limiting factor in the Indian Ocean (Figure 2.4b). In situ observations are only available at a few locations. However, the measurements show globally among the highest values of diazotrophic biomass of $> 100 \text{ mg C m}^{-3}$ (Figure 2.1b). It is known that the northeastern monsoon promotes blooms of *Trichodesmium* (Bergman, 2001; Lugomela *et al.*, 2002). Satellite data (Gower and Carpenter, 1992; Sarangi *et al.*, 2005; Westberry and Siegel, 2006) and other global models (e.g., Moore *et al.*, 2004; Monteiro *et al.*, 2010) further support the potential of the Indian Ocean in playing a significant role in global N₂ fixation.

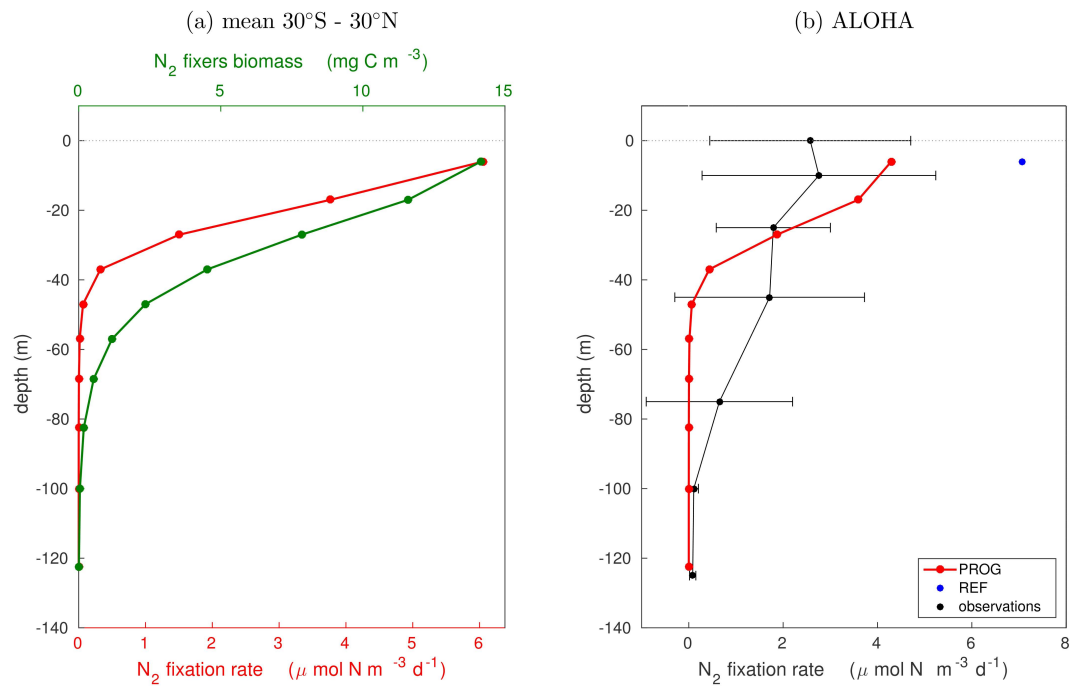


Figure 2.5: **(a)** Vertical profiles of 100 year mean modeled N₂ fixers biomass (mg C m⁻³) (green, upper x-axis), and N₂ fixation rates (μmol N m⁻³ d⁻¹) (red, lower x-axis), averaged over an area of 30°S to 30°N in PROG. **(b)** Vertical profiles of N₂ fixation rate at the station ALOHA, for PROG (red, 100 year mean), for REF (blue, 100 year mean), and for observations (black, mean and standard deviation of data from 2005 to 2010 taken from the database of Luo et al. (2012)).

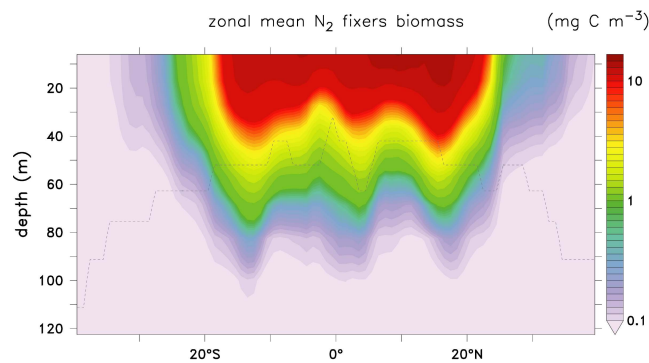


Figure 2.6: Vertical section of 100 year mean zonally averaged N₂ fixers biomass (mg C m^{-3}) in PROG. The gray dashed line displays the zonally averaged mixed layer depth.

Vertical distribution

Highest modeled N₂ fixers concentrations and fixation rates are located at the surface, where high light intensities promote diazotrophic growth (Figures 2.5a and 2.6). Following the exponential decrease of light, the vertical profiles of modeled concentration and fixation decline rapidly with depth. Biomass declines less rapidly than the fixation rates (Figures 2.5a), since biomass that is mixed downwards to greater depths is not necessarily able to grow and fix N₂ due to too low light availability. The largest fraction of biomass and fixation is located in the upper 40 m, where 99 % of the total fixation takes place (85 % in the upper 20 m, respectively).

Regionally, the total vertical extent of diazotrophs in the water column varies considerably (Figure 2.6). Zonally averaged concentrations of $> 0.1 \text{ mg C m}^{-3}$ reach depths levels between 70 to 110 m in the meridional band of 25°S to 25°N. In general, highest modeled concentrations develop within the mixed layer (Figure 2.6). Comparing both hemispheres, in the upper 40 m, higher zonally averaged concentrations occur on the northern hemisphere compared to the southern hemisphere (Figure 2.7). This is probably due to the overall high values present in the eastern tropical North Pacific (Figures 2.1a and 2.1c). Observational evidence regarding the distribution of biomass and fixation rates with depth is equivocal. Several studies, using net tows, found concentrations restricted to the nearest surface (e.g., *Carpenter and Price, 1977; McCarthy and Carpenter, 1979; Orcutt et al., 2001*). However, measurements with a novel optical method revealed a more uniform distribution of *Trichodesmium* colonies over the water column than previously thought (*Davis and McGillicuddy, 2006*), supporting the vertical distribution as simulated by our model. The database of *Luo et al. (2012)* confirms the abundance of diazotrophs and N₂ fixation over greater depths (down to $\sim 250 \text{ m}$).

Long-term measurements of the vertical profile of N₂ fixation rates are only available at the ALOHA station, providing values approximately once per month over

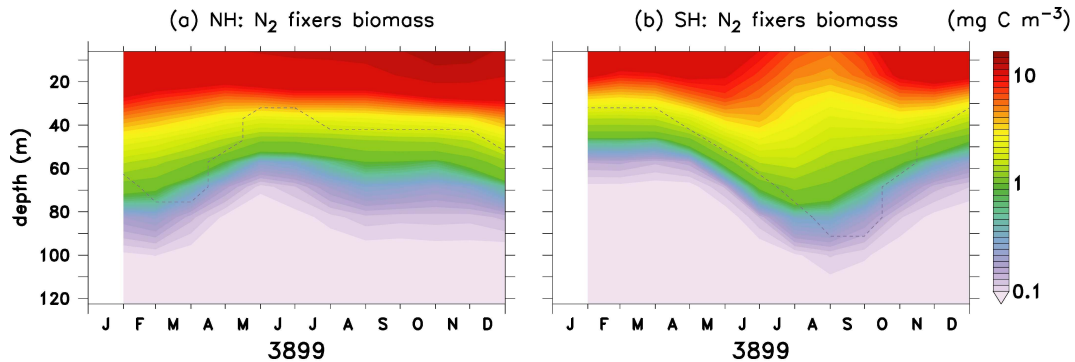


Figure 2.7: Seasonal evolution (100 year mean) of the vertical distribution of N_2 fixers biomass (mg C m⁻³) in PROG on the northern hemisphere (NH) (a) and southern hemisphere (SH) (b). The concentrations are averaged over an area of 40°N to the equator and 40°S to the equator, respectively. The gray dashed line displays the mixed layer depth averaged over the same area.

the period of 2005–2010 (Luo *et al.*, 2012). In general, comparisons between observations at single geographical positions and simulations with a coarse resolution model are difficult. We choose a location in the model with a similar seasonal cycle of sea surface temperature to the one observed at ALOHA, located $\sim 4^\circ$ latitude further south of the actual geographical position. The simulated mean vertical profile of N_2 fixation at this location lies within the range of observed values (Figure 2.5b). However, the decrease of N_2 fixation with depth is steeper in the model than in observations. The measurements show a quite homogenous profile with considerable fixation rates of about $1 \mu\text{mol N m}^{-3} \text{d}^{-1}$ reaching down to a depth of about 75 m. Whereas the modeled rates in the upper levels (0–20 m) fall into the upper range of observations, below a depth of 30 m the model values are rather too small compared to the observed ones. However, it has to be kept in mind, that the ocean model is driven by a climatological forcing, which produces an overall smaller interannual variability in the modeled N_2 fixation rates than present in reality. The high variability of N_2 fixation existent at this location is indicated by the large standard deviations observed for the single depth levels (Figure 2.5b). The new parameterization improves the vertical distribution of N_2 fixation rates compared to the diagnostic formulation, in which the total input of ‘new’ nitrogen was added by definition to the surface layer (for ALOHA: Figure 2.5b, blue dot).

2.3.3 Seasonal variability of diazotrophic biomass and N_2 fixation rates

The modeled biomass and fixation rates show a pronounced seasonal cycle, mainly driven by physical conditions like temperature and light. Thereby, the northern and southern boundary of its occurrences move slightly polewards in summer, and

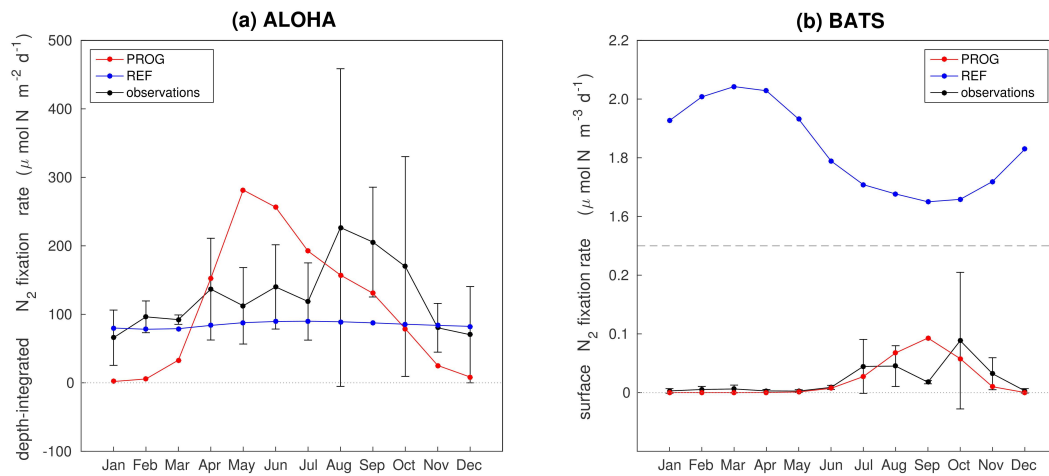


Figure 2.8: **(a)** Seasonal cycle of depth-integrated N₂ fixation ($\mu\text{mol N m}^{-2} \text{d}^{-1}$) at ALOHA: PROG (red, 100 year mean), REF (blue, 100 year mean), and observations (black, mean and standard deviation of data from 2005 to 2010 taken from the database of Luo et al. (2012)). **(b)** Surface N₂ fixation rates at BATS: PROG (red, 100 year mean), REF (blue, 100 year mean), observations (black, mean and standard deviation of approx. monthly data from 1995 to 1997 taken from the database of Luo et al. (2012)). Note the different scaling on the y-axis.

equatorwards in winter of the respective hemispheres (by approximately 10° latitude). In the northern hemisphere, highest surface concentrations, as well as shallow reaching biomass occur in August to November (Figure 2.7a); in the southern hemisphere in December to May (Figure 2.7b). During winter and spring of the respective hemisphere, enhanced mixing of N₂ fixers downwards, as well as stronger light limitation, lead to lower surface concentrations. The expansions to greater depths due to downward mixing are probably supported by better growth conditions due to a weaker self shading effect (i.e., light absorption by biomass lying above) in the upper layers.

Observed timeseries of biomass and N₂ fixation rates (measured approximately once per month) are available at two locations, the long-term monitoring stations ALOHA (Church et al., 2009; Luo et al., 2012), and BATS (Orcutt et al., 2001; Luo et al., 2012). Figure 2.8a shows the observed and modeled N₂ fixation rates at station ALOHA. For the model-observation comparison of the seasonal cycle, we take a model position corresponding to the physical conditions at the location of ALOHA, as already done for the comparison of the vertical profile (Section 2.3.2). The magnitudes of the modeled prognostic depth-integrated N₂ fixation rates (PROG), and also its seasonal pattern with lowest values at the end/beginning of the year and highest values in the middle of the year, generally agree with the observed ones. However, the peak in the modeled fixation rates occurs too early, in May instead of August. Furthermore, the values at the end and beginning of the year (November–March) appear to be underestimated by the model. The N₂ fixation in experiment

REF produces higher values during this period which better agree with the observed ones. However, the diagnostic formulation is not able to produce a reasonable seasonal cycle. The monthly mean values do not spread much around the annual mean of $84.7 \mu\text{mol N m}^{-2} \text{d}^{-1}$, which is generally too low in comparison to the observed annual mean of $126.7 \mu\text{mol N m}^{-2} \text{d}^{-1}$. The mean fixation rate of PROG with $110.3 \mu\text{mol N m}^{-2} \text{d}^{-1}$ matches the observational record better.

At BATS, long-term measurements of N_2 fixation are only available for the surface seawater. The seasonal cycle of the model results of PROG at the corresponding geographical coordinates are conform with the observed ones, showing highest surface fixation rates from July to October, and lowest, which approach even zero, during the rest of the year (Figure 2.8b). A discrepancy is seen in September, where observations show a rather low value of $0.02 \mu\text{mol N m}^{-3} \text{d}^{-1}$, with low standard deviation, whereas the model has its maximum of about $0.1 \mu\text{mol N m}^{-3} \text{d}^{-1}$ in this month. In general, the fixation rates are rather low at this position, both in observations and in the model. On the contrary, experiment REF strongly overestimates the observed values of surface N_2 fixation at BATS by more than a factor of 20 throughout the whole year (Figure 2.8b). In the diagnostic formulation, by definition the fixed nitrogen is added to the first model layer. Even if distributing the integrated fixation rate ($\sim 21.5 \mu\text{mol N m}^{-2} \text{d}^{-1}$) over the upper 30 m, the resulting value for the volumetric rate is still too large ($\sim 0.72 \mu\text{mol N m}^{-3} \text{d}^{-1}$). Furthermore, the seasonal cycle is opposite to the observed one. Hence, the diagnostic formulation is neither able to produce fixation rates in the right order of magnitude at this location (see Section 2.3.2), nor a reasonable seasonal cycle.

In the Indian Ocean, PROG shows a pronounced seasonal cycle of N_2 fixers biomass and N_2 fixation rates, with highest values from September to February (not shown). This strong seasonal pattern is also reported from observations, and roughly corresponds to the timing of the monsoon, with highest biomass promoted by the northeast monsoon (November–April) when water conditions are generally calm and warm, and lowest values during the southwest monsoon (June–October) (Carpenter and Capone, 1992; Bergman, 2001; Lugomela et al., 2002).

The comparison of the results of the two treatments of N_2 fixation (PROG and REF) shows that prognostic growth dynamics are needed to produce reasonable seasonal dynamics of N_2 fixation. In contrast to REF, the variable growth rate in PROG is able to respond to the seasonally changing physical conditions like temperature and light, and acts on the variable standing stock of N_2 fixers instead of prescribing a constant rate.

Besides the pronounced seasonal cycle, variability on shorter timescales is present in the modeled diazotrophic biomass. The temporal evolution of N_2 fixers concentration shows episodic events of high concentrations which last for a few weeks or even months (not shown). Yet, as the simplification of a linear decay rate in the pa-

parameterization neglects mortality of N₂ fixers due to abrupt cell death or viruses which potentially are important (e.g., Hewson *et al.*, 2004), the model does not capture the very short-lived behaviour of blooms reported from observations (e.g., Bar-Zeev *et al.*, 2013). As a result, the abundances of N₂ fixers in the model may be less patchy and more stable than observed for *Trichodesmium*. Longer durations of blooms up to several months that have been observed (e.g., Devassy and Goes, 1988) are better represented in the model.

2.4 Effects of N₂ fixers on the mean biogeochemical model state

In general, the mean states of both experiments PROG and REF are similar, and comparable to the coupled model run described in detail in Ilyina *et al.* (2013). However, as the novel prognostic N₂ fixers in PROG affect the other biogeochemical model pools, differences in the fluxes and inventories compared to the simulation with diagnostic N₂ fixation (REF) occur. Concurrently, changes in the biogeochemical state variables between the two model runs emerge. In the following, we discuss differences between the two simulations PROG and REF with regard to fluxes and inventories within the euphotic zone, as well as with regard to state variables. We use observations from the World Ocean Atlas (WOA) 2013 (<https://www.nodc.noaa.gov/OC5/woa13/>) for evaluation of the state variables. Thereby, we focus on the distribution of nitrate, phosphate, and oxygen, since these are the key variables relevant for biological processes. Iron is not considered, as its spatial pattern is largely determined by the applied dust deposition field. The derived quantity P* ($\text{PO}_4 - \text{NO}_3/16$), a measure of the excess of P relative to the Redfield N quota (e.g., Deutsch *et al.*, 2007; Somes *et al.*, 2010), is additionally applied to assess the model skill with respect to phosphate and nitrate.

2.4.1 Effects on organic matter fluxes and inventories within the euphotic zone

The main fluxes and inventories of the model pools within the euphotic zone of the two experiments are summarized in Table 2.2. The global annual N₂ fixation rate in the simulation with the prognostic diazotrophs (PROG) of 135.6 Tg N yr⁻¹ is similar to the simulation with diagnostic N₂ fixation (REF) with 132.6 Tg N yr⁻¹. In REF, the input of 'new' nitrogen enters by definition directly into the nitrate pool of the surface layer. In PROG N₂ is utilized for the production of diazotrophic biomass, and reaches the nitrate pool indirectly via remineralization. Hence, in contrast to REF, the input of 'new' nitrogen does not exclusively occur in the uppermost model

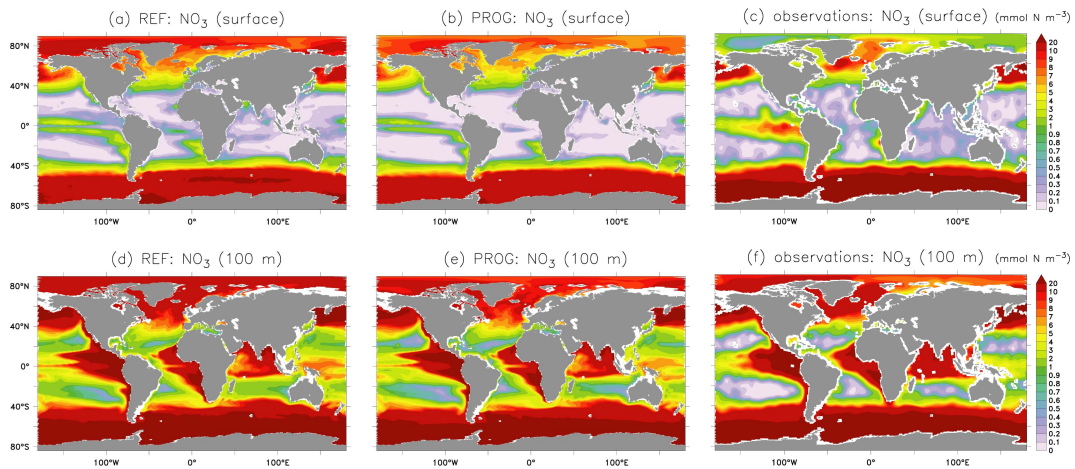


Figure 2.9: 100 year mean fields of nitrate (mmol N m^{-3}) at the surface (top), and at a depth of 100 m (bottom), in REF (left), PROG (middle), and observations (right).

layer. In both simulations global N_2 fixation approximately balances denitrification ($141.9 \text{ Tg N yr}^{-1}$ in PROG and $135.0 \text{ Tg N yr}^{-1}$ in REF).

The bulk phytoplankton standing stock is similar between the two runs (0.62 Gt C in REF and 0.61 Gt C in PROG). Since diazotrophs, unlike bulk phytoplankton, can grow in the nitrate depleted oligotrophic tropical and subtropical oceans, the total standing stock of autotrophs increases to 0.71 Gt C in PROG when adding the diazotrophic biomass of 0.10 Gt C . Globally, N_2 fixers represent about 14 % of the mean phytoplankton biomass. In the tropical regions they often locally constitute up to 90 %. This large proportion of diazotrophic biomass in distinct regions of the ocean is in accordance with observations (Capone *et al.*, 2005; Mahaffey *et al.*, 2005).

Although the global biomass of bulk phytoplankton is very similar between the two model runs, the global value of net primary production (NPP) by bulk phytoplankton is considerably lower in PROG ($45.53 \text{ Gt C yr}^{-1}$) compared to REF ($61.01 \text{ Gt C yr}^{-1}$). This decrease in NPP results from the competition with diazotrophs, which regionally prevail over bulk phytoplankton in the tropics and subtropics. Furthermore, lower nitrate concentrations in high latitudes, as will be discussed in Section 2.4.1, result in stronger growth limitation of bulk phytoplankton and hence additionally reduce NPP. Adding the fraction of NPP produced by N_2 fixers ($3.23 \text{ Gt C yr}^{-1}$), yields an overall value of $48.76 \text{ Gt C yr}^{-1}$ for the experiment PROG. The global value of NPP is generally not well constrained, and both model states lie within the spread of published estimates ranging from about 40 to 70 Gt C yr^{-1} (e.g., Carr *et al.*, 2006; Westberry *et al.*, 2008).

Along with a smaller NPP in PROG, the fluxes from the phytoplankton pool into the zooplankton pool (grazing) as well as into the DOM pool decrease, together with a decrease in the respective inventories ('DOM': 5.88 Gt C in REF and 4.64 Gt C

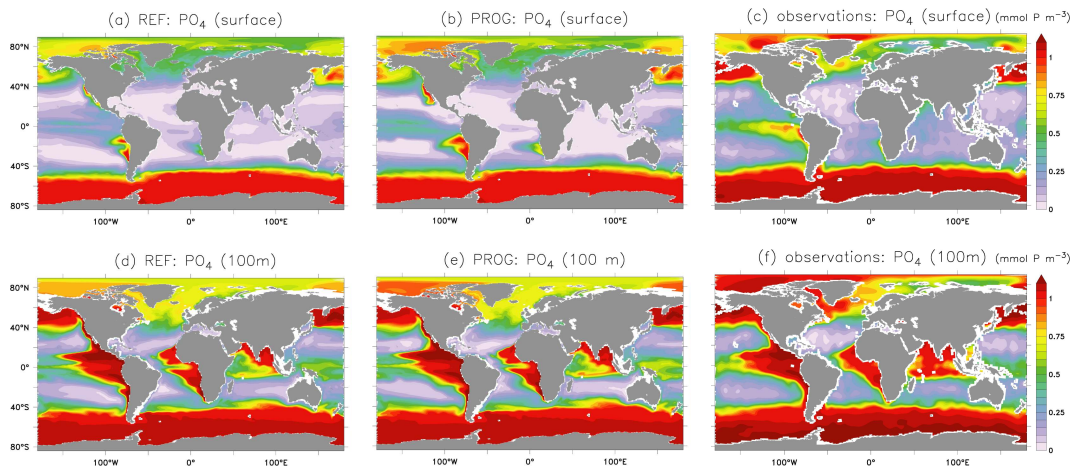


Figure 2.10: 100 year mean fields of phosphate (mmol P m^{-3}) at the surface (top), and at a depth of 100 m (bottom), in REF (left), PROG (middle), and observations (right).

in PROG; 'ZOO': 0.51 Gt C in REF and 0.39 Gt C in PROG). Accordingly, also the fluxes from bulk phytoplankton and zooplankton into the detritus pool are reduced, whereas the inventory of the detritus pool stays similar (1.62 Gt C in REF and 1.57 Gt C in PROG) due to the contribution from N₂ fixers. Export production in 90 m depth is almost the same in the two experiments (7.24 Gt C yr⁻¹ in REF and 7.46 Gt C yr⁻¹ in PROG). The difference is negligible against the background of the large range of reported estimates (3–20 Gt C yr, *Najjar et al. (2007)*). The DOC pool fed by diazotrophs (DOM_{Diaz} , 0.82 Gt C) is about 15 % of the total DOC pool (5.44 Gt C). As not much is known about the partitioning of DOM into various refractory pools, it is difficult to evaluate this number.

Effects on the global distribution of nitrate, phosphate, and oxygen

Accounting for diazotroph's dynamics does not fundamentally change the large scale patterns of surface nitrate and phosphate in the model (Figures 2.9 and 2.10). But regionally, differences occur. Although the global mean N₂ fixation rate is very similar in the two experiments (Table 2.2), the spatial distribution of nitrate influx is very different. In REF the nitrate influx takes place almost all over the global ocean (Figure 2.3) and by definition adds directly nitrate into the surface layer. In PROG, nitrate addition occurs where after N₂ fixation the biomass of diazotrophs is remineralized, thus primarily in the tropical and subtropical ocean (Figures 2.2a and 2.2c). As N₂ fixation is absent in high latitudes in PROG, surface nitrate concentrations are lower, regionally up to 2.5 mmol N m⁻³. In contrast, surface phosphate concentrations are higher here (up to 0.1 mmol P m⁻³) (Figure 2.10), since lower nitrate concentrations lead to a decrease of bulk phytoplankton growth in high latitudes. The lower nitrate and higher phosphate concentrations in high latitudes are

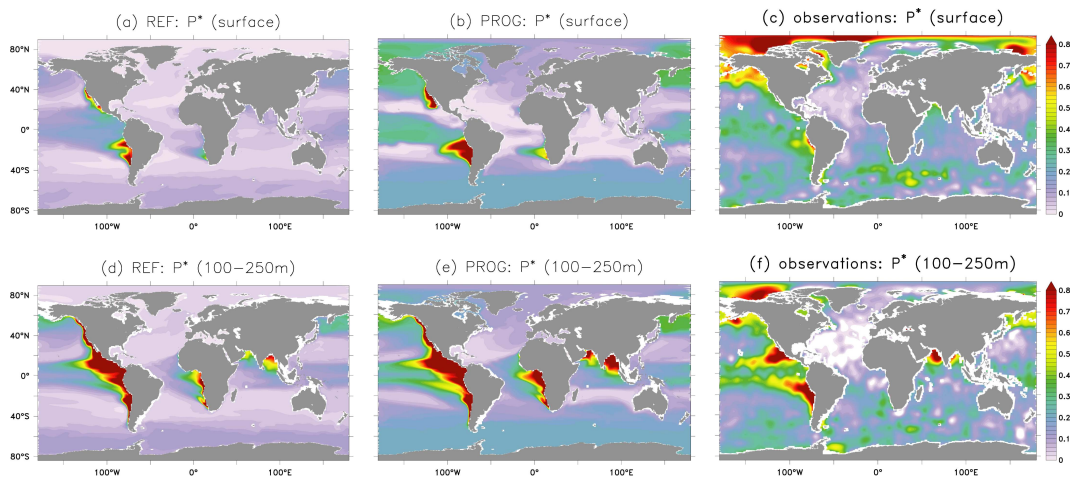


Figure 2.11: 100 year mean fields of P^* ($PO_4 - NO_3/16$) at the surface (top), and at a depth of 100-250 m (bottom), in REF (left), PROG (middle), and observations (right).

more realistic, as indicated by comparing simulated spatial patterns of P^* to observations (Figure 2.11). In the process of N_2 fixation, only phosphate and no nitrate is consumed (reducing P^*). During growth of non-fixing phytoplankton, in contrast, nitrate and phosphate are consumed proportionally (conserving P^*). The absence of N_2 fixation in high latitudes as well as in the central equatorial Pacific in PROG leads to an increase of P^* in the respective regions, which is in better agreement with observations than the rather low values present in REF.

In the tropics and subtropics, the upwelling of P^* rich water from denitrification sites (Figure 2.11) promotes N_2 fixation. As discussed above, N_2 fixation then reduces phosphate and P^* at the surface. The too strong depletion of surface phosphate and P^* in regions of highest N_2 fixation indicates either an overestimation of N_2 fixation in the respective regions, or a shortcoming in the growth parameterization. An overestimation of N_2 fixation might be caused by too strong denitrification, or, in case of the eastern tropical Pacific, by too high dust deposition. With respect to the model shortcoming, one potential cause for the phosphate and P^* depletion could be the low N:P ratio that is prescribed for diazotrophs in the model (see Section 2.2.2). Furthermore, a missing process in the growth parameterization with respect to the phosphorus source (like dissolved organic phosphorus utilization or the vertical movement to depths of higher phosphate concentrations, as discussed in Section 2.3.2) might be responsible for the strong depletion of phosphate and P^* at the surface. Surface nitrate is also more depleted in PROG in the regions of diazotrophic growth compared to REF (regionally up to $0.8 \text{ mmol N m}^{-3}$). This is because the prognostic N_2 fixers first consume the available nitrate before utilizing N_2 for growth. As the physical growth conditions are mostly favorable in the tropical and subtropical regions, diazotrophs grow unhindered until nutrients are

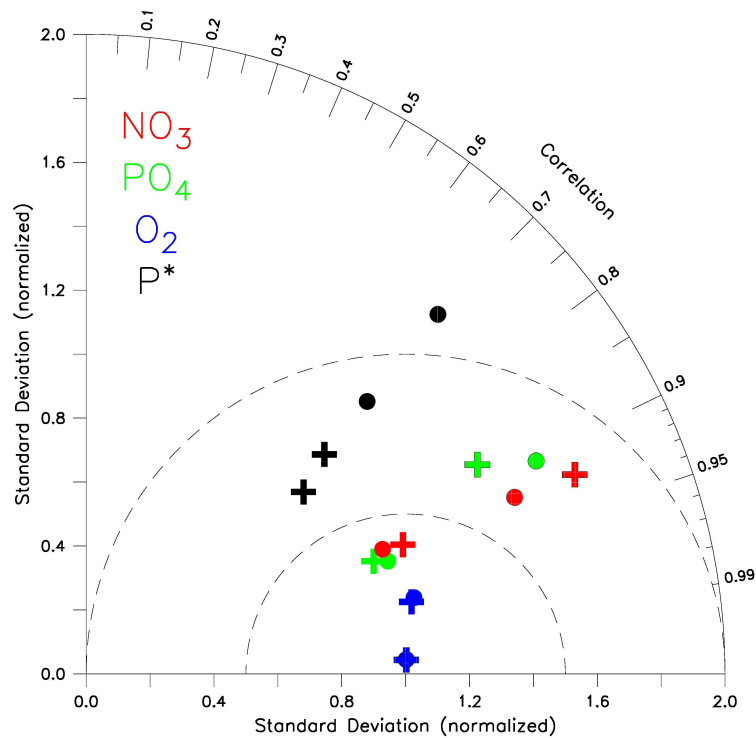


Figure 2.12: Taylor diagram of nitrate (red), phosphate (green), oxygen (blue), and P* (black); at the surface (checked) and at 100 m depth (filled); for the experiments PROG (crosses) and REF (circles). Global 100 year means of spatial correlations and standard deviations are shown. The observations (WOA 2013) are represented by a standard deviation and correlation of 1.

exhausted. Thus, although N₂ fixers add ‘new’ nitrate to the system, the associated production of biomass, and the subsequent sinking of a large fraction of the decaying material (detritus), leads to a depletion of the nitrate in the surface layer, rather than to an accumulation.

Highest differences in nitrate and phosphate between the model runs occur at the surface. Already at a depth of 100 m the concentrations do not differ notably between the two model states (Figures 2.9 and 2.10). In case of nitrate, both experiments show generally slightly higher concentrations in the centers of the subtropical gyres compared to observations. In experiment PROG this discrepancy is partly reduced. Below 100 m, in case of phosphate no deviations between the two models are visible (not shown). Differences in oxygen between the two experiments, both at the surface and at 100 m depth, are marginal and the respective maps are not shown here. Also at greater depth, PROG neither improves the OMZs which are generally too enhanced, nor the nitrate concentrations which are generally too low in HAMOCC (Ilyina *et al.*, 2013).

The overall consistency between the two mean model states is affirmed by a Taylor

diagram (Figure 2.12), which visualizes the model skill compared to observations (Taylor, 2001). In the graphs, the observational dataset (WOA 2013) is represented by a correlation and standard deviation of 1. Deviations from 1 display the discrepancy of the modeled to observed variables. For surface nitrate, the model performance shows a slightly higher mismatch to observations in PROG than in REF. For surface phosphate it is the other way around, PROG slightly reduces the model deficiency. At 100 m, nitrate and phosphate are equally well represented in both experiments. The relation between phosphate and nitrate, measured by P^* , is considerably improved in PROG compared to REF. Both at the surface and at a depth of 100 m, the values are closer to 1 in PROG compared to REF. For oxygen, values of standard deviation and correlation are almost identical for both experiments at both depth levels.

2.5 Sensitivity of prognostic N_2 fixers to selected parameters

A number of biological model parameters, such as the growth and decay rate, as well as the half saturation constants for the uptake of nutrients, have been tuned in order to produce reasonable results with respect to N_2 fixers biomass and fixation rates. As the biological parameters are not well constrained by measurements and can vary between different diazotrophic groups, additional sensitivity experiments have been conducted in order to assess the impact of the uncertainties in these parameters on the model results. The parameters of maximum growth rate and decay rate only modify the magnitudes, rather than the spatial distribution of N_2 fixers and fixation rates. In contrast, the half saturation constants of iron K_{Fe} and phosphate K_P , which enter the limiting functions of growth (Equation 2.8 and 2.9), affect also the spatial patterns. Further, the buoyancy velocity w_{Diaz} affects the vertical distribution of N_2 fixers and fixation rates in the model. The motility is a characteristic feature of *Trichodesmium* and does not apply for the other diazotrophic groups. However, it is of interest to test the sensitivity of the model to the buoyancy velocity since *Trichodesmium* constitutes a considerable portion of the diazotrophic community (e.g., LaRoche and Breitbarth, 2005).

Simulations were started from the equilibrium model state described in Section 2.3.2, and run for another 50 years with the modified parameter values for K_P , K_{Fe} , and w_{Diaz} , respectively. Applied parameter values and the respective model response with regard to N_2 fixation are summarized in Table 2.3.

Table 2.3: Applied values in the sensitivity experiments for the half saturation constants of phosphate K_P (left) and iron uptake K_{Fe} (middle), and the buoyancy velocity w_{Diaz} (right); and resulting values of N₂ fixation. The values with a gray background correspond to the reference run PROG.

Phosphate		Iron		Buoyancy	
K_P	N ₂ fixation	K_{Fe}	N ₂ fixation	w_{Diaz}	N ₂ fixation
[kmol P m ⁻³]	[Tg N yr ⁻¹]	[nmol Fe m ⁻³]	[Tg N yr ⁻¹]	[m d ⁻¹]	[Tg N yr ⁻¹]
0.1 · 10 ⁻⁸	145.4	0.032	150.6	0	134.6
0.5 · 10 ⁻⁸	140.1	0.160	145.7	1	135.6
1.0 · 10 ⁻⁸	135.6	0.320	135.6	2	135.3
2.0 · 10 ⁻⁸	125.6	0.640	84.3	10	135.3
10.0 · 10 ⁻⁸	57.1	3.200	13.7	50	134.8

2.5.1 Sensitivity to the half saturation constant of phosphate and iron

For the half saturation constant of phosphate K_P , values of 0.1, 0.5, 2, and 10 times the reference value of $K_P=1\cdot 10^{-8}$ kmol P m⁻³ were applied (Table 2.3). They were chosen as to cover a large range of available global estimates of N₂ fixation. An approximate linear relationship between K_P and the resulting global N₂ fixation appears to hold. This can be explained by the hyperbolic form of the applied limiting function following Michaelis Menten kinetics (Equation 2.9). As the reference value of $K_P=1\cdot 10^{-8}$ kmol P m⁻³ is in the order of magnitude of the ambient phosphate concentrations, changes around this value result in approximately linear changes in the growth rate. Furthermore, as the horizontal gradients of phosphate are rather small in the area where N₂ fixers occur, this results in an overall linear change of the global N₂ fixation. Decreasing K_P (0.1·10⁻⁸ and 0.5·10⁻⁸ kmol P m⁻³) leads only to a small increase of overall N₂ fixers concentrations, without a notable change in the inhabited area (Figures 2.13a and 2.13b). The global N₂ fixation rate only slightly increases (140.1 and 145.4 Tg N yr⁻¹ compared to 135.6 Tg N yr⁻¹ in PROG). Increasing K_P (2·10⁻⁸ and 10·10⁻⁸ kmol P m⁻³), on the other hand, shows a more pronounced effect, both on the global N₂ fixation rate (125.6 and 57.1 Tg N yr⁻¹ compared to 135.6 Tg N yr⁻¹ in PROG), and on the extent of the diazotrophic habitat (Figures 2.13c and 2.13d). For a ten times higher K_P , N₂ fixers almost completely vanish in the West Pacific and subtropical South Pacific. Also the North Pacific, the Atlantic, and the Indian Ocean show considerably lower values of depth-integrated biomass.

Analogous to phosphate, values of 0.1, 0.5, 2, and 10 times the reference value of $K_{Fe}=0.32$ nmol Fe m⁻³ were tested (Table 2.3). The resulting N₂ fixation rates (except for the highest K_{Fe}) suggest an exponential relationship, indicating the model's sensitivity to this parameter, and to the iron distribution in general. Horizontal gradients are large in the surface iron concentrations, and hence small changes in K_{Fe}

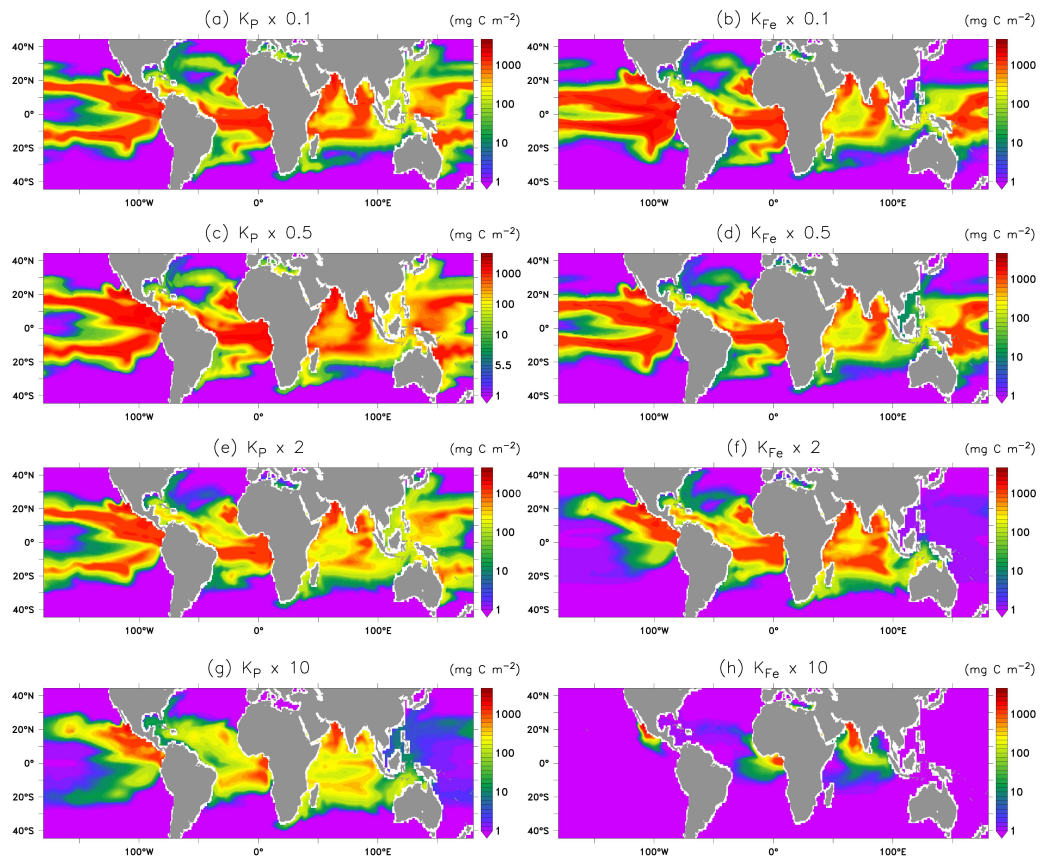


Figure 2.13: Depth-integrated N_2 fixers biomass (mg C m^{-2}) for the sensitivity experiments with varying half saturation constant for phosphate uptake (left, a-d), and iron uptake (right, e-h). Applied values from top to bottom: 0.1, 0.5, 2, and 10 times the original value of $K_P=1e^{-8} \text{ kmol P m}^{-3}$ and $K_{Fe}=0.32 \text{ nmol Fe m}^{-3}$ used in PROG.

lead to large changes in the spatial distribution of N₂ fixers (Figures 2.13e-h). Largest changes can be seen in the Pacific Ocean, where, except in the east, rather low surface iron concentrations prevail. Decreasing the original K_{Fe} by 0.5 leads to a small increase of the global fixation (145.7 Tg N yr⁻¹ compared to 135.6 Tg N yr⁻¹). The increase in global fixation is larger for a tenfold smaller value of K_{Fe} (150.7 Tg N yr⁻¹), mainly visible in the occupation of N₂ fixers of the equatorial Pacific area, where they were not present before (Figures 2.13e and 2.13f). With increasing K_{Fe} , the areal extent of N₂ fixers effectively decreases, mainly in the Pacific, where a doubling of K_{Fe} leads to almost vanishing existence of N₂ fixers in the west and south of the basin (Figure 2.13g). Further increasing K_{Fe} to a 10 times higher value shrinks the area covered by N₂ fixers to the hotspots of the atmospheric iron input, which are located in the North East Pacific, the Gulf of Guinea, and the Arabian Sea (Figure 2.13h). The global N₂ fixation in this case yields only 13.7 Tg N yr⁻¹.

The sensitivity experiments indicate that iron limitation is an important controlling factor in the modeled distribution of N₂ fixers, especially in the Pacific Ocean. An increasing iron limitation leads to a decoupling of N₂ fixation from denitrification sites and to a tighter coupling to the atmospheric iron source which is in agreement with the study of *Weber and Deutsch* (2014). As knowledge about the iron distribution is very limited, especially in the Pacific Ocean, the dependency of the model performance on iron limitation constitutes a source of uncertainty. Furthermore, we include constant half saturation rates for both phosphate and iron in our model. In reality, large (e.g. *Trichodesmium*) and small diazotrophs (e.g. unicellular cyanobacteria) have very different values. Including this diversity could affect the regional spatial patterns of the simulated habitat, as shown in the sensitivity experiments.

2.5.2 Sensitivity to the buoyancy velocity

The buoyancy velocity of *Trichodesmium* is poorly constrained by observations. The work by *Brodhagen* (2015) indicated that the simulated vertical distribution of cyanobacteria strongly depends on their prescribed rising velocity. Reported observed values range from even a negative buoyancy velocity (sinking), to a rising rate of about 260 m d⁻¹ (*Walsby*, 1978; *Villareal and Carpenter*, 2003; *Guidi et al.*, 2012). The extreme rising velocities of 200 m d⁻¹ and more are probably only rarely reached, and a mean value of 3 m d⁻¹ was reported to hold (*Guidi et al.* (2012), and references therein). We tested values between 0 m d⁻¹ (no buoyancy), and 50 m d⁻¹, which can be considered as a high value when taken as a global mean. It corresponds to a rising time of only two days to the surface if diazotrophs are mixed down to a depth of 100 m.

Our model results show, that the global N₂ fixation rate is not sensitive to w_{Diaz} (Table 2.3). First, this is because already for a velocity of 1 m d⁻¹ a major fraction of N₂

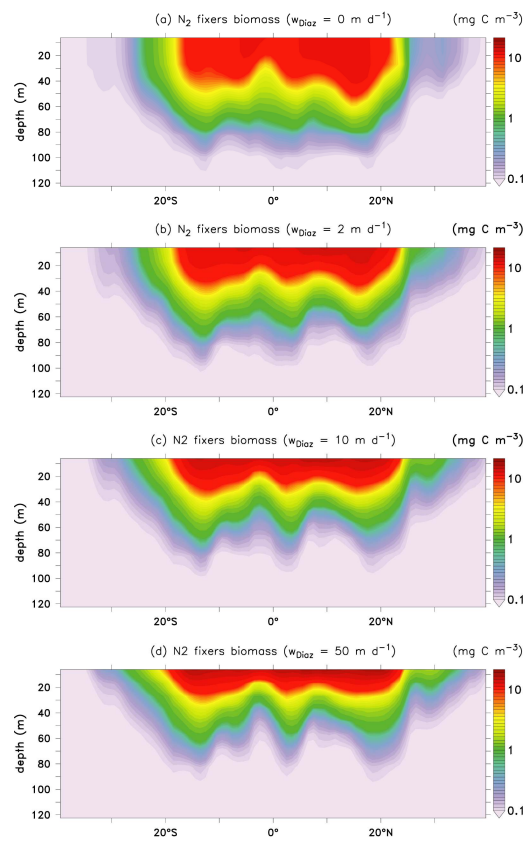


Figure 2.14: Vertical section of zonal mean N_2 fixers biomass (mg C m^{-3}) with varying buoyancy velocities w_{Diaz} . From top to bottom: 0 m d^{-1} , 2 m d^{-1} , 10 m d^{-1} , 50 m d^{-1} .

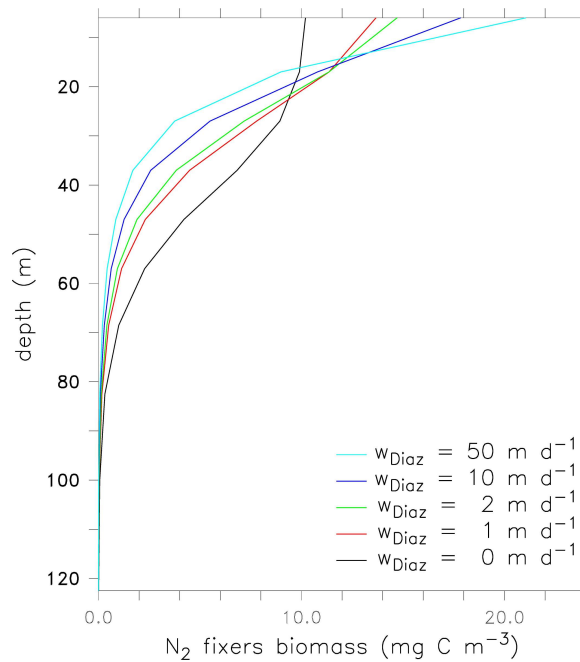


Figure 2.15: Vertical profiles of mean N₂ fixers biomass (mg C m^{-3}) for varying buoyancy velocities w_{Diaz} , averaged over an area of 30°S to 30°N. Black: 0 m d^{-1} , red: 1 m d^{-1} (used in the reference run PROG), green: 2 m d^{-1} , blue: 10 m d^{-1} , light blue: 50 m d^{-1} .

fixation takes place in the first model layer (12 m). Hence, higher velocities do only slightly modify the global value of N₂ fixation. Second, P-limitation gets stronger with increasing buoyancy velocity, restricting further growth and fixation. Also the global map of depth-integrated biomass shows only minor changes for different applied values of buoyancy velocity (not shown). However, varying w_{Diaz} affects the surface pattern (Figure 2.14), as well as the vertical profiles of biomass and fixation rates (Figure 2.15). Global maps of surface N₂ fixers concentrations generally display higher surface concentrations for higher buoyancy velocities. Related to that, the areal extent in the central Pacific with very low concentrations below 0.1 mg C m^{-3} decreases. Maps of zonally averaged biomass for the different applied buoyancy velocities indicate that the surface area covered by concentrations above 10 mg C m^{-3} extends towards higher latitudes with increasing w_{Diaz} (Figure 2.14). At the same time, the depth range of N₂ fixers abundance gets shallower and more concentrated at the surface. These changes with changing w_c are also reflected by the mean vertical profiles of biomass. Whereas for the case with $w_{Diaz} = 0$ the concentrations in the upper two model layers (22 m) are almost homogenous due to the mixing by the physical model, all experiments with positive w_{Diaz} (already for a velocity of 1 m d^{-1}) start to show a gradient in this depth range, as the buoyancy counteracts the downward mixing. The highest sensitivity of the change of concentration with depth is seen for parameter values between 0 and 1 m d^{-1} , since vertical mixing is

in this order of magnitude. Between 1 and 10 m d^{-1} the differences are relatively small, however, the surface concentrations further increase with increasing rising rate.

The current state of knowledge about the vertical distribution of N_2 fixers biomass and fixation rates is limited, however, observations of vertical profiles will probably increase in the future. Our sensitivity experiments indicate that the buoyancy velocity plays a crucial role in influencing the vertical distribution.

2.6 Summary and Conclusions

N_2 fixation plays a relevant role in ocean biogeochemical cycles and carbon sequestration (e.g., Capone, 2001). Yet, until now N_2 fixation has only been very simplistically represented in HAMOCC, the ocean biogeochemical component of the MPI-ESM. The diagnostic formulation of N_2 fixation used hitherto was solely aimed at compensating the nitrogen loss due to denitrification. The resulting N_2 fixation was closely coupled to the upwelling sites of nitrogen-depleted water masses and neither captured the spatial distribution, nor the seasonal dynamics of observed N_2 fixation. The implementation of prognostic N_2 fixers, as presented in this paper, leads to a considerable improvement of the model's representation of present-day N_2 fixation. The new model component is included in the standard model MPI-ESM1.2, which will be used inter alia in the upcoming CMIP6 experiments.

Our growth parameterization of bulk N_2 fixers is based on physiological characteristics of the cyanobacterium *Trichodesmium*, which are thought to largely represent the ecological niche of N_2 fixers in general (Monteiro et al., 2010, 2011). N_2 fixers in our model differ from bulk phytoplankton by their ability to use both NO_3 and N_2 , a slower maximum growth rate, stronger iron limitation, buoyancy, and a specific optimum temperature range.

The prognostic parameterization reproduces the large scale distribution of autotrophic N_2 fixers biomass and fixation rates, confined to the tropical and subtropical oceans between $40^\circ S$ and $40^\circ N$. In addition to fixed N deficits, the spatial patterns of N_2 fixation are controlled by temperature, phosphate, and iron limitation, and thus are partially decoupled from the upwelling areas of nitrogen-depleted water masses. The global N_2 fixation rate yields $135.6 \text{ Tg N yr}^{-1}$, which lies within the range of recently reported estimates ($80\text{--}200 \text{ Tg N yr}^{-1}$, e.g., Gruber and Galloway (2008); Voss et al. (2013)).

N_2 -fixing diazotrophs are found in the upper 100 m with a major fraction of biomass confined to the upper 40 m, where about 99 % of the total N_2 fixation occurs (85 % in the upper 20 m, respectively). The diazotrophic activity concentrated in the upper tens of meters is in agreement with observations (Davis and McGillicuddy, 2006;

Luo *et al.*, 2012), and the simulated vertical profile of N₂ fixation at the location of ALOHA matches well the long-term measurements.

The prognostic growth dynamics, responding to seasonal changes in physical conditions and acting on a variable standing stock of N₂ fixers, are capable of producing a reasonable seasonal variability of N₂ fixation. The observed seasonal cycles at the long-term monitoring station BATS and ALOHA with highest fixation rates in northern summer/fall are adequately simulated, though the timing of the peak at ALOHA occurs a few months too early in the model.

The inclusion of N₂ fixers has marginal effects on the surface distribution of nitrate and phosphate. This is due to the changes in the spatial distribution of nitrate influx by N₂ fixation into the upper ocean, and due to the intensified nutrient turnover by the diazotrophic phytoplankton dynamics. However, the large scale patterns of nutrients resemble the observations as in the previous model version without prognostic diazotrophs. The spatial patterns of P* are improved, indicating that the changes in the spatial distribution of fixed nitrogen input improve the relative abundance of nitrate to phosphate. However, the prescribed low N:P ratio of 16:1 for diazotrophs causes a depletion of P* in areas of high N₂ fixation. The simulated annual net primary production of 48.76 Gt C yr⁻¹ and the export production of 7.46 Gt C yr⁻¹ are within the reported ranges of 40–70 Gt C yr⁻¹ (e.g., Carr *et al.*, 2006; Westberry *et al.*, 2008) and 3–20 Gt C yr⁻¹ (Najjar *et al.*, 2007), respectively.

The fact that the essential characteristics of bulk N₂ fixation are captured by the model gives confidence that the main controlling factors are included in the parameterization based on *Trichodesmium*. However, the absence of N₂ fixers at some locations in our simulation where N₂ fixation has actually been measured (e.g. in the central equatorial Pacific and in Peruvian upwelling region in the South Pacific) indicates that the ecological niche of diazotrophs is not completely covered by our growth parameterization. Sensitivity experiments show that different half saturation constants for nutrient uptake of various diazotroph types might be relevant for regional spatial patterns of the total diazotroph habitat. In general, future research on the physiology of more uncharacterized N₂-fixing groups, e.g. symbiotic diazotrophs, and unicellular cyanobacteria that grow in cooler water (e.g., Needoba *et al.*, 2007; Moisander *et al.*, 2010), will potentially give more insights into if and how other diazotrophic groups should be accounted for in the model. Especially for representing the response of N₂ fixers to variability and climate change it might be important to include a higher level of diazotrophic diversity.

The underestimation of simulated N₂ fixers biomass and fixation rates within the North Atlantic subtropical gyre indicates a lacking mechanism that supplies N₂ fixers with sufficient phosphorus to grow in this region. Proposed mechanisms are the ability of *Trichodesmium* to utilize dissolved organic phosphorus (e.g., Landolfi *et al.*, 2015), and a potential vertical migration of *Trichodesmium* from the phosphate

depleted surface layer to the phosphate rich thermocline (*Karl et al.*, 1992). More profound knowledge of the respective processes is required to include them in the model parameterization.

Sensitivity experiments show that iron limitation is an important factor controlling the distribution of diazotrophs and N₂ fixation in our model, especially in the Pacific Ocean. Our model assigns the Eastern Pacific Ocean a large potential for N₂ fixation, mainly driven by a pattern of high dust deposition. As knowledge of dust deposition and the iron cycle is limited, more direct measurements of N₂ fixation are needed to sufficiently evaluate the model results in this part of the ocean.

The high sensitivity of N₂ fixers to iron as found in our study supports the idea that prospective changes in the atmospheric dust deposition might affect the future evolution of global N₂ fixation (e.g., *Krishnamurthy et al.*, 2007, 2009). Observations indicate that additional physiological sensitivities of N₂ fixers (which are not accounted for in the current model), like pH-dependent growth (e.g., *Barcelos e Ramos et al.*, 2007), and temperature adaptation (*Thomas et al.*, 2012), could also play a role. The parameterization of prognostic N₂ fixers presented in this paper provides the basis for further studies on the influence of different environmental factors on N₂ fixation, which could give indications for the response of N₂ fixation to potential conditions in a future climate.

Chapter 3

Sensitivity of the tropical climate system to light absorption by marine cyanobacteria

3.1 Introduction

Phytoplankton pigments, predominantly chlorophyll, absorb light and thereby modify the vertical distribution of radiative heating in the upper ocean (e.g., *Lewis et al.*, 1990; *Strutton and Chavez*, 2004). Numerous model studies, using ocean-only and coupled ocean-atmosphere model setups, show that the biologically-induced redistribution of heat in the water column considerably impacts on ocean temperature and circulation (e.g., *Murtugudde et al.*, 2002; *Manizza et al.*, 2008; *Löptien et al.*, 2009), as well as on climate mean state and variability (e.g., *Wetzel et al.*, 2006; *Anderson et al.*, 2007; *Patara et al.*, 2012).

One phytoplankton type that is observed to have an particularly strong local heating effect on sea surface temperature (SST) are positively buoyant cyanobacteria (*Kahru et al.*, 1993; *Capone et al.*, 1998). Cyanobacteria are abundant throughout the tropical and subtropical ocean, where they often represent a dominant fraction of total phytoplankton biomass (e.g., *Carpenter and Romans*, 1991; *Capone et al.*, 1997; *Luo et al.*, 2012). The unique capability of cyanobacteria to fix nitrogen gas (N_2) enables them to grow at the edges of and partly within the nitrate-depleted downwelling regions of the subtropical gyres (e.g., *Luo et al.*, 2012). Accounting for the major input of new nitrogen to the upper ocean, cyanobacteria play a crucial role in global ocean biogeochemical cycling (e.g., *Capone*, 2001). Besides affecting biogeochemistry, cyanobacteria can affect their physical environment by absorbing light. Cyanobacteria organisms, largely positively buoyant, have the capacity to form sur-

face blooms extending over up to several millions of square kilometres (e.g., *Capone et al.*, 1998). Although the chlorophyll content of cyanobacteria is in general rather low compared to that of other phytoplankton (e.g., *Berman-Frank et al.*, 2001; *Carpenter et al.*, 2004; *Sathyendranath et al.*, 2009), the dense accumulations of biomass in cyanobacteria blooms result in high chlorophyll concentrations (e.g., *Subramaniam et al.*, 2001; *Westberry and Siegel*, 2006) and hence strong light absorption and heat trapping at the ocean surface. Observations showed a local heating effect of 1.5–5.0 K caused by cyanobacteria blooms (*Kahru et al.*, 1993; *Capone et al.*, 1998).

Idealized model studies support the view that positively buoyant cyanobacteria affect the local temperature distribution and mixed layer dynamics (*Hense*, 2007; *Sonntag and Hense*, 2011; *Sonntag*, 2013). The authors simulated a local heating effect of up to 2 K and a mixed layer depth shoaling of up to 20 m. These idealized model studies, however, only give evidence on a local, at the best, regional scale. As cyanobacteria are abundant throughout large parts of the tropical and subtropical ocean – which is at the same time a region where the atmosphere is especially sensitive to changes in SST – cyanobacteria may likely have the potential to play a role in the climate system on a more global scale.

All global model studies, however, only consider the effect of phytoplankton light absorption in general, without differentiating between individual phytoplankton types (e.g., *Patara et al.*, 2012, and references therein). Moreover, none of the biogeochemical models used in these studies contains positively buoyant cyanobacteria. Some recent global model studies, however, demonstrated that water turbidity within the subtropical gyres and in the eastern tropical regions overlying the oxygen minimum zones – exactly the regions inhabited by cyanobacteria – is particularly relevant in affecting tropical SST and climate (*Anderson et al.*, 2007, 2009; *Gnanadesikan and Anderson*, 2009). This underpins our hypothesis that cyanobacteria might affect the upper ocean heat budget and climate on the large scale. The respective studies, however, did not apply interactive biogeochemistry but a satellite based climatological map of chlorophyll. This approach entails various limitations, including a missing vertical as well as temporal variability in chlorophyll concentrations, a potential inconsistency of the chlorophyll field with the model circulation field, and, most importantly, a missing feedback from changes in ocean physics onto chlorophyll itself.

In order to investigate the full interactive feedback from cyanobacteria radiative heating on the climate system, we apply the Max Planck Institute Earth System Model (MPI-ESM) which contains a realistic representation of positively buoyant, N₂-fixing cyanobacteria (*Paulsen et al.*, 2017, Chapter 2 of this thesis). We include cyanobacteria in complement to bulk phytoplankton in affecting the depth of shortwave attenuation, and, by varying the chlorophyll content per cyanobacteria biomass (and thereby the strength of light absorption) we can separate the effects of

cyanobacteria from those of bulk phytoplankton in the model. We assess how the local redistribution of heat induced by cyanobacteria affects climate on the large scale, and further, how respective changes feed back on ocean biogeochemistry. Moreover, we obtain a better understanding of the sensitivity of the involved processes to the strength of light absorption, and how changes in this parameter propagate through the climate system.

3.2 Model description and experimental setup

3.2.1 The MPI-ESM

We use MPI-ESM, which consists of the coupled general circulation models for the atmosphere ECHAM6 (*Stevens et al., 2013*), and the ocean MPIOM (*Jungclaus et al., 2013*), and the ocean biogeochemistry model HAMOCC5.2 (*Ilyina et al., 2013*) extended by prognostic N₂-fixing cyanobacteria (*Paulsen et al., 2017*, Chapter 2 of this thesis), and the land carbon and vegetation model JSBACH (*Reick et al., 2013; Schneek et al., 2013*). We apply a grid configuration referred to as LR (GR15 for MPIOM, T63L47 for ECHAM6). In the atmosphere, the horizontal resolution is T63 in spectral space (approximately 1.75° on a Gaussian grid) with 47 vertical σ -hybrid layers. The time step is 450 seconds. In the ocean, the bipolar grid GR15 has poles over Antarctica and Greenland and a horizontal resolution of approx. 1.5°, gradually varying between 15 km in the Arctic and about 184 km in the Tropics. In the vertical, there are 40 unevenly spaced layers with level thicknesses increasing with depth, whereby eight layers are located within the upper 90 m. The time step is 2700 seconds. MPIOM is a z-coordinate global general circulation model solving the primitive equations under the hydrostatic and Boussinesq approximation on a C-grid with a free surface (*Marsland et al., 2003; Jungclaus et al., 2013*). Momentum, heat and freshwater fluxes are coupled daily between ECHAM and MPIOM using the Ocean Atmosphere Sea Ice Soil (OASIS3-MCT; *Valcke, 2013*) coupler. Incoming shortwave radiation is passed also daily from ECHAM to MPIOM.

The global ocean biogeochemistry model HAMOCC as component of MPI-ESM serves to simulate carbon cycling in the ocean. The spatial and temporal resolution of HAMOCC is inherited from MPIOM. Details on the coupling of HAMOCC and MPIOM are given in *Maier-Reimer et al. (2005)*. We use the version HAMOCC5.2 (*Ilyina et al., 2013*), extended by a prognostic representation of N₂-fixing cyanobacteria (*Paulsen et al., 2017*, Chapter 2 of this thesis). HAMOCC includes biogeochemical processes in the water column, the sediment, and at the air-sea interface. Biogeochemical tracers in the water column are fully advected, mixed and diffused by the flow field of the physical model. Biogeochemistry dynamics, which are premised on an extended NPZD (nutrients, phytoplankton, zooplankton, detritus) model

approach (*Six and Maier-Reimer, 1996*), include the compartments nutrients (phosphate, nitrate, and iron), oxygen, silicate, opal, calcium carbonate, dissolved inorganic carbon, alkalinity, phytoplankton (bulk phytoplankton and N₂ fixers), zooplankton, dissolved organic matter, and detritus. Organic material is composed following a constant Redfield ratio (C:N:P:O₂ = 122:16:1:-172) based on *Takahashi et al. (1985)* and of the micronutrient iron (Fe:P = 366·10⁻⁶:1) (*Johnson et al., 1997*). Below 100 m, the sinking speed of organic matter increases linearly with depth after *Martin et al. (1987)*. Atmospheric deposition of iron is accounted for by applying the present-day climatology of monthly atmospheric dust deposition from *Mahowald et al. (2006)*. It is assumed that a fixed fraction of the dust deposition (3.5 %) is iron, of which 1 % is biologically available. Iron complexation by organic substances (ligands) takes place at dissolved iron concentrations larger than 0.6 nmol L⁻¹. Dissolved iron is removed from the water column with a constant rate (*Archer and Johnson, 2000; Parekh et al., 2005*).

Phytoplankton is represented by two tracers in the model, N₂-fixing cyanobacteria (Cya) and bulk phytoplankton (Phy). The growth parameterization of cyanobacteria is based on physiological characteristics of the cyanobacterium *Trichodesmium* (*Paulsen et al., 2017, Chapter 2 of this thesis*). The major difference between N₂ fixers as compared to bulk phytoplankton in the model is their ability to fix N₂. In contrast to bulk phytoplankton, cyanobacteria are hence not limited by nitrate. However, when available, cyanobacteria nevertheless take up nitrate. Furthermore, cyanobacteria are positively buoyant (in contrast to bulk phytoplankton which are neutrally buoyant). Cyanobacteria have a specific optimum temperature range, with an optimum at 28°C (in contrast to bulk phytoplankton for which the Eppley curve is applied, see *Ilyina et al., 2013*). Cyanobacteria grow slower than bulk phytoplankton and have a high iron limitation. A detailed description of the parameterization as well as evaluation of the model performance with respect to cyanobacteria are given in *Paulsen et al. (2017)* (Chapter 2 of this thesis).

3.2.2 Parameterization of radiative heating in the water column and experimental setup

Incoming shortwave radiation I_0 is attenuated by seawater itself and by phytoplankton. Chlorophyll is thereby used as a measure of strength of light absorption by phytoplankton. The vertical light field $I(z)$ in the model is described by the scheme after *Zielinski et al. (2002)*:

$$I(z) = I_0 \cdot f_{vis} \cdot \left[\sigma \cdot \exp(-z \cdot k_r) + (1 - \sigma) \cdot \exp(-z \cdot k_w - k_{Chl} \cdot \int_0^z Chl(z) dz) \right]. \quad (3.1)$$

Here, f_{vis} is the visible light fraction (0.58), covering the wavelength range of 400–700 nm which has the potential to penetrate into deeper layers. The light spectrum is divided at 580 nm, prescribed by $\sigma = 0.4$, into two domains: Whereas for larger wavelengths (red domain) attenuation is dominated by sea water with the attenuation coefficient k_r (0.35 m^{-1}), for shorter wavelengths (blue/green domain) the absorption by chlorophyll with the absorption coefficient k_{Chl} (0.04 m^{-1}) is considered in addition to clear water with the absorption coefficient k_w (0.03 m^{-1}). Chlorophyll (Chl) is assumed to be a linear function of the concentrations of bulk phytoplankton and cyanobacteria:

$$Chl(z) = \frac{1}{R_{Phy}} \cdot Phy(z) + \frac{1}{R_{Cya}} \cdot Cya(z). \quad (3.2)$$

The observed C:Chl ratio (R) in phytoplankton varies from about 12 to more than 200 mg C (mg Chl) $^{-1}$ depending on species, light conditions, nutrient limitation and temperature (e.g., *Taylor et al.*, 1997). We choose $R_{Phy} = 60 \text{ mg C (mg Chl)}^{-1}$ for bulk phytoplankton (*Ilyina et al.*, 2013) and $R_{Cya} = 120 \text{ mg C (mg Chl)}^{-1}$ for cyanobacteria. Cyanobacteria generally contain less chlorophyll than other phytoplankton and the chosen value lies in the middle of the large observed range of ~ 40 to $200 \text{ mg C (mg Chl)}^{-1}$ for *Trichodesmium* (e.g., *Berman-Frank et al.*, 2001; *Carpenter et al.*, 2004). The lower chlorophyll content of cyanobacteria compared to bulk phytoplankton prescribed in the model implies that under the same level of incoming shortwave radiation, the presence of cyanobacteria of the same biomass than bulk phytoplankton reduces the attenuation depth only half as efficient as bulk phytoplankton.

The radiative heating of water is accounted for by an internal source of heat in the temperature equation, proportional to the vertical derivative of the light field $I(z)$:

$$\frac{\partial T}{\partial t} = \frac{1}{\rho \cdot c_p} \cdot \frac{\partial I(z)}{\partial z} \quad (3.3)$$

with ρ as the density and c_p the specific heat capacity of seawater. Thereby, it is assumed that the total absorbed light is converted into heat. Biological fluorescence mostly converts into heat, and the absorbed energy stored in biomass is generally small and can be neglected (*Lewis et al.*, 1983, and references therein).

Three experiments are conducted (Table 3.1), which all apply the chlorophyll-dependent radiative heating. In the first experiment, PHY_ONLY, cyanobacteria are set to transparent with respect to shortwave radiation, that means to $0 \text{ mg Chl (mg C)}^{-1}$. Light is thus only absorbed by bulk phytoplankton, not by cyanobacteria. In the second experiment, PHY_CYA, light is absorbed by bulk phytoplankton and by cyanobacteria ($R_{Cya} = 120 \text{ mg C (mg Chl)}^{-1}$). Finally, because

Table 3.1: Experiment names and descriptions.

Experiment name	Description
PHY_ONLY	light absorption by bulk phytoplankton only (cyanobacteria are set to transparent)
PHY_CYA	light absorption by bulk phytoplankton and cyanobacteria
PHY_CYA _{x2}	light absorption by bulk phytoplankton and cyanobacteria, with doubled Chl content of cyanobacteria

the light absorption strength by cyanobacteria is not well constrained, we consider a sensitivity experiment, PHY_CYA_{x2}, in which we increase the strength of cyanobacteria light absorption by doubling their chlorophyll content per biomass to a value of $R_{C_{ya}} = 60 \text{ mg C (mg Chl)}^{-1}$. The different light absorption parameterizations are only applied for the heat budget in the physical model. For light limitation of photosynthesis in the biogeochemical model, in all experiments the same self shading effect is applied in order to exclude direct effects on phytoplankton (C:Chl 60:1 $\text{mg C (mg Chl)}^{-1}$).

All three experiments are run for 300 years with prescribed preindustrial (1850) atmospheric CO_2 concentrations (284.7 ppm). For all analyses the mean of the last 100 years is evaluated, in which the upper ocean ($\sim 500 \text{ m}$) shows no considerable drifts anymore. All experiments are started from a preindustrial control run in steady state, in which light absorption is prescribed by a globally uniform exponential profile of light (the default setup in MPI-ESM, see Appendix Ch3 for details).

3.3 Global distribution of cyanobacteria and chlorophyll

Cyanobacteria in the model occur between 40°S and 40°N (Figure 3.1), where they constitute an important fraction ($\sim 18\%$) of total phytoplankton biomass (in certain regions up to 90% of the local concentrations). The ecological niche of cyanobacteria in the model is mainly determined by their ability to fix N_2 , their positive buoyancy, a high optimum temperature, and a strong iron limitation (*Paulsen et al., 2017*, Chapter 2 of this thesis). The global depth-integrated N_2 fixation rate of $116.6 \text{ Tg N yr}^{-1}$ lies within the range of reported estimates of $\sim 80\text{--}200 \text{ Tg N yr}^{-1}$ (e.g., *Karl et al., 2002*; *Großkopf et al., 2012*). The simulated maximum annual mean surface concentrations reach values of $\sim 400 \text{ mg C m}^{-3}$ (depth-integrated $\sim 700 \text{ mg C m}^{-2}$), and surface fixation rates of $\sim 300 \text{ } \mu\text{mol N m}^{-3} \text{ d}^{-1}$ (depth-integrated $\sim 5000 \text{ } \mu\text{mol N m}^{-2} \text{ d}^{-1}$). The major fraction of biomass and N_2 fixation ($\sim 85\%$) is thereby confined to the upper 20 m. The orders of magnitudes of biomass and fixation rates as well as the large scale spatiotemporal patterns are in agreement with observations (*Luo et al., 2012*). In the North Atlantic subtropical gyre, the model is characterized by an underestimation of cyanobacteria concentrations and N_2 fixation rates in comparison

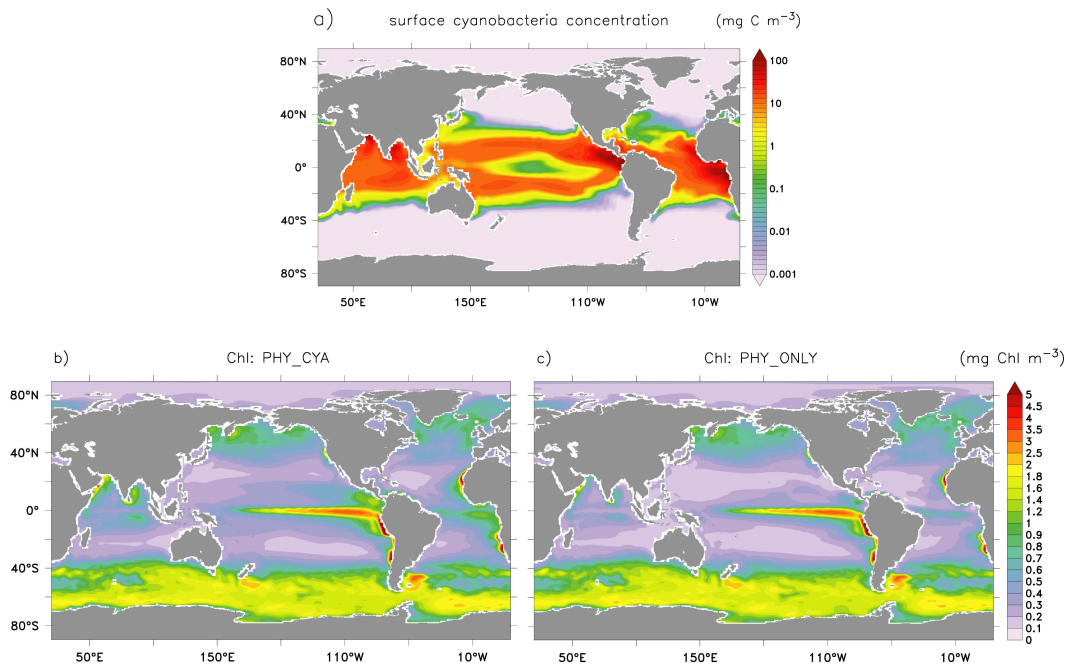


Figure 3.1: a) Climatological annual mean surface (0–22 m) cyanobacteria concentrations [mg C m^{-3}] in PHY_CYA. Note the nonlinear color scale. b) Climatological annual mean global surface (0–22 m) chlorophyll concentrations [mg Chl m^{-3}] of bulk phytoplankton and cyanobacteria, and c) of bulk phytoplankton only (used for calculating the radiative heating in PHY_CYA (b) and PHY_ONLY (c) (Equation 3.2)).

to observations. In the eastern tropical Pacific, on the other hand, concentrations and fixation rates are probably overestimated by the model due to a too high dust input. The lack of observations, however, limits the evaluation of the model in this part of the ocean. For a detailed description and model evaluation, see *Paulsen et al.* (2017) (Chapter 2 of this thesis).

Chlorophyll is used as a measure of strength of phytoplankton light absorption in this study (Equations 3.1,3.2). Figure 3.1b shows the simulated global annual mean distribution of total surface chlorophyll (bulk phytoplankton and cyanobacteria) of the upper 22 m (first two model layers). The simulated distribution qualitatively reproduces the main global patterns and seasonal dynamics (not shown) of chlorophyll observed by satellite (e.g., *SeaWiFS Project*, 2003). High simulated values of chlorophyll occur in high latitudes north and south of 40° latitude (annual mean $\sim 0.5\text{--}3 \text{ mg Chl m}^{-3}$, with a pronounced seasonal cycle), as well as in the nutrient rich upwelling regions at the equator and along the eastern boundaries of the continents (annual mean $\sim 1\text{--}5 \text{ mg Chl m}^{-3}$). In the equatorial Pacific, chlorophyll values are strongly overestimated by the model, caused by too strong upwelling and hence too large biological production (*Ilyina et al.*, 2013). Low chlorophyll values, on the other hand, are present in the oligotrophic areas of the downwelling regions in

the central subtropical gyres (annual mean $\sim 0.1\text{--}0.3$ mg Chl m^{-3}). The values are slightly higher than satellite estimates of chlorophyll ($0.03\text{--}0.2$ mg Chl m^{-3}) (*SeaWiFS Project*, 2003), probably due to the missing depth dependent C:Chl ratio of bulk phytoplankton in the model. At the margins of the subtropical gyres, simulated values of $\sim 0.3\text{--}1.0$ mg Chl m^{-3} are in line with satellite estimates.

Setting cyanobacteria to transparent with respect to shortwave radiation (Figure 3.1c), as done in experiment PHY_ONLY, leads to a reduction of annual mean surface chlorophyll in the tropical and subtropical ocean in the order of $0.1\text{--}0.3$ mg C (mg Chl) $^{-1}$, regionally, however, by up to 0.8 mg Chl m^{-3} (Figure 3.2a). This represents up to 80% of the total surface chlorophyll concentrations in certain regions (e.g. in the eastern equatorial Atlantic and Pacific). The large contribution of cyanobacteria to overall surface chlorophyll can be explained, first, by their capability to grow in nitrate-depleted regions (in contrast to bulk phytoplankton), and second, by the fact that they are, as mentioned above, concentrated rather at the surface due to their positive buoyancy (in contrast to bulk phytoplankton, which shows a deep chlorophyll maximum at roughly 50–100 m in large parts of the tropical and subtropical ocean in summer months, not shown). If the simulated chlorophyll content of cyanobacteria of the first model layer (12 m) with an annual mean concentration of up to 0.9 mg Chl m^{-3} (not shown) was confined more to the surface (e.g. to the upper first meter, which is more realistic in surface bloom conditions), this would refer to a value of 10.8 mg Chl m^{-3} , which lies within the range of reported values for *Trichodesmium* blooms ($\sim 0.8\text{--}40$ mg Chl m^{-3} ; e.g., *Subramaniam et al.*, 2001; *Westberry and Siegel*, 2006; *Mohanty et al.*, 2010). Overall, the simulated values of cyanobacteria chlorophyll are hence in a plausible order of magnitude.

3.4 Effects of cyanobacteria light absorption on the mean tropical climate state

In order to assess the added impact of including prognostic cyanobacteria in complement to bulk phytoplankton in affecting the depth of shortwave radiation attenuation, we subtract the mean state PHY_ONLY from PHY_CYA (mean of the last 100 years of the simulations). In the subsequent sections, we first show the effects on ocean temperature and mixed layer depths and explain the underlying mechanisms. Then, we describe the response of the atmosphere to SST changes, both with respect to wind patterns and precipitation. Afterwards, implied alterations in ocean circulation and concomitant feedbacks on phytoplankton growth itself are elucidated.

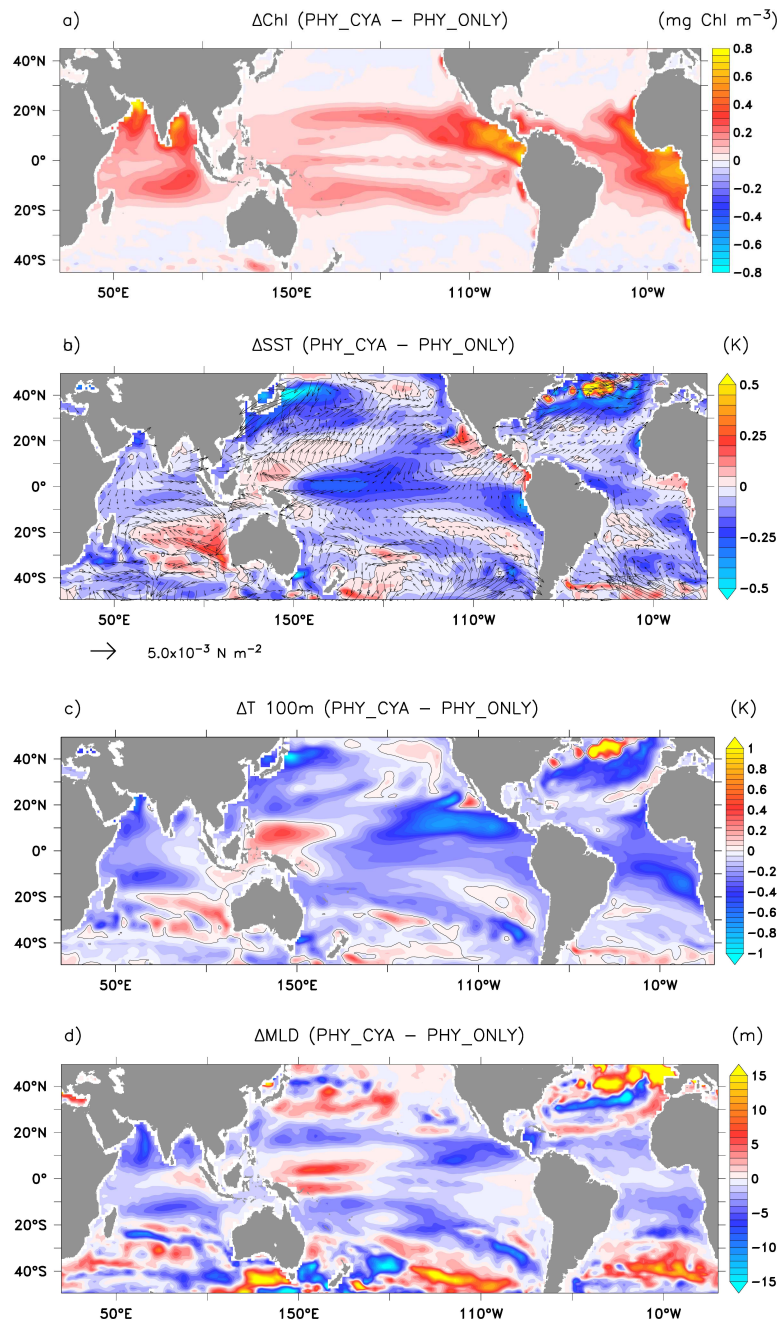


Figure 3.2: Change in the climatological annual mean between PHY_ONLY and PHY_CYA of a) surface Chl (0–22 m) [mg Chl m^{-3}], b) SST [K], c) mean temperature at a depth of 100 m [K], and d) mixed layer depth [m]. The vectors in b) display anomalies of wind-stress (PHY_CYA - PHY_ONLY) on the ocean. The reference vector represents a value of $5.0 \cdot 10^{-3} \text{ N m}^{-2}$. The isolines in b) and c) display the zero-isoline of SST anomalies and temperature anomalies, respectively.

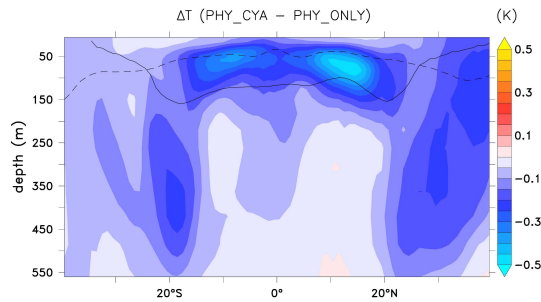


Figure 3.3: Change in the climatological global zonal mean temperature [K] in the upper 550 m between PHY_ONLY and PHY_CYA. The dashed black line shows the global zonal mean MLD and the solid black line the global zonal mean thermocline depth (defined as the depth of the 20°C isotherm) in PHY_ONLY.

3.4.1 Effects on ocean temperature and mixed layer depth

Including light absorption by cyanobacteria in addition to bulk phytoplankton has an overall cooling effect on the tropical surface ocean (Figure 3.2b). Although the change in the mean tropical SST (20°S–20°N) is only small (0.07 K), regionally, negative SST anomalies reach values of up to 0.5 K. The strongest negative signals occur at the equator and in the eastern boundary upwelling systems off the South American and African continents.

The surface cooling can be explained by the following mechanism. The presence of cyanobacteria increases light absorption in the upper layers. Radiative heating is thus more confined to the surface, causing a shoaling of the mixed layer depth (MLD) by up to 10 m (Figure 3.2d) and a shoaling of the thermocline depth (shown for the equatorial Pacific in Figure 3.4). At the same time, deeper layers receive less radiation, which leads to a decrease in subsurface temperature (Figure 3.2c), in the global zonal mean by up to 0.5 K (Figure 3.3). The cold signal reaches below the MLD and down to the thermocline (defined here as the depth of the 20°C isotherm). This subsurface water feeds the shallow overturning cells and is transported equatorward along the thermocline, which is equivalent with the pycnocline in the Tropics. At the equator, the relatively cooler subsurface water is upwelled, where it outweighs the direct heating effect due to local cyanobacteria light absorption at the surface. The upwelled water is spread laterally via the poleward surface Ekman transport and leads to a cooling in large parts of the tropical and subtropical ocean. Hence, instead of a surface heating, which one would expect from the direct effect of cyanobacteria, i.e. the higher light absorption, the advective process brings relatively cooler subsurface water to the surface and cools the surface ocean. In addition, the atmospheric cooling above the eastern equatorial Pacific spreads throughout the troposphere and enhances the surface cooling in other regions due to the associated heat flux directed from the ocean into the atmosphere (not shown).

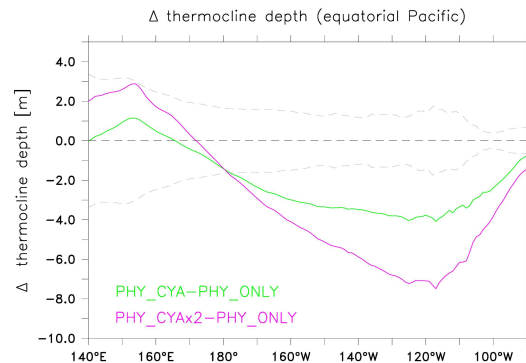


Figure 3.4: Change in the climatological mean thermocline depth [m] between PHY_CYA and PHY_ONLY (green) and PHY_CYAx2 and PHY_ONLY (purple). To provide a sense for the variability, the grey dashed lines show \pm two times the standard deviation of eight 100 year periods of experiment CTRL (see Appendix Ch3).

The origin of the relatively colder subsurface water that reaches the surface in the upwelling areas is in the regions where cyanobacteria are abundant and shade the deeper layers (Figure 3.2a). These regions include two different regimes. The first regime are the downwelling regions of the subtropical gyres in which the cooler water is subducted within the shallow meridional overturning cells and then transported equatorward along the thermocline. In the second regime, the eastern equatorial upwelling regions at the margins of the subtropical gyres, overall high cyanobacteria concentrations are present, which strongly shade and hence cool the subsurface layers. Although these regions are less ventilated than the subtropical gyres, the water from here finally also ends up in the shallow meridional overturning cells and the equatorial upwelling system, contributing to the cold SST signal seen at the Equator. Due to the complexity of the circulation system and the exchange pathways between the tropical and subtropical ocean, it is not possible to separate the contributions from the subtropical gyres and from its margins to the cooling signal.

Besides the SST decrease, which dominates in large parts of the tropical and subtropical ocean, there are regions with an annual mean SST warming signal (Figure 3.2b). These include the eastern equatorial Atlantic and the eastern equatorial Pacific adjacent to the coast. In these regions, the direct heating by high cyanobacteria concentrations, in combination with the decrease in upwelling strength (as will be discussed in Section 3.4.3), outweighs the upwelling effect of cooler subsurface water and results in a surface warming.

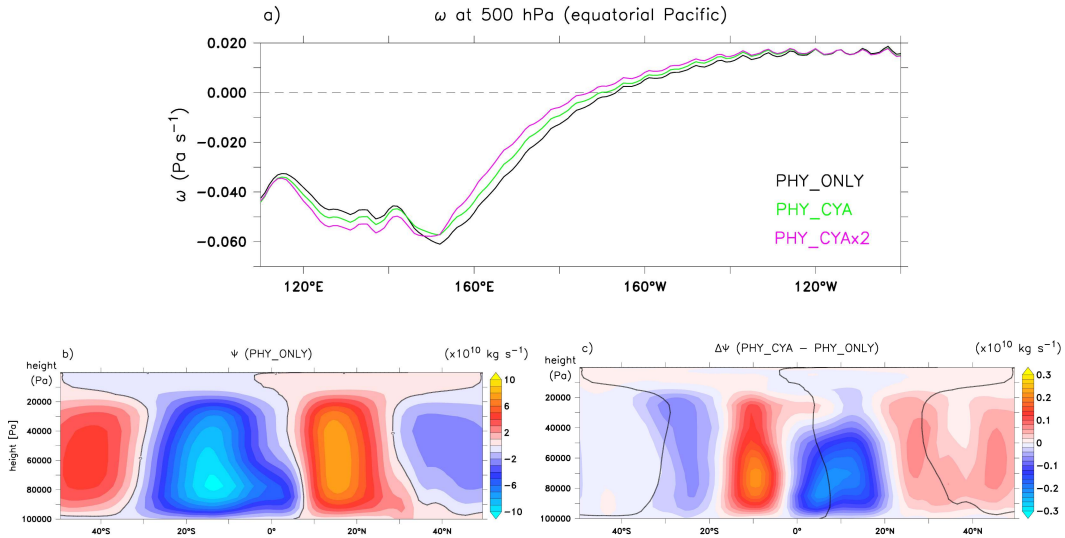


Figure 3.5: a) Climatological mean vertical velocity ω [Pa s^{-1}] at 500 hPa above the equatorial Pacific (5°S – 5°N) in PHY_CYA (green), PHY_ONLY (black) and PHY_CYA $\times 2$ (purple). b) Climatological zonal mean meridional mass flux Ψ [$10^{10} \text{ kg s}^{-1}$] in PHY_ONLY. The zero-isoline is overlaid in black. (c) The difference in the climatological zonal mean meridional mass flux Ψ [$10^{10} \text{ kg s}^{-1}$] between PHY_ONLY and PHY_CYA. The zero-isoline of PHY_ONLY is overlaid in black.

3.4.2 Effects on wind patterns and precipitation

The cooling of the cold tongue in the eastern and central equatorial Pacific, in conjunction with the heating of the warm pool in the west, intensifies the zonal SST gradient (Figure 3.2b). A stronger SST gradient implies a strengthening of the Walker circulation (Figure 3.5a). The ascent of the air over the warm pool is enhanced west of 150°E by roughly 6% (vertical velocity ω at 500 hPa averaged from 120 – 140°E), and the descent of air in the east by roughly 15% (averaged from 120 – 160°W , respectively) (Figure 3.5a). The equatorial westward winds are intensified west of 200°E , enhancing the westward windstress on the ocean (Figure 3.2b). Furthermore, the transition zone between convection and subsidence of the Walker circulation is shifted eastward by $\sim 3^{\circ}$ longitude. In other words, the convection gets stronger, but more confined to the western part of the Pacific basin.

Besides the zonal tropical wind system, also the meridional wind system is affected by the change in SST. The strong negative SST signal at the Equator generally reduces the meridional temperature gradient between the equatorial zone and the Extratropics (Figure 3.2b). This results in damped trade winds above the Atlantic and the eastern part (east of 200°E) of the Pacific, as visible in the reduced wind stress over the ocean (Figure 3.2b). Related to the weaker trade winds, the strength of the Hadley circulation is reduced, as discernable in the Stokes streamfunction,

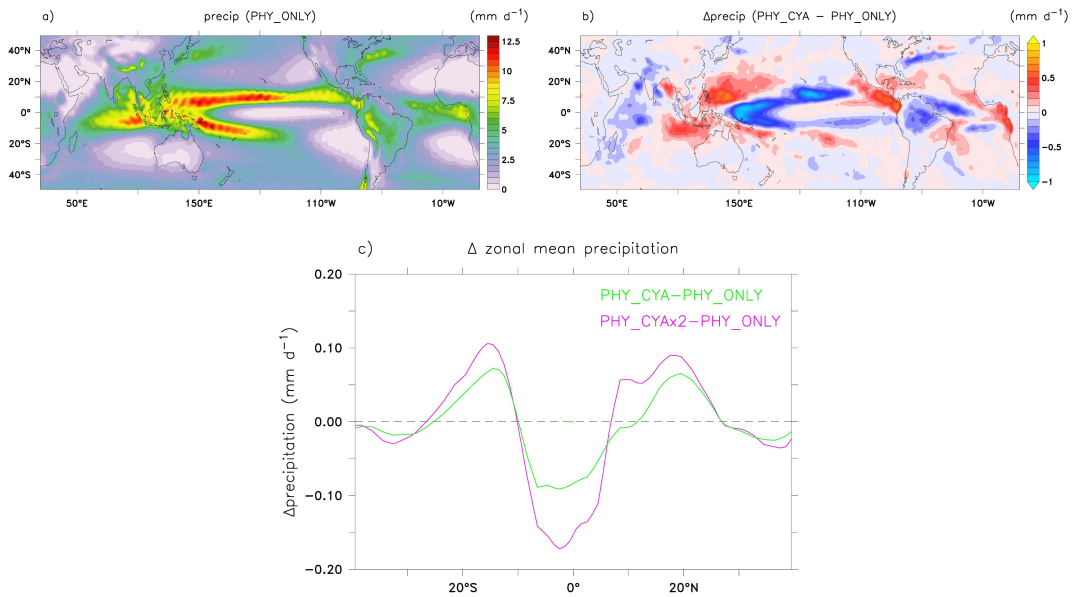


Figure 3.6: a) Climatological annual mean precipitation [mm d^{-1}] in PHY_CYA. b) Difference in the climatological annual mean precipitation [mm d^{-1}] between PHY_ONLY and PHY_CYA. c) Difference in the climatological annual zonal mean precipitation [mm d^{-1}] between PHY_CYA and PHY_ONLY (green), and PHY_CyAx2 and PHY_ONLY (purple).

which displays the zonal mean meridional mass flux (Figure 3.5b,c). The equatorward parts of the cells are weakened, whereas the poleward parts are slightly strengthened, both in the southern and Northern Hemisphere. This dipole pattern of change in the streamfunction indicates a slight expansion of the Hadley cells poleward.

Changes in SST and the wind system induce changes in precipitation. The strongest signal in precipitation can be seen over the western equatorial Pacific (Figure 3.6b). Here, the strong decrease in equatorial SST at 160°E (Figure 3.2b) and the zonal displacement of the Walker circulation (Figure 3.5a) lead to a change in the location and strength of convection and precipitation. Precipitation decreases with a maximum centered at $\sim 160^{\circ}\text{E}$ by up to 1.0 mm d^{-1} , and extending, shaped like a horseshoe, off-Equator in latitudinal bands at about 10°S and 10°N towards the east. A decrease is also seen above the cold SST anomalies in the western Indian Ocean, as well as the western tropical Atlantic and over the Amazon region. In the eastern parts of the ocean basins, the eastern equatorial Atlantic, Pacific and Indian Ocean, relatively warmer surface water, on the other hand, increases convection and hence precipitation by up to 0.8 mm d^{-1} . Zonally averaged over the globe, the precipitation rates are decreased in the equatorial zone between 10°S – 10°N by 2.5%, and increased between 10 – 25°S and 10 – 25°N by 2.5–3.5%, indicating the poleward extent of the tropical rain belt associated with the poleward expansion of the Hadley

cells (Figure 3.6c).

3.4.3 Effects on ocean circulation

The weakening of the Hadley cells implies a weakening of the wind driven ocean circulation. The barotropic streamfunction Ψ , which describes the large-scale horizontal ocean circulation, decreases in magnitudes both in the subtropical- as well as in the equatorial gyres (Figure 3.7a,b). The dipole anomaly patterns within the subtropical gyres indicate a poleward shift of its boundaries. This feature is most dominant in the North Atlantic, where the weakening in the southern part and strengthening in the northern part reflects a northward shift of the position of the Gulf Stream and the North Atlantic Current, respectively. The northward shift is also visible in the strong negative temperature anomaly which is present at the surface (Figure 3.2b) and reaches down to greater depth (Figure 3.3).

In the North Pacific, the increase in annual mean prevailing southward wind-stress along the Pacific coast (Figure 3.2b) reduces the warm water transport of the Kuroshio Current. Together with the slight shift of the western boundary current northward, this leads to a strong negative SST signal, which reaches into the interior of the ocean basin (Figure 3.2b).

In the Indian Ocean, both the subtropical and the equatorial gyres are generally weaker and the boundary between them is slightly shifted southwards (Figure 3.7a,b). The reduced strength of the Indian Ocean subtropical gyre is accompanied by a weakening of the so-called Southern Hemisphere "supergyre" (e.g., Speich *et al.*, 2007), which extends into the South Atlantic. The associated reduced transport of warm water from the Indian Ocean into the South Atlantic ocean is visible in the cold SST signal around the tip of South Africa (Figure 3.2b). This cooling effect enhances the negative SST signal which occurs at the eastern margin of the South Atlantic due to the upwelling of colder subsurface water in the Benguela Upwelling system.

In the Atlantic Ocean, the reduction of the trade winds and the related windstress on the ocean (Figure 3.2b) reduces equatorial divergence. The related weakening of the overturning cells damps equatorial upwelling and reduces downwelling in the subtropical gyres (Figure 3.7c). Hence, the atmospheric response to the SST anomaly pattern does not amplify the negative equatorial SST signal, but rather damps it, by transporting less cold subsurface water to the surface. In combination with the local heating due to high cyanobacteria concentrations, this results in a positive SST signal at the eastern boundary (Figure 3.2b). In the Pacific Ocean, a similar behavior of weaker trade winds and equatorial upwelling (Figure 3.7d) can be seen in the eastern part of the basin (east of 160°W). In the western part, on the contrary, the strengthening of the westward surface current related to the change in the Walker

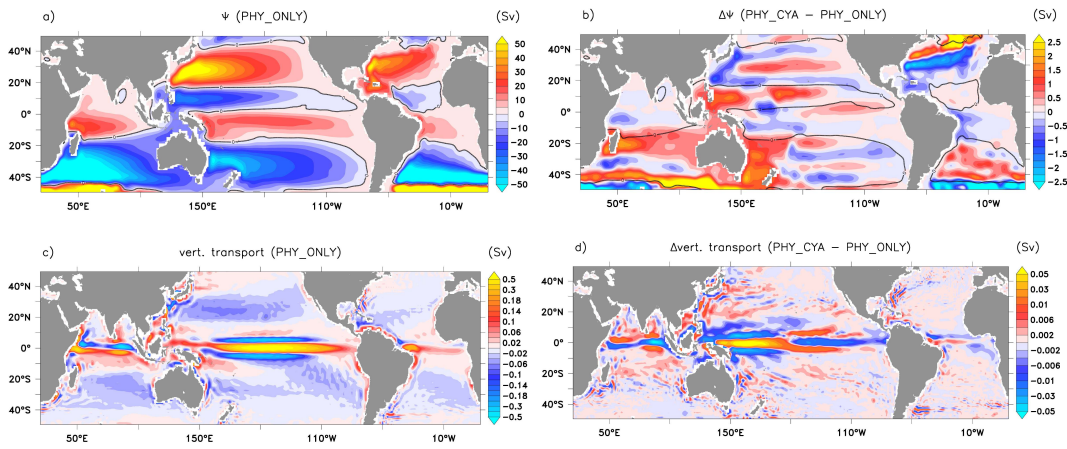


Figure 3.7: **Top:** a) Climatological mean barotropic streamfunction Ψ [Sv] in PHY_ONLY. The zero-isoline is overlaid in black. b) The difference in the climatological mean Ψ [Sv] between PHY_CYA and PHY_ONLY. The zero-isoline of PHY_ONLY is overlaid in black. **Bottom:** c) Climatological mean vertical transport [Sv] in PHY_ONLY. Note the non-linear color scaling with 0.01 Sv between -0.2 and 0.2 Sv and 0.1 Sv for the remaining range. d) The difference in the climatological annual mean vertical transport [Sv] between PHY_ONLY and PHY_CYA. Note the non-linear color scaling with 0.001 Sv between -0.01 and 0.01 Sv and 0.01 Sv for the remaining range.

circulation increases equatorial upwelling. Here, the atmospheric feedback intensifies the surface cooling effect. This explains the larger SST signal in the western central Pacific compared to the east. In summary, the atmospheric feedback amplifies the SST signal in the western Pacific by enhancing the upwelling strength, and damps it, on the other hand, in the eastern Pacific and the Atlantic Ocean by reducing the upwelling strength.

Besides the effects on the large scale ocean circulation, changes in the wind patterns regionally influence the coastal upwelling strengths along the eastern boundaries. The upwelling strengths in three of the four major upwelling systems (Benguela, Peru/Chile, California) are slightly increased due to stronger coastal winds (Figure 3.7c,d), which further contributes to the surface cooling effect. Off North West Africa, on the other hand, upwelling is slightly decreased due to weaker southward coastal winds. Nevertheless, surface cooling prevails owing to the upwelling of relatively cooler subsurface water.

3.4.4 Feedback on phytoplankton abundance

The changes in temperature and ocean circulation induced by cyanobacteria light absorption feed back on the growth conditions of cyanobacteria and bulk phytoplankton itself. Globally integrated, the two mean states PHY_CYA and

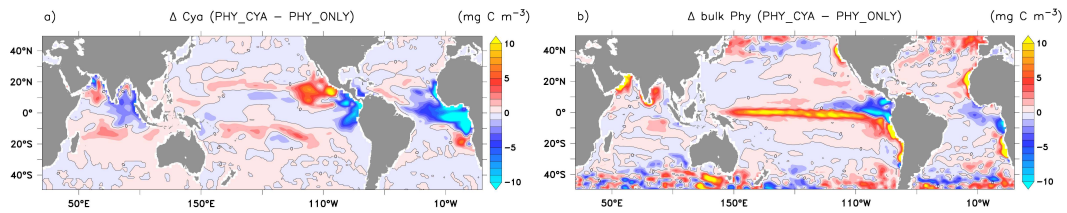


Figure 3.8: Change in a) climatological annual mean surface cyanobacteria concentrations [mg C m^{-3}] and b) surface bulk phytoplankton concentrations [mg C m^{-3}] between PHY_CYA and PHY_ONLY. The zero-isolines are overlaid in black.

PHY_ONLY do not differ notably from each other. Regionally, however, considerable changes up to 25% in the concentrations of bulk phytoplankton and cyanobacteria occur (Figure 3.8). Thereby, phytoplankton concentrations, both of cyanobacteria and bulk phytoplankton, do not uniformly decrease or increase, but show a more complex pattern of change. Hence, we cannot generally refer to a positive or negative feedback between ocean physics and cyanobacteria light absorption. A positive feedback would mean that the induced changes in ocean circulation and temperature would result in an increase in cyanobacteria biomass, which further enhances the initial perturbation - that means the increase in light absorption strength. This is indeed the case in the subtropical bands of the Pacific ocean. Here, the cyanobacteria abundance results in cooling of equatorial SST (Figure 3.2b), which shifts the Walker circulation westward (Figure 3.5a), implying an increase in upwelling strength in the western equatorial Pacific (Figure 3.7d). The related increased abundance of nutrients at the surface is spread poleward via Ekman transport and promotes growth of cyanobacteria in the subtropical bands at about $\sim 10\text{--}20^\circ\text{S}$ and $\sim 10\text{--}20^\circ\text{N}$, closing the positive feedback loop. In the eastern tropical Atlantic and Indian Ocean, as well as the eastern equatorial Pacific, the decrease in upwelling strength and the increase in SST above the optimum temperature of 28°C impairs cyanobacteria growth conditions and results in a strong decline in cyanobacteria concentrations up to 25% (Figure 3.8a). This results in rather a negative feedback, that means damping the effect of light absorption. The strong increase in bulk phytoplankton in the equatorial Pacific, as well as in the eastern boundary upwelling areas (Figure 3.8b), probably also rather damps the cooling effect due to the large increase in surface light absorption directly at the upwelling sites.

3.4.5 Synthesis and discussion of the mean state changes

The surface cooling effect due to cyanobacteria which we see in our simulation on climatological time scale is rather counterintuitive and in contrast to satellite observations, which showed a heating effect due to the presence of a cyanobacteria blooms instead (Kahru *et al.*, 1993; Capone *et al.*, 1998). These observations, how-

ever, only represent snapshots of episodic heating events. Also one-dimensional model studies did not account for the advective effect and showed, in contrast to our study, a local surface warming induced by cyanobacteria (Sonntag and Hense, 2011). Within the framework of the Earth system model used in this study, we are able to show that the surface heating effect of cyanobacteria acting locally, transfers into a cooling on climatological large scale due to the upwelling of cooler subsurface water. Cyanobacteria, by remotely affecting regions relevant for biogeochemistry and climate variability, might thus play a role on a larger scale than indicated by observations locally.

Other global model studies concur with the relevance of the advective redistribution of heat and also diagnosed a SST cooling along the equator caused by the presence of phytoplankton (Nakamoto *et al.*, 2001; Sweeney *et al.*, 2005; Anderson *et al.*, 2007; Gnanadesikan and Anderson, 2009). In particular, the studies of Anderson *et al.* (2007) and Gnanadesikan and Anderson (2009) focused on similar regions than we do in this study. The authors showed that especially the water turbidity in off-equatorial regions, more precisely in the subtropical gyres and the eastern tropical regions overlying the oxygen minimum zones, leads, in agreement with our study, to a surface cooling with similar patterns and effects on the mean climate state. The concordance about the sensitivity of the Walker and Hadley circulation as well as precipitation patterns to the changes in SST between the two coupled models (this study and Gnanadesikan and Anderson (2009)) gives confidence about the robustness of our model results. The use of a satellite climatology map of chlorophyll, as done in Gnanadesikan and Anderson (2009), however, involves a number of limitations, including a potentially non-consistent chlorophyll and model circulation field, missing vertical and temporal variations in chlorophyll concentrations, and, most importantly, the missing feedback on chlorophyll itself. We, instead, applied a full biogeochemical model with interactive biogeophysical feedback and identified the phytoplankton type that is largely responsible for the light absorption in the areas already considered important by Gnanadesikan and Anderson (2009), namely cyanobacteria. Cyanobacteria, provided with the ability to fix N_2 , inhabit exactly the regions which have a regulative effect on tropical SST due to the shading of the subsurface water that enters the meridional cells. Moreover, cyanobacteria are positively buoyant and hence mainly concentrated in the upper 20 m, where highest incoming radiation is present, and where effects on light absorption thus have strongest effects on temperature. Based on idealized model setups, Sonntag and Hense (2011) and Hense *et al.* (2017) already suggested the relevance of "surface mat producers", such as positively buoyant cyanobacteria, to be included in Earth system models – a suggestion which we confirm with our study.

The cooling effect due to off-equatorial turbidity which we see in our coupled simulations was also stressed in global ocean-only studies. By considering the zonal

momentum budget integrated over the mixed layer, the authors argue that stronger light absorption and related shallower MLDs in the regions off-Equator enhance the meridional transport and equatorial upwelling, which causes the simulated SST decrease at the Equator (Sweeney *et al.*, 2005; Löptien *et al.*, 2009; Park *et al.*, 2014). In our coupled model setup, on the contrary, we show that the atmospheric feedback on ocean circulation largely outweighs the density driven effect, and results, instead, in a decrease in upwelling strength in most parts. In the coupled system, the shading and hence cooling of the subsurface water that is eventually upwelled is responsible for the cooling effect, rather than an increase in upwelling strength itself. This discrepancy between the results of the ocean-only and the coupled model setup demonstrates the importance of using an Earth system model to study biogeophysical feedbacks in order to include feedbacks between the components of the Earth system.

The use of an Earth system model with full biogeochemistry instead of a chlorophyll climatology furthermore allows us to study the feedback on ocean biogeochemistry. The positive feedback which we found in some regions, such as the subtropical bands of the Pacific Ocean, is in line with idealized model studies (Hense, 2007; Sonntag and Hense, 2011; Sonntag, 2013). In our simulation, however, the positive feedback is not acting locally via changes in temperature (as is the case in the studies mentioned above), but mainly via non-local processes, i.e. changes in the upwelling strength and hence the supply of nutrients. In large regions, these circulation changes, however, lead to a decline in phytoplankton concentrations in our simulation, which rather constitutes a negative feedback.

3.5 Effects on temporal variability

3.5.1 Effects on seasonal dynamics of SST and cyanobacteria concentrations

Besides the climatological annual mean state, light absorption by cyanobacteria also affects the seasonal dynamics of ocean physical and biogeochemical quantities. In case of SST, the changes are mainly caused by two counteracting processes: first, the direct heating due to local cyanobacteria biomass, and second, the indirect cooling due to upwelling of subsurface water (and its subsequent lateral transport). Both processes have their own seasonal dynamics (whereby the seasonal variability of the first process is already a combination of seasonal cycle of cyanobacteria abundance and the seasonal cycle of the incoming shortwave radiation). In addition, changes in heat fluxes between the ocean and atmosphere are involved. In the end, the complex interactions between the different dynamics result in modifications of the seasonal dynamics of SST.

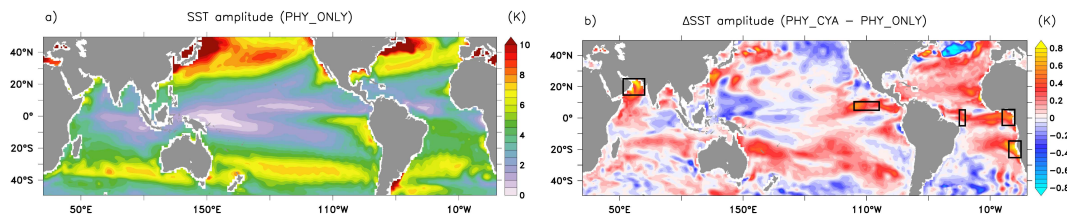


Figure 3.9: a) Climatological mean amplitude of the seasonal signal in SST [K] in PHY_ONLY. b) Change in the climatological mean amplitude of the seasonal signal in SST [K] between PHY_CYA and PHY_ONLY. The black boxes display the locations discussed in Section 3.5.1 (Figure 3.10).

In general, including cyanobacteria light absorption increases the amplitude of the climatological mean seasonal cycle of SST in large parts of the tropical and subtropical ocean, regionally by up to 20% (Figure 3.9). This is caused by either an increase in the maximum annual (monthly mean) temperature, or by a decrease of the minimum annual (monthly mean) temperature, or a combination of both. We exemplarily select different locations (Figure 3.9b, black boxes) to illustrate that – depending on the region – different factors play a role.

In the western Atlantic equatorial upwelling region, surface cooling prevails year-round (Figure 3.10a) due to upwelling of relatively cooler subsurface water. The decrease is stronger from July to September, resulting in an increased amplitude of the seasonal cycle (13.5%). Cyanobacteria concentrations are decreased at the beginning of the year due to a lower upwelling strength (Figure 3.10b). In the eastern equatorial Atlantic (Gulf of Guinea), the maximum temperatures between December and March are increased due to the surface heating effect due to high local cyanobacteria concentrations in this time, which also leads to an enhanced amplitude of the SST seasonal cycle (17.0%, Figure 3.10c). As the temperature is above the optimum value of 28°C, cyanobacteria growth and concentrations are reduced (Figure 3.10d). In the South Atlantic Benguela upwelling region, a combination of both effects leads to the increase in the seasonal SST amplitude (10.2%, Figure 3.10e). Temperatures are slightly increased in spring, when highest cyanobacteria concentrations occur. In fall, temperatures are decreased due to the upwelling of cooler subsurface water. Cyanobacteria almost completely vanish in all three experiments during this season due to generally low temperatures (Figure 3.10f). In the eastern Pacific, SST is slightly increased in the first half of the year when cyanobacteria concentrations are high (February to May) and slightly decreased during the rest of the year (Figure 3.10g). The amplitude between minimum and maximum SST is increased by 18.8%. Cyanobacteria concentrations, on the other hand, show a strong increase of the maximum value by roughly 30% from November to February (Figure 3.10h). In the Arabian Sea, apart from slightly higher SSTs in May, a cooling dominates

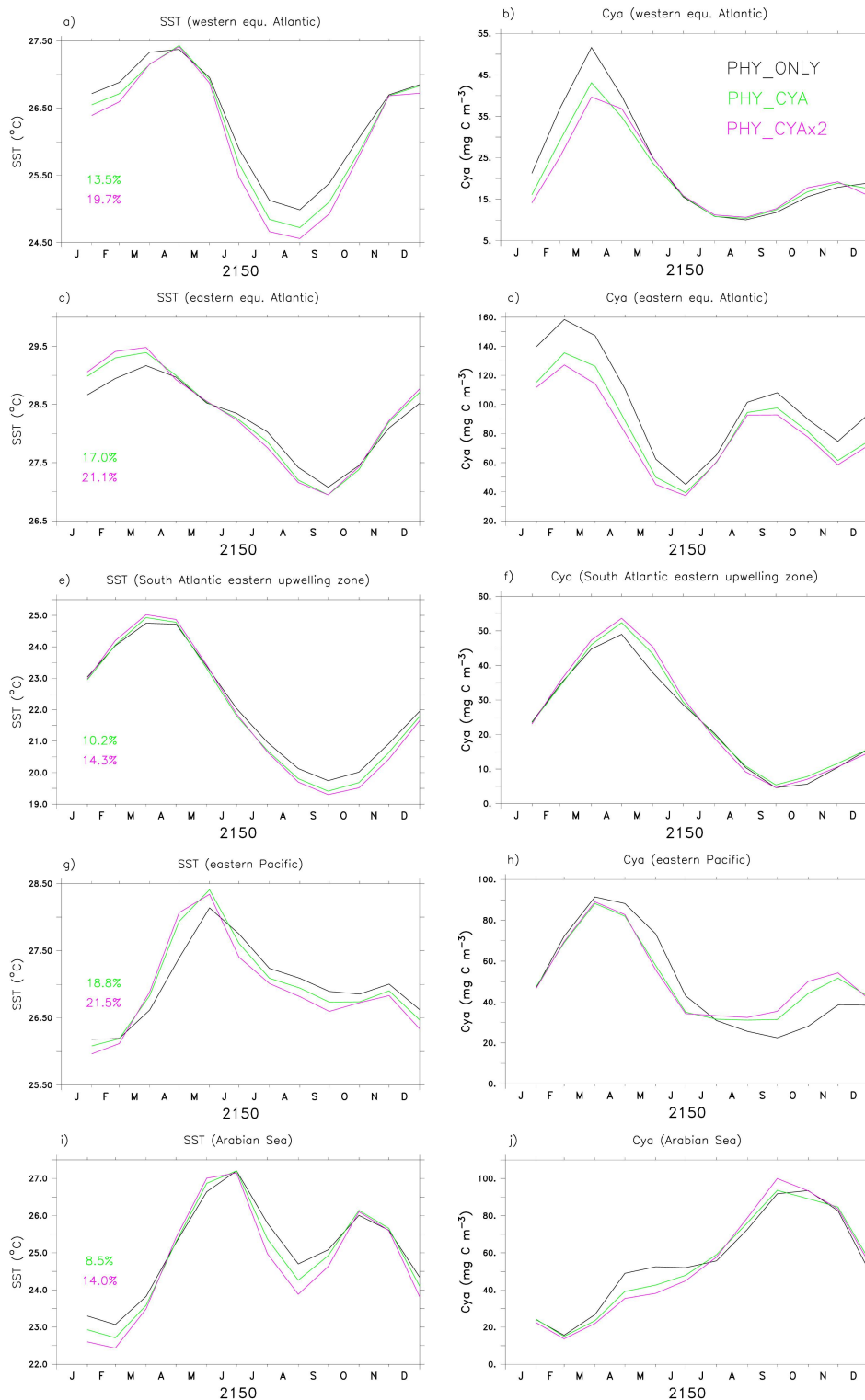


Figure 3.10: Left column: Climatological monthly mean seasonal cycle of SST [K] at distinct locations in PHY_ONLY (black), PHY_CYA (green), and PHY_CYAx2 (purple). The displayed numbers show the change in the amplitude in percent. Left column: Climatological mean seasonal cycle of surface cyanobacteria concentrations [kmol P m⁻³] at distinct locations in PHY_ONLY (black), PHY_CYA (green), and PHY_CYAx2 (purple). The locations are shown as black boxes in Figure 3.9b (from top to bottom): western equatorial Atlantic (a,b), eastern equatorial Atlantic (c,d), South Atlantic eastern boundary upwelling zone (e,f), eastern Pacific (g,h), and Arabian Sea (i,j).

throughout the rest of the year, with a maximum in August (Figure 3.10i). The amplitude is increased by 8.5%.

The exemplary changes in seasonal cycles of SST and cyanobacteria concentrations at different locations shown here indicate the complexity of the processes which are involved when including the dynamic feedback from cyanobacteria on the ocean heat balance. The regional amplification of the amplitude in seasonal cycle of SST by up to 20% which we see in our simulation has indeed the potential to affect also other quantities such as wind strength and precipitation, as well as the temperature dependent strength of CO₂ uptake/outgassing.

3.5.2 Effects on the tropical Pacific interannual variability

Among the strongest effect on climatological mean SST can be seen in the tropical Pacific (Figure 3.2b) – a region, where the atmosphere is particularly sensitive to changes in SST. The comparison of the spatial maps of the annual mean standard deviation of SST between PHY_CYA and PHY_ONLY indicates that including light absorption by cyanobacteria increases variability in the eastern equatorial Pacific by roughly 30% (Figure 3.11a,b). To provide a sense for the variability on centennial timescales (the average period over which the model is evaluated), we calculate the standard deviation of eight 100 year periods of the simulation CTRL (see Appendix Ch3 for a description of the simulation), for which a longer integration is available. Figure 3.11c shows only signals larger than two times the standard deviation of the eight 100 year subintervals. The signal of increasing variability in the equatorial Pacific is larger than this variability and hence seems to be robust. The increase in variability is probably caused by two factors: first, the increased asymmetry in zonal SST due to the cooling of the cold tongue (Figure 3.2b), and second, the shoaling of the thermocline (Figure 3.4). Both factors are generally proposed to increase variability of tropical SST and El Niño-Southern Oscillation (ENSO) (e.g., Collins *et al.*, 2010; Meehl *et al.*, 2001). Cyanobacteria, although mainly present off-Equator, seem to influence ENSO due to their non-local effects of modifying SST and the thermocline depth at the Equator.

The seasonality of ENSO variability seems also to be affected. Figure 3.11d shows the monthly mean standard deviation of the Nino3.4 index (SST anomalies averaged over the area 5°S–5°N and 170°W–120°W). PHY_CYA has generally a higher standard deviation compared to PHY_ONLY. The annual mean value is increased by 16% (PHY_CYA: 0.80 K, PHY_ONLY: 0.69 K). Largest differences of up to 64% occur from May to August. The large variability even on 100 year averages (indicated by the standard deviation of eight 100 year periods of the simulation CTRL, shown in blue errorbars around the blue line in Figure 3.11d), however, has to be kept in mind.

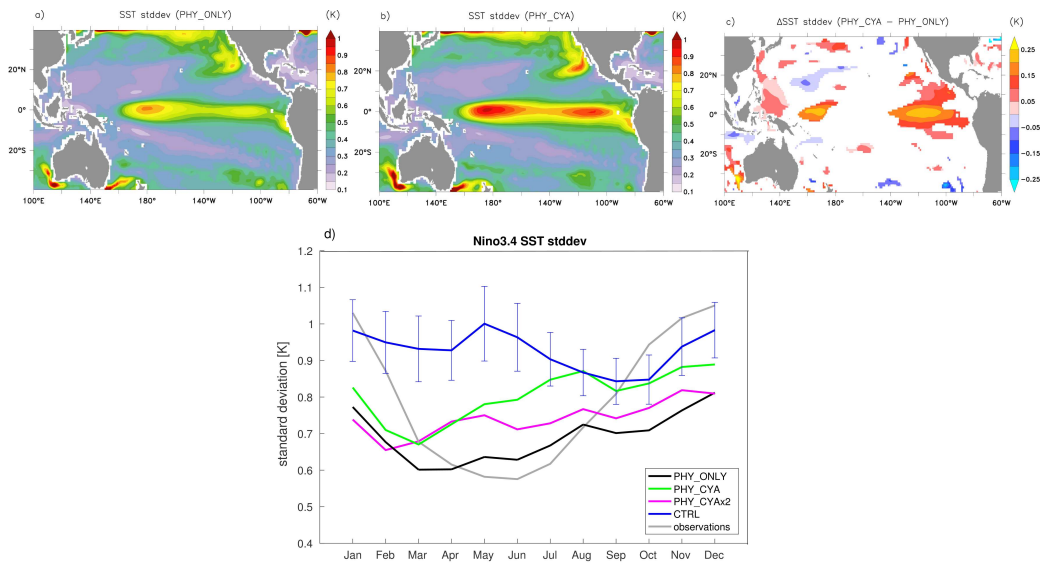


Figure 3.11: Standard deviation of SST [K] in the tropical Pacific in a) PHY_ONLY and b) PHY_CYA, and c) the difference between PHY_CYA and PHY_ONLY. In c), only values larger than two times the standard deviation of eight 100 year periods of experiment CTRL (Appendix Ch3) are shown. d) Seasonal cycle of the standard deviations of the Nino3.4 SST index (SST anomalies averaged over the area 5°S–5°N, 170°W–120°W) for the experiments PHY_ONLY (black), PHY_CYA (green), PHY_CYAx2 (purple), CTRL (blue) and observations (HadISST1, Rayner *et al.*, 2003) (grey). The blue errorbars on the blue curve for CTRL show the standard deviation of eight 100 year periods of CTRL (Appendix Ch3).

The fact that including the retroaction of phytoplankton on the surface ocean heat budget affects ENSO dynamics has already been suggested by numerous model studies (e.g., Timmermann and Jin, 2002; Marzeion *et al.*, 2005; Jochum *et al.*, 2010). Many of the studies, however, hold chlorophyll located at the Equator accountable for this effect. Our study indicates, in agreement with Anderson *et al.* (2009), that especially light absorption off-equator plays a relevant role by modifying equatorial SST and thermocline depth. As cyanobacteria are strongly contributing to the light absorption strength off-equator, they might impose further complexity on the ENSO dynamics which has not been taken into account until now.

3.6 Sensitivity of the results to the strength of cyanobacteria light absorption

As described in Section 3.2.2, the chlorophyll content per cyanobacteria biomass, which is used in this study as a measure of strength of light absorption, is not well constrained. To test the sensitivity and robustness of the results to this parame-

ter, and to assess the possible range of impact, we now compare PHY_CYA_{x2} to PHY_ONLY. In PHY_CYA_{x2}, the chlorophyll content is doubled, that means R_{Cya} is set to a value of 60 mg C (mg Chl)⁻¹, which is roughly at the lower limit of observed values of 40 and 200 mg C (mg Chl)⁻¹ (e.g., *Berman-Frank et al.*, 2001; *Carpenter et al.*, 2004). The maximum difference in surface chlorophyll between the two experiments now reaches values of 1.6 mg Chl m⁻³ in the annual mean (Figure 3.12a).

The patterns of change in SST in PHY_CYA_{x2} compared to PHY_ONLY are consistent with PHY_CYA (Figure 3.12b and 3.2b, respectively). The magnitudes are, however, strongly enlarged. Increasing the surface light absorption strength enhances the shading effect of the subsurface, leading to a stronger subsurface cooling (up to ~1.1 K in the zonal mean compared to ~0.6 K in PHY_CYA, not shown). The water upwelled at the Equator is consequently cooler, resulting in a stronger decrease of SST (e.g. equatorial Pacific: ~0.6 K compared to ~0.3 K in PHY_CYA). Analogous to PHY_CYA, this relatively cooler water is spread laterally and cools large parts of the tropical and subtropical ocean. Also the positive SST signals in the eastern equatorial Atlantic and the eastern tropical Pacific north of the Equator are more pronounced in PHY_CYA_{x2} due to a stronger surface thermal heating effect of local cyanobacteria.

Associated with stronger SST signals, also the response of the atmosphere is enhanced. The stronger zonal SST gradient in the equatorial Pacific results in a Walker circulation more intensified (by 12%, instead of 6% as in PHY_CYA), and shifted more to the west by roughly a factor of two (~6° longitude, instead of ~3° longitude as in PHY_CYA) (Figure 3.5a). The Hadley cells are weakened by 2-5% (instead of 1-3% as in PHY_CYA), together with a more pronounced poleward shift of the outer boundaries, as well as the northward shift of the equatorial boundary between the two cells (not shown). The patterns of change in precipitation are also consistent, however, with enhanced magnitudes (the dominant signal in the western central equatorial Pacific is up to 1.6 mm d⁻¹ (instead of 1.0 mm d⁻¹ as in PHY_CYA). The enhanced response is also visible in the zonal mean precipitation changes (Figure 3.6c). The stronger effects on the atmosphere impose stronger impacts on the ocean circulation, respectively. Upwelling in the western Pacific is intensified (not shown), contributing to the enhanced cooling signal at the surface.

Stronger effects on temperature and circulation (and hence transport of nutrients) imply stronger effects on biological growth and hence phytoplankton concentrations. The patterns of change in bulk phytoplankton and cyanobacteria concentrations are similar, and as for the other quantities, the magnitudes of the signals are enhanced (not shown). This confirms the positive feedback between cyanobacteria light absorption and circulation in the subtropical Pacific as proposed in Section 3.4.4. The stronger absorption strength leads to stronger upwelling and hence enhanced supply of nutrients to the surface, which amplifies the increase

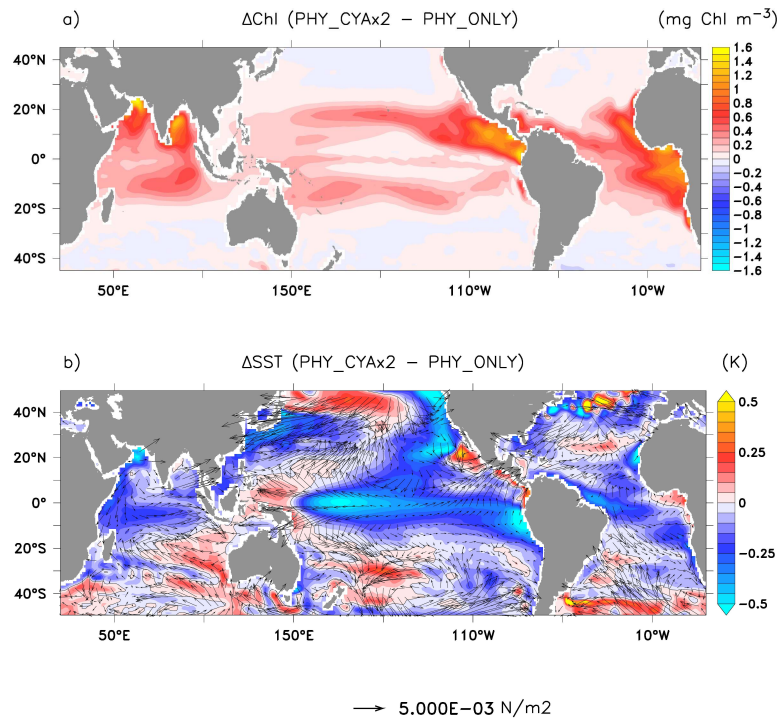


Figure 3.12: Change in the climatological annual mean a) surface (0-20 m) chlorophyll [mg Chl m^{-3}], and b) SST [K] between PHY_CYAx2 and PHY_ONLY. The vectors in b) display windstress anomalies (PHY_CYAx2 - PHY_ONLY) on the ocean.

of cyanobacteria within the subtropical gyres, which further stimulates the process due to a higher shading effect.

Associated with a stronger effect on surface temperature as well as on upwelling strengths, also the amplitude of the seasonal cycle in SST and cyanobacteria concentrations is strongly enhanced (Figure 3.10).

With respect to the effect on ENSO dynamics, the stronger decrease in equatorial SST and thermocline depth in PHY_CYAx2 compared to PHY_CYA would let expect a higher variability in ENSO. This is, however, not the case (Figure 3.11d). The limits of the short experiment period relative to the rather large variability even on centennial timescales have, however, to be kept in mind.

It can be summarized that the response patterns to light absorption by cyanobacteria, both in physical and in biogeochemical quantities, are in general consistent in the two experiments PHY_CYA and PHY_CYAx2. This can be seen as a proof of concept that the signals and proposed mechanisms are indeed robust. The magnitudes of the signals, however, strongly depend on the prescribed strength of light absorption per cyanobacteria biomass. Since this parameter is not well constrained, there is a considerable potential range of impact of cyanobacteria light absorp-

tion. Chlorophyll concentrations, which are used as a measure of strength of light absorption in this study, are derived linearly from the phytoplankton concentrations and thus have to be seen as a rough first order approximation. The value of $60 \text{ mg C (mg Chl)}^{-1}$ as applied in PHY_CYAx2, is situated in the upper range of observations (e.g., *Berman-Frank et al.*, 2001; *Carpenter et al.*, 2004; *Sathyendranath et al.*, 2009). The effects in this experiment can thus be roughly seen as upper limit. However, although chlorophyll is the primary absorber, cyanobacteria contain other pigments, like phycocyanin, which also absorb shortwave radiation in the visible range (e.g., *Navarro Rodriguez*, 1998), but are not accounted for in the model parameterization. In addition to uncertainties in the light absorption strength per cyanobacteria biomass, also uncertainties in the cyanobacteria distribution itself affect the validity of the model results. As discussed in *Paulsen et al.* (2017) (Chapter 2 of this thesis), the model underestimates cyanobacteria concentrations in the North Atlantic subtropical gyre. Related to that, the surface cooling effect might be underestimated. On the other hand, the model seems to overestimate cyanobacteria concentrations in the tropical east Pacific, and thus also likely the cooling effect of the Pacific cold tongue. Although more observations are needed to further constrain the effects of cyanobacteria on the climate system, the results nevertheless indicate the potential of this phytoplankton group to play a relevant role in the Earth system.

3.7 Implications for the Earth system model

In this study, we focused on the added impact of including prognostic cyanobacteria in complement to bulk phytoplankton in the dynamic biological shortwave heating on the Earth system. In the standard model MPI-ESM (e.g., *Jungclaus et al.*, 2013; *Ilyina et al.*, 2013), the interactive retroaction of phytoplankton on the heat budget is, however, not accounted for at all. Instead, a globally uniform optical water type is applied (Appendix Ch3), as done in many climate models. In the following, we set the results of the present study in the context of the standard model version and observations.

Figure 3.13a shows the SST bias of the standard model version (CTRL, see Appendix Ch3) in comparison to the PHC3 climatology (a blend of the *Levitus et al.* (1998) data with an updated data set for the Arctic from *Steele et al.* (2001)). Including the active biogeophysical feedback of both phytoplankton groups (PHY_CYA) reduces some of the model biases in comparison to CTRL (Figure 3.13b). In particular, the clearer water in the subtropical gyres in PHY_CYA compared to the constant attenuation depth of 17 m in CTRL (which roughly refers to $0.44 \text{ mg Chl m}^{-3}$) leads to a warming of the subsurface water that is eventually upwelled at the equator. This reduces the Pacific cold bias by 0.7 K (~25%) and improves the precipitation bias in the western equatorial Pacific (not shown). Without cyanobacteria in the

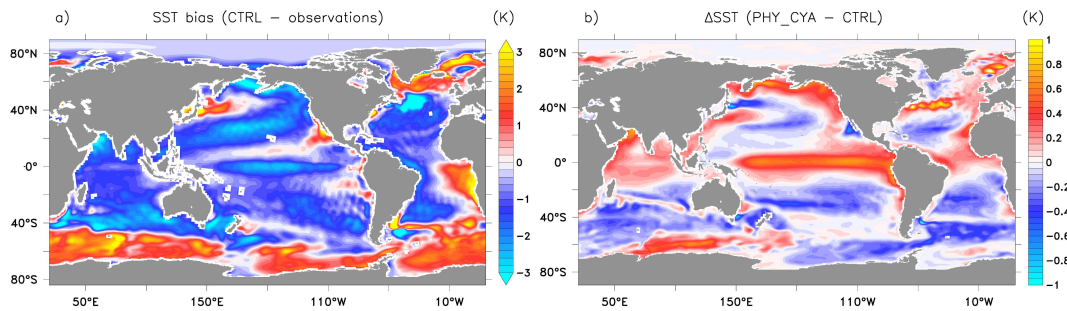


Figure 3.13: a) SST [K] bias of CTRL (Appendix Ch3) compared to observations (PHC3 climatology). b) Difference in SST [K] between PHY_CYA and CTRL.

feedback, that means light absorption only by bulk phytoplankton (PHY_ONLY), the heating of the Pacific cold tongue – and hence the improvement with respect to the Pacific SST bias – compared to CTRL is even larger than is the case for PHY_CYA (the cooling effect shown in Figure 3.2b of 0.3 K has to be subtracted). The fact that a better SST pattern exists when not accounting for cyanobacteria might have two reasons. First, as mentioned in Section 3.3, the chlorophyll of bulk phytoplankton in the subtropical gyres is slightly overestimated in comparison to satellite data (potentially due to the missing depth dependent C:Chl ratio). This model deficit might lead to an underestimation of the subsurface heating and the related equatorial surface warming. Second, the model is tuned to best possibly represent the climate state in a model version without the biogeophysical feedback. The fact that including cyanobacteria, which to our best knowledge should improve the representation of distribution of light absorption, does however regionally deteriorate the model biases, might indicate the demand for a retuning of certain model parameters. In particular, the parameterization of mixing at the base of and below the mixed layer could play a role (Ballabrera-Poy *et al.*, 2007; Gnanadesikan and Anderson, 2009).

What should, however, be emphasized with regard to the results, is the regulative effect that including cyanobacteria has on equatorial SST. Considering cyanobacteria in complement to bulk phytoplankton in the feedback changes the signal (compared to only bulk phytoplankton) by $\sim 30\%$ (PHY_CYA - CTRL: 0.7 K, PHY_ONLY - CTRL: 1.0 K). This magnitude (0.3 K) is comparable to differences in equatorial Pacific SST which is seen between different model resolution configurations, MPI-ESM-MR and MPI-ESM-LR, of ~ 0.75 K (Jungclaus *et al.*, 2013).

Associated with a reduction of the SST bias of the Pacific cold tongue due to including the interactive biogeophysical feedback, also the representation of tropical Pacific variability is improved compared to observations. All simulations with feedback included (PHY_ONLY, PHY_CYA, PHY_CYA $\times 2$) seem to be closer to observations with respect to the seasonal cycle of variability than CTRL (Figure 3.11d).

Without accounting for cyanoacteria, the agreement, again, seems to be slightly better. This demonstrates that the relevance of details in the distribution of marine biota also counts for tropical climate variability.

In certain regions, such as the eastern boundary upwelling regions off South America and Africa, the cooling effect caused by including cyanobacteria reduces the SST bias in the model in PHY_CYA compared to PHY_ONLY (relative to CTRL). The magnitude of the reduction is, however, small compared to other relevant factors, such as the resolution of the atmospheric model which was shown to be largely responsible for the bias in MPI-ESM (*Milinski et al.*, 2016). Nevertheless, our results show that the sensitivity of SST to details in the spatial distribution of light absorption by marine biota, indeed, adds another level of complexity which is largely independent of the model resolution and which should be taken into account in considerations of the model biases.

This study has to be seen as first attempt to include and understand the effects of distinct phytoplankton groups in the absorption feedback in a climate model. What the results already reveal is that uncertainties in the simulated distribution of marine biota and light absorption strength, which undoubtedly exist, propagate through the Earth system with effects on climate relevant scales and magnitudes. More attention should hence be paid to the representation of marine biota and its impact on radiative heating in climate models. We show that the functional group of surface buoyant, N₂-fixing cyanobacteria is a potential candidate to be of climatic importance in the Earth system, not only due to its role in the marine nitrogen cycle and the carbon-climate feedback, but also its role in the light absorption feedback.

3.8 Summary and Conclusions

We apply the comprehensive Earth system model MPI-ESM to study the effects of light absorption by marine cyanobacteria on the climate system. We find that accounting for prognostic cyanobacteria in addition to bulk phytoplankton in the attenuation depth of light has regional but sizeable effects in the Earth system model in areas relevant for ocean biogeochemistry and climate variability.

Cyanobacteria induce a surface cooling on mean tropical SST on the large scale. This is because cyanobacteria biomass, located throughout the tropical and subtropical ocean, shades and hence cools the subsurface water that is upwelled at the equator and in eastern boundary upwelling regions, reducing mean SST by up to 0.5 K in these areas. The advective process of bringing cooler subsurface water to the surface outweighs the direct heating effect that was indicated by observations and idealized one-dimensional studies locally. Implications of the regional cooling effect for the climate system include a strengthening (~6%) and westward shift (~3°

longitude) of the Walker circulation, as well as changes in the precipitation patterns by up to 1.0 mm d^{-1} . Changes in ocean temperature and circulation feed back on cyanobacteria growth itself, imposing complex patterns of positive and negative feedback loops. Furthermore, the amplitude of the seasonal cycle of SST in areas where cyanobacteria are abundant is increased by up to 20%. Tropical Pacific variability is enhanced by roughly 30%. The magnitudes of all effects are thereby sensitive to the prescribed strength of light absorption per cyanobacteria biomass.

Apart from the cooling in the southeastern Atlantic and Pacific coastal upwelling regions, which reduces the model warm bias here, the changes induced by including cyanobacteria do generally not improve the model state in comparison to observations. The importance of the results lies rather in the demonstrated sensitivity of the simulated climate mean state and variability to details in the distribution and representation of marine biota. In light of the uncertainties in the spatial distribution and light absorption strength of phytoplankton, the results stress the need for more observations to further constrain and better represent the effects of biological light absorption on climate in Earth system models. Our results indicate that cyanobacteria, due to their remote, regulative effect on tropical SST in areas relevant for ocean biogeochemistry and climate variability, are important to be considered.

Appendix Ch3: Standard MPI-ESM version with globally uniform light absorption

In the standard model MPI-ESM (e.g. used in CMIP5; *Jungclaus et al., 2013*), which is applied in experiment CTRL, the vertical distribution of light $I(z)$ in the ocean is prescribed by a globally uniform exponential profile after *Paulson and Simpson (1977)*:

$$I(z) = I_0 \cdot f_{blue} \cdot \exp(k_{blue} \cdot z) \quad (3.4)$$

with I_0 as the incoming shortwave radiation that reaches the sea surface. The attenuation coefficient k_{blue} of 0.06 m^{-1} (attenuation depth: 17 m) and the blue water fraction f_{blue} of 0.41 roughly correspond to the Jerlov optical water type 1A (*Jerlov, 1976; Kara et al., 2005*). The attenuation depth of 17 m is in the order of magnitude of values typically used in climate models (*Patara et al., 2012*, and references therein).

Chapter 4

Impacts of phytoplankton light absorption on climate under rising CO₂

4.1 Introduction

The feedback from phytoplankton light absorption on the upper ocean heat budget considerably influences climate mean state and variability (e.g., *Wetzel et al.*, 2006; *Patara et al.*, 2012). Under global warming, the distribution of phytoplankton – and concomitantly light absorption – is expected to change (e.g., *Bopp et al.*, 2013). How these changes in the abundance and biogeography of phytoplankton feed back on the changing climate itself remains unknown. We apply a comprehensive Earth system model to explore the potential of changes in phytoplankton light absorption to alter climate projections under rising CO₂.

Phytoplankton, dependent on the availability of light, grows exclusively in the upper sunlit ocean. By converting the absorbed light into heat, phytoplankton modifies the temperature distribution in the water column. Model studies consistently show considerable effects of this feedback on the ocean heat budget, with implications for ocean circulation as well as for the climate mean state and variability (e.g., *Wetzel et al.*, 2006; *Anderson et al.*, 2007; *Patara et al.*, 2012). Although previous studies differ with respect to the simulated magnitudes and signs of the effects (*Patara et al.*, 2012, and references therein), all studies agree on the importance of including the feedback from phytoplankton on the ocean heat budget in climate models. Some CMIP5 models indeed already include the biogeophysical feedback (*Hense et al.*, 2017, and references therein).

With a changing climate, the phytoplankton abundance and biogeography – and

hence feedback strengths and patterns – will change. Nearly all previous model studies dealing with the biogeophysical feedback from phytoplankton on climate, however, only applied a constant climate state and did not consider the effects of long-term changes in the phytoplankton distribution. The only exception is the study of *Park et al.* (2015) who showed in transient simulations that in the Arctic a positive feedback between sea ice and phytoplankton could amplify Arctic warming. Thereby, a decline in sea ice promotes phytoplankton growth and hence surface light absorption, which, in turn, promotes warming and sea ice melting. Apart from the Arctic, the effects of changes in phytoplankton on other regions of the Earth are unexplored.

A region where large long-term changes in phytoplankton abundance (and consequently water turbidity) are expected under greenhouse warming is the tropical and subtropical ocean. Increased stratification and reduced ventilation decrease the supply of nutrients to the surface and impair growth conditions of phytoplankton (*Behrenfeld et al.*, 2006; *Falkowski and Oliver*, 2007). Model studies concordantly project a decline in net primary production in the tropical and subtropical ocean (*Bopp et al.*, 2013; *Laufkötter et al.*, 2015). Satellite observations support the simulated negative trend in phytoplankton abundance and indicate an expansion of the low-chlorophyll ocean deserts of the subtropical gyres (*Polovina et al.*, 2008).

At the same time, it is known that particularly in the tropical and subtropical ocean changes in turbidity have large effects on climate mean state and variability (Chapter 3 of this thesis; *Gnanadesikan and Anderson*, 2009; *Anderson et al.*, 2007). Hence, the question arises how the projected decline in phytoplankton in the tropical and subtropical ocean – and associated changes in water turbidity – alter climate's response to increasing CO₂. Do related changes in the biogeophysical feedback regionally amplify or damp the effects of transient CO₂ forcing? It is speculated that a decline in phytoplankton would cool the surface ocean due to decreased surface light absorption and thus counteract the warming associated with climate change (*Patara et al.*, 2012). Other model studies, on the contrary, would rather suggest the opposite effect, that means an amplified surface warming, due to advective processes (Chapter 3 of this thesis; *Anderson et al.*, 2007, 2009; *Gnanadesikan and Anderson*, 2009; *Jochum et al.*, 2010). However, until now no transient simulations have been done to further investigate these diverging hypotheses.

To address this question we apply the state of the art Earth system model of the Max Planck Institute for Meteorology (MPI-ESM). We perform idealized 1% atmospheric CO₂ increase per year scenarios with and without including the full biogeophysical feedback of phytoplankton light absorption and assess the relative difference in the response of climate to the transient CO₂ forcing. We thereby focus on the tropics and subtropics, and analyze effects on ocean and atmosphere temperatures, wind and precipitation patterns, as well as the feedback from changes in physics on phy-

toplankton growth itself.

As mentioned above, models (including MPI-ESM) generally agree on the decline in primary production and phytoplankton concentrations in the tropical and subtropical ocean under rising CO₂ (Bopp *et al.*, 2013). The validity of these projections is, however, quite uncertain and the projected decline still a matter of debate (Sarmiento *et al.*, 2004; Boyce *et al.*, 2010; Laufkötter *et al.*, 2015). The representations of ecosystems in the global biogeochemistry models as part of Earth system models rely on rather simple underlying assumptions that control the biogeochemical processes. Some key phytoplankton groups, however, respond differently than bulk phytoplankton to climate stressors and may benefit from climate change. In particular, cyanobacteria, which represent an important phytoplankton group in the tropical and subtropical ocean (Capone *et al.*, 1997), and further have been shown to play a relevant role in the light absorption feedback (Chapter 3 of this thesis; Sonntag and Hense, 2011; Sonntag, 2013), are expected to benefit under increasing temperatures and stratification (Paerl and Huisman, 2008) and decreasing pH (Hutchins *et al.*, 2007; Levitan *et al.*, 2007; Barcelos e Ramos *et al.*, 2007; Kranz *et al.*, 2009). Furthermore, the ability to utilize dissolved organic phosphorus (DOP) in addition to phosphate (PO₄) (Sohm and Capone, 2006; Dyhrman *et al.*, 2006) might help cyanobacteria to cope with the intensified phosphate limitation under global warming. If these potential physiological advantages and adaptations are however sufficient to lead to an overall increase in the abundance of cyanobacteria is quite uncertain (Hutchins and Fu, 2017). Moreover, to what extent cyanobacteria could counteract the decline in overall phytoplankton, and thereby alter the effects of the biogeophysical feedback associated with light absorption, is unresolved. To address these questions, we run one additional future scenario in which we modify the growth parameterization of the prognostic cyanobacteria in the model by providing them with a set of proposed potential physiological advantages and adaptation mechanisms. This additional scenario serves two goals. First, we further explore the hypothesis that cyanobacteria might increase under rising CO₂ given the potential physiological advantages and adaptations. And second, the scenario serves as a test case to assess how sensitive climate's evolution reacts to a different development of the phytoplankton distribution in the tropical and subtropical ocean.

The remaining chapter is organized as follows. Section 4.2.1 gives a brief overview of MPI-ESM, followed by a description of the parameterization of light absorption in the different setups, as well as the experimental strategy (Section 4.2.2). Section 4.3 compares the respective preindustrial control states from which the scenarios are started. The evolution of phytoplankton in the transient simulations is given in Section 4.4, before we describe the resulting effects on climate (Section 4.5). Afterwards, we show the results of the modified parameterization of cyanobacteria in Section 4.6 and how the different evolution of phytoplankton affects the respective response of

climate to rising CO₂. In the end, we discuss the major findings and implications (Section 4.7) and present our conclusions (Section 4.8).

4.2 Model description and experimental setup

4.2.1 The MPI-ESM

We use MPI-ESM, which consists of the coupled general circulation models for the atmosphere ECHAM6 (*Stevens et al., 2013*), and the ocean MPIOM (*Jungclaus et al., 2013*), and the ocean biogeochemistry model HAMOCC5.2 (*Ilyina et al., 2013*) extended by prognostic N₂-fixing cyanobacteria (*Paulsen et al., 2017*, Chapter 2 of this thesis), and the land carbon and vegetation model JSBACH (*Reick et al., 2013; Schneek et al., 2013*). We apply a grid configuration referred to as LR (GR15 for MPIOM, T63L47 for ECHAM6). In the atmosphere, the horizontal resolution is T63 in spectral space (approximately 1.75° on a Gaussian grid) with 47 vertical σ -hybrid layers. The time step is 450 seconds. In the ocean, the bipolar grid GR15 has poles over Antarctica and Greenland and a horizontal resolution of approx. 1.5°, gradually varying between 15 km in the Arctic and about 184 km in the tropics. In the vertical, there are 40 unevenly spaced layers with level thicknesses increasing with depth, whereby eight layers are located within the upper 90 m. The time step is 2700 seconds. MPIOM is a z-coordinate global general circulation model solving the primitive equations under the hydrostatic and Boussinesq approximation on a C-grid with a free surface (*Marsland et al., 2003; Jungclaus et al., 2013*). Momentum, heat and freshwater fluxes are coupled daily between ECHAM and MPIOM using the Ocean Atmosphere Sea Ice Soil (OASIS3-MCT; *Valcke, 2013*) coupler. Incoming shortwave radiation is passed also daily from ECHAM to MPIOM.

The global ocean biogeochemistry model HAMOCC as component of MPI-ESM serves to simulate carbon cycling in the ocean. The spatial and temporal resolution of HAMOCC is inherited from MPIOM. Details on the coupling of HAMOCC and MPIOM are given in *Maier-Reimer et al. (2005)*. We use the version HAMOCC 5.2 (*Ilyina et al., 2013*), extended by a prognostic representation of N₂-fixing cyanobacteria (*Paulsen et al., 2017*, Chapter 2 of this thesis). HAMOCC includes biogeochemical processes in the water column, the sediment, and at the air-sea interface. Biogeochemical tracers in the water column are fully advected, mixed and diffused by the flow field of the physical model. Biogeochemistry dynamics, which are premised on an extended NPZD (nutrients, phytoplankton, zooplankton, detritus) model approach (*Six and Maier-Reimer, 1996*), include the compartments nutrients (phosphate, nitrate, and iron), oxygen, silicate, opal, calcium carbonate, dissolved organic carbon, alkalinity, phytoplankton (bulk phytoplankton and N₂ fixers), zooplankton, dissolved organic matter, and detritus. Organic material is composed following a

Table 4.1: Experiment names and descriptions.

Experiment name	Description
NoFB_pi	pi-control run, no feedback
NoFB_1%	1% atm. CO ₂ increase per year, no feedback
FB_pi	pi-control run, with feedback
FB_1%	1% atm. CO ₂ increase per year, with feedback
FBcya_pi	pi-control run, with feedback, modified cyanobacteria param.
FBcya_1%	1% atm. CO ₂ increase per year, with feedback, modified cyanobacteria param.

constant Redfield ratio (C:N:P:O₂ = 122:16:1:-172) based on *Takahashi et al.* (1985) and of the micronutrient iron (Fe:P = 366·10⁻⁶:1) (*Johnson et al.*, 1997). Below 100 m, the sinking speed of organic matter increases linearly with depth after *Martin et al.* (1987). Atmospheric deposition of iron is accounted for by applying the present-day climatology of monthly atmospheric dust deposition from *Mahowald et al.* (2006). It is assumed that a fixed fraction of the dust deposition (3.5 %) is iron, of which 1 % is biologically available. Iron complexation by organic substances (ligands) takes place at dissolved iron concentrations larger than 0.6 nmol L⁻¹. Dissolved iron is removed from the water column with a constant rate (*Parekh et al.*, 2005; *Archer and Johnson*, 2000).

Phytoplankton is represented by two tracers in the model, N₂-fixing cyanobacteria (Cya) and bulk phytoplankton (Phy). The growth parameterization of cyanobacteria is based on physiological characteristics of the cyanobacterium *Trichodesmium* (*Paulsen et al.*, 2017, Chapter 2 of this thesis). The major difference between N₂ fixers as compared to bulk phytoplankton in the model is their ability to fix N₂. In contrast to bulk phytoplankton, cyanobacteria are hence not limited by nitrate. However, when available, they nevertheless take up nitrate. Furthermore, cyanobacteria in the model are positively buoyant and have a specific optimum temperature range, with an optimum at 28.0°C (in contrast to bulk phytoplankton for which the Eppley curve is applied, see *Eppley*, 1972). Cyanobacteria grow slower than bulk phytoplankton and have a high iron limitation. A detailed description of the parameterization as well as evaluation of the model performance with respect to cyanobacteria are given in *Paulsen et al.* (2017) (Chapter 2 of this thesis).

4.2.2 Parameterizations of radiative heating in the ocean and experiment description

The radiative heating of the water column in the ocean general circulation model is accounted for by an internal source of heat in the temperature equation, proportional to the vertical derivative of the light profile $I(z)$:

$$\frac{\partial T}{\partial t} = \frac{1}{\rho \cdot c_p} \cdot \frac{\partial I(z)}{\partial z} \quad (4.1)$$

with ρ as the density and c_p the specific heat capacity of seawater.

In order to assess the effects of including the feedback from phytoplankton on climate projections under rising CO₂, we conduct three sets of experiments with different parameterizations of the light field $I(z)$ (Table 4.1). The first set of experiments prescribes a globally uniform exponential profile of light based on an optical water type. In the second set, the feedback from phytoplankton on the light field is activated. The third set is analogous to the second set. In addition, we introduce potential physiological advantages and adaptation mechanisms of cyanobacteria which allow them to better cope with the environmental stressors associated with climate change under rising CO₂. Details about the three experimental setups are given in the following.

First set of experiments: Globally uniform light absorption

In the first setup (NoFB), heat is distributed in the ocean using a globally uniform exponential profile of light $I(z)$ prescribed after *Paulson and Simpson (1977)*:

$$I(z) = I_0 \cdot f_{blue} \cdot \exp(k_{blue}z). \quad (4.2)$$

I_0 [$W\ m^{-2}$] is the incoming shortwave radiation that reaches the sea surface. The applied attenuation coefficient k_{blue} of $0.06\ m^{-1}$ (attenuation depth: 17 m) and the blue water fraction f_{blue} of 0.41 roughly correspond to the Jerlov optical water type 1A (*Jerlov, 1976; Kara et al., 2005*). This formulation is used in the standard version of MPI-ESM (e.g., *Jungclaus et al., 2013*). The attenuation depth of 17 m is in the order of magnitude as often used in climate models (*Patara et al., 2012*, and references therein).

Second set of experiments: Phytoplankton-dependent light absorption

In the second set of experiments (FB), we include the interactive feedback from phytoplankton on the heat budget. Chlorophyll is thereby used as a measure of strength of light absorption. We apply the chlorophyll-dependent light absorption scheme after *Zielinski et al. (2002)* as described in Chapter 3 of this thesis:

$$I(z) = I_0 \cdot f_{vis} \left[\sigma \cdot \exp(-z \cdot k_r) + (1 - \sigma) \cdot \exp(-z \cdot k_w - k_{Chl} \cdot \int_0^z Chl(z) dz) \right]. \quad (4.3)$$

Here, f_{vis} is the visible light fraction (0.58), covering the wavelength range of 400–700 nm which has the potential to penetrate into deeper layers. The light spectrum is divided at 580 nm, prescribed by $\sigma = 0.4$, into two domains: Whereas for larger

wavelengths (red domain) attenuation is dominated by sea water with the attenuation coefficient k_r (0.35 m^{-1}), for shorter wavelengths (blue/green domain) the absorption by chlorophyll with the absorption coefficient k_{Chl} (0.04 m^{-1}) is considered in addition to clear water with the absorption coefficient k_w (0.03 m^{-1}). Chlorophyll (Chl) is a linear function of the concentrations of bulk phytoplankton and cyanobacteria:

$$Chl(z) = \frac{1}{R_{Phy}} \cdot Phy(z) + \frac{1}{R_{Cya}} \cdot Cya(z). \quad (4.4)$$

The observed C:Chl ratio (R) in phytoplankton varies from about 12 to more than $200 \text{ mg C (mg Chl)}^{-1}$ depending on species, light conditions, nutrient limitation and temperature (e.g., *Taylor et al.*, 1997). We choose $R_{Phy} = 60 \text{ mg C (mg Chl)}^{-1}$ for bulk phytoplankton (*Ilyina et al.*, 2013) and $R_{Cya} = 120 \text{ mg C (mg Chl)}^{-1}$ for cyanobacteria. Cyanobacteria generally contain less chlorophyll than other phytoplankton and the chosen value lies in the middle of the observed range of ~ 40 to $200 \text{ mg C (mg Chl)}^{-1}$ (e.g., *Sathyendranath et al.*, 2009; *Carpenter et al.*, 2004; *Berman-Frank et al.*, 2001). This implies that under the same level of incoming shortwave radiation, the presence of cyanobacteria of the same biomass than bulk phytoplankton reduces the attenuation depth only half as efficient as bulk phytoplankton. It is assumed that the total absorbed light is converted into heat. Biological fluorescence mostly converts into heat, and the absorbed energy stored in biomass is generally small and can be neglected (*Lewis et al.*, 1983, and references therein).

Third set of experiments: Phytoplankton-dependent light absorption and additional physiological characteristics and adaptation mechanisms of cyanobacteria

Several studies propose cyanobacteria to become one of the "winners" of climate change (*Hutchins and Fu*, 2017, and references therein). Besides the ability to fix N_2 , a number of other physiological traits and adaptation mechanisms have been proposed to help cyanobacteria to benefit from changes in the environmental conditions. We therefore run one additional scenario, in which we provide cyanobacteria with these potential traits. This additional scenario serves, on the one hand, to further explore the hypothesis that cyanobacteria increase their abundance under global warming. On the other hand, we use the additional experiment to test the sensitivity of the results with respect to the feedback on climate to a different evolution of phytoplankton and chlorophyll.

In this third set of experiments (FBcya), the feedback from phytoplankton on temperature is active, analogous to the setup FB (Section 4.2.2), however, three modifications are done – at the same time – to the growth (g) parameterization of cyanobacteria. The growth rate (g) of cyanobacteria is given by multiplying the maximum

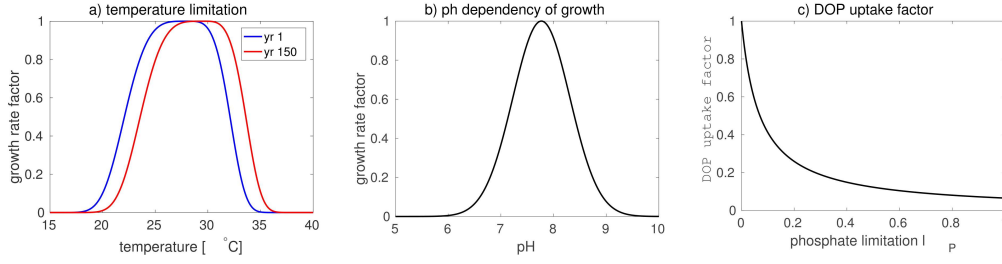


Figure 4.1: Modified growth characteristics of cyanobacteria in the setup FBcya: a) Temperature limitation l_T at the beginning of the simulation FBcya_1% (blue) and at the end of the simulation (red) (Equation 4.6,4.7). b) pH-dependency of growth (as in Equation 4.8 but divided by the maximum growth rate μ_{max}). c) Function of the DOP uptake factor f_{DOP} (Equation 4.10).

growth rate μ_{max} with the respective limiting functions:

$$g = \mu_{max} \cdot l_L \cdot l_T \cdot l_{Fe} \cdot l_P. \quad (4.5)$$

with l_L light limitation, l_T temperature limitation, l_{Fe} iron limitation, and l_P phosphate limitation (see Chapter 2 for a detailed description). The three modifications in setup FBcya are as follows: (1) We let cyanobacteria adapt to higher temperatures by adjusting the optimum temperature towards higher values. (2) We apply a pH-dependent growth rate. (3) We allow cyanobacteria to take up DOP as additional phosphorus source. Although some studies propose the increased dust deposition to be an important factor in driving higher N₂ fixation (e.g., *Krishnamurthy et al.*, 2009), in our simulations, iron seems not to be the limiting factor under rising CO₂ (see Section 4.4). Hence, we focus on the three factors listed above, which will be explained in more detail in the following.

(1) Temperature adaptation Cyanobacteria are known to have a high optimum temperature. The default parameter value for the optimum temperature is set to 28.0°C in the model, based on the observed value for *Trichodesmium* (*Breitbarth et al.*, 2007). Temperature limitation is described by a modified Gaussian function around this optimum temperature based on *Sonntag* (2013):

$$l_T(T, T_{opt}) = \exp \left[-\frac{(T - T_{opt})^4}{(T_1 - T_2 \cdot \Gamma)^4} \right], \quad \text{with } \Gamma = \begin{cases} -1 & \text{for } T < T_{opt} \\ 0 & \text{for } T = T_{opt} \\ 1 & \text{for } T > T_{opt} \end{cases} \quad (4.6)$$

with $T_1 = 5.5$ °C and $T_2 = 1$ °C.

With increasing CO₂ forcing, temperatures exceed 28.0°C by far in the tropical ocean. As species may respond with genetic adaptation to alterations in the environmental conditions, which can generally occur on relatively short time scales (e.g.,

Padfield et al., 2016), we shift the optimum temperature of cyanobacteria linearly with time from $T_{opt_0} = 28.0^\circ\text{C}$ at the beginning of the simulation to $T_{opt_{150}} = 29.5^\circ\text{C}$ at the end of the simulation (Figure 4.1a):

$$T_{opt}(\text{yr}) = T_{opt_0} + \frac{T_{opt_{150}} - T_{opt_0}}{150 \text{ yrs}} \text{ yr} \quad (4.7)$$

Here, yr is the year in the simulation period between 1 and 150. The time dependent optimum temperature enters the formulation of temperature limitation of growth l_T (Equation 4.6).

(2) pH-dependent growth rate Culture studies show stimulated N_2 fixation rates of the open ocean cyanobacterium *Trichodesmium* by 35% to 65% from present-day (375–380 ppm) to projected year 2100 atmospheric pCO_2 (~750 ppm) (*Hutchins et al.*, 2007; *Levitan et al.*, 2007; *Barcelos e Ramos et al.*, 2007; *Kranz et al.*, 2009). Related to this, similar increases in carbon fixation and/or growth rates by increased CO_2 (decreased pH) were observed. Based on this observational evidence, we introduce a pH-dependent growth rate of cyanobacteria in our model. We use a Gauss curve fitted to the observations of *Trichodesmium* (*Barcelos e Ramos et al.*, 2007), based on the work of *Hinners* (2014) (Figure 4.1b), and replace μ_{max} in Equation 4.5 by μ_{max_pH} :

$$\mu_{max_pH}(\text{pH}) = \mu_{max} \exp \left[\frac{-(\text{pH} - \text{pH}_{opt})^2}{\text{pH}_{slope}} \right] \quad (4.8)$$

with $\text{pH}_{opt} = 7.7$ and $\text{pH}_{slope} = 0.59$. The maximum growth rate, μ_{max} , which has a value of 0.2 d^{-1} in the first two model setups (*Paulsen et al.*, 2017, Chapter 2 of this thesis), is adjusted to a value of 0.25 d^{-1} , so that for a preindustrial surface pH value of 8.15 (spatial average over 40°S – 40°N) a growth rate μ_{max_pH} of roughly 0.2 d^{-1} holds.

(3) Uptake of DOP Cyanobacteria growth is strongly limited by phosphate (e.g., *Sohm et al.*, 2011). Under global warming, this limitation will probably become stronger. Several studies, however, propose cyanobacteria to be able to utilize DOP to meet their phosphorus needs (*Sohm and Capone*, 2006; *Dyhrman et al.*, 2006; *Sohm et al.*, 2011). We account for this potential additional phosphorus source by letting cyanobacteria – depending on the strength of phosphate limitation – grow on DOP in addition to phosphate. As DOP is not prognostically represented in the model but part of the dissolved organic matter (DOM) pool, we parameterize the DOP uptake (or DOM uptake, respectively) as follows. Cyanobacteria grow on available phosphate as described in *Paulsen et al.* (2017) (Chapter 2 of this thesis). Additionally,

cyanobacteria can use DOP (DOM). Growth on DOP (DOM) is formulated analogous to growth on phosphate, only that the phosphate concentrations in the limiting function l_P are exchanged by the DOP fraction of the DOM pool:

$$l_{DOP} = f_{DOP} \frac{DOP}{K_P + DOP}. \quad (4.9)$$

Hereby, f_{DOP} is a function that describes the ability to utilize DOP depending on the phosphate limitation (l_P) (Figure 4.1c). The stronger the phosphate limitation (that means the lower l_P), the higher is the ability to utilize DOP:

$$f_{DOP} = 1 - \frac{l_P}{0.07 + l_P} \quad (4.10)$$

with

$$l_P = \frac{PO_4}{K_P + PO_4}. \quad (4.11)$$

Due to the higher energetic expense of utilizing DOP compared to PO₄ (Landolfi *et al.*, 2015, and references therein), we reduce the maximum growth rate to two third of the value for PO₄ in case of growth on DOP. The half saturation constant K_P of $1 \cdot 10^{-8}$ kmol P m⁻³ is also applied for DOP. As all other compounds besides phosphorus, i.e., carbon, nitrogen, and iron, are part of the DOM pool (according to the Redfield ratio), the concentrations of the respective pools (nitrate, carbon, and iron) are not altered in the process of cyanobacteria growth on DOP (DOM). Furthermore, no N₂ fixation takes place.

Experimental strategy

For each of the three sets of experiments (NoFB, FB, and FBcya), we run a preindustrial (1850) control simulation with constant atmospheric CO₂ concentrations (284.7 ppm), NoFB_pi, FB_pi, and FBcya_pi, respectively. The simulations NoFB_pi and FB_pi are run for 400 years, until the upper ocean has adjusted to the feedback from biology on physics in FB_pi and shows no considerable trends anymore. FBcya_pi is started from the end of the simulation FB_pi and integrated for another 125 years. Starting from these three preindustrial control states, we perform idealized transient 1% atmospheric CO₂ increase per year scenarios with prescribed atmospheric CO₂ concentrations, NoFB_1%, FB_1%, and FBcya_1%, for 150 years. The CO₂ concentrations are thereby doubled after 70 years, and quadrupled after 140 years. All other forcings are as in the control simulations. For the first two setups (NoFB_1%, FB_1%) three realizations are conducted and for the third setup (FBcya_1%) two realizations.

By comparing the evolution of climate relative to the respective preindustrial (pi) control climate state we assess the effects of the changing phytoplankton distribution on climate's response to increasing CO₂. We evaluate the difference at the end of the simulation (ensemble mean of the last 20 years) against the mean climate of the control state (mean of the last 100 years).

Before we compare the transient simulations, we first evaluate the two preindustrial control climate states NoFB_pi and FB_pi from which the scenarios are started against each other (last 100 year means).

4.3 Comparison of the preindustrial control climate states with globally uniform light absorption and with phytoplankton-dependent light absorption

Including the feedback from phytoplankton light absorption on the upper ocean heat budget alters the simulated preindustrial climate mean state and variability compared to the standard model which applies a globally uniform exponential profile of light. As a consequence, the respective idealized CO₂ increase scenarios start from different control states. Here, we briefly summarize the differences in the respective climate states of the control runs NoFB_pi, FB_pi, and FBcya_pi. As the climate states in the two setups with active feedback, FB_pi and FBcya_pi are similar, we describe only the differences between NoFB_1% and FB_1%.

Global mean surface air temperatures and sea surface temperatures (SSTs) are nearly identical in NoFB_pi and FB_pi (surface air temperature 13.9°C, SST 17.5°C, in both setups). In the regional patterns, however, sizeable differences occur (Figure 4.2a). The main effect of including the chlorophyll-dependent light absorption comes about through the deeper penetration of light within the low-chlorophyll subtropical gyres. The attenuation depth of 17 m as used in NoFB_pi corresponds to a surface chlorophyll value of roughly 0.44 mg Chl m⁻³ in Equation 4.3 (if transferred into units of chlorophyll). In the subtropical gyres, where chlorophyll derived from the biogeochemical model is considerably lower, shortwave radiation penetrates deeper into the water column in FB_pi, which leads to a cooling of the surface and heating of the subsurface in FB_pi compared to NoFB_pi, zonally averaged in the order of 1 K (Figure 4.2b), but regionally up to 2 K (not shown). This warm anomalous subsurface water is transported within the subtropical shallow overturning cells towards the equator, where it is upwelled and results in the strong surface warming. This warming in the upwelling regions is enhanced by the direct effect of strong light absorption due to high abundance of chlorophyll here. The resulting warming signal of ~0.8 K reduces the cold bias in the equatorial Pacific by ~25%. Going along with the warming of the Pacific cold tongue, a weakening and eastward shift of the

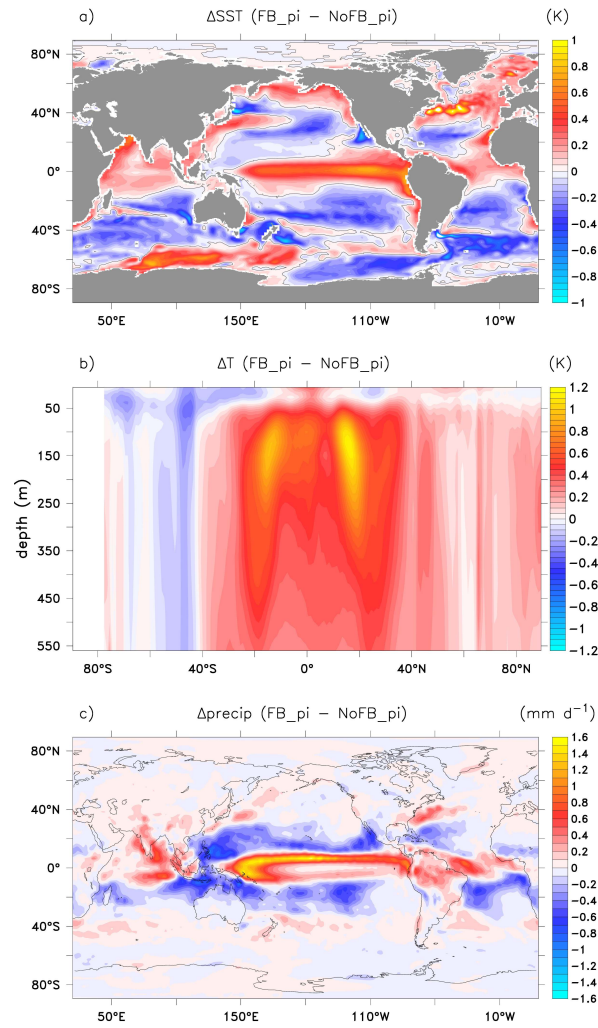


Figure 4.2: a) SST difference [K] between FB_pi and NoFB_pi (100 year means). b) Zonal mean temperature difference [K] in the upper 500 m between FB_pi and NoFB_pi (100 year means). c) Precipitation difference [mm d^{-1}] between FB_pi and NoFB_pi (100 year means).

Walker circulation takes place (not shown), as well as an increase in precipitation in the tropical Pacific (reducing the Pacific dry bias) (Figure 4.2,c).

Regarding ocean biogeochemistry, the control states are similar with respect to global inventories such as global net primary production (NPP, 52.1 Pg C yr⁻¹ in FB_pi and 51.7 Pg C yr⁻¹ in NoFB_pi), global export production at 90 m (7.6 Pg C yr⁻¹ in both setups), and global N₂ fixation (114.9 Tg N yr⁻¹ in FB_pi and 121.1 Tg N yr⁻¹ in NoFB_pi).

All in all, the evaluation confirms that the new mean climate and ocean biogeochemical states in the model with interactive biogeochemical feedback of phytoplankton light absorption in FB_pi (and FBcya_pi, respectively) are in reasonable states and can be used as starting point for the transient experiments.

4.4 Change in the phytoplankton and chlorophyll distributions under rising atmospheric CO₂ concentrations

In the following, we describe the response of marine biota to the transient atmospheric CO₂ forcing in simulation FB_1%. We compare the last 20 year ensemble mean of FB_1% to the last 100 year mean of FB_pi.

In the tropical and subtropical ocean, the area we focus on in this study, both simulated phytoplankton groups, bulk phytoplankton and cyanobacteria, mostly decline under global warming (Figure 4.3d-i). The total standing stock of phytoplankton (bulk phytoplankton and cyanobacteria) is reduced from 498.6 Gt C to 430.3 Gt C (13.7%) in the area from 40°S to 40°N (Table 4.2). Thereby, cyanobacteria, which decline by 35% (from 88.5 to 57.3 Gt C) strongly contribute to the overall decrease. The standing stock of bulk phytoplankton is reduced by 9.1% (from 410.1 to 373.0 Gt C) in the area from 40°S to 40°N. Coupled to this, net primary production (NPP) in this area is strongly reduced from 38.3 to 31.1 Pg C yr⁻¹ (18.3%). The decline in NPP under rising CO₂ in this part of the ocean is in accordance with the general consensus of CMIP5 models (Bopp *et al.*, 2013; Laufkötter *et al.*, 2015). Global N₂ fixation is reduced from 114.9 Tg N yr⁻¹ to 70.05 Tg N yr⁻¹ (39.9%).

For bulk phytoplankton, nutrient limitation is the main limiting factor driving the decrease in the transient simulations (Figure 4.4). Although higher temperatures are beneficial for bulk phytoplankton in the model and increase their growth rate following the temperature dependency of the Eppley curve (1.066^T , Eppley, 1972) (Figure 4.4d-f), increased stratification, reduced ventilation and reduced upwelling strengths, decrease the supply of nitrate (the least available nutrient) to the surface ocean and overall strengthen nutrient limitation (Figure 4.4a-c). Furthermore, the poleward expansion of the subtropical gyres due to the expansion of the Hadley

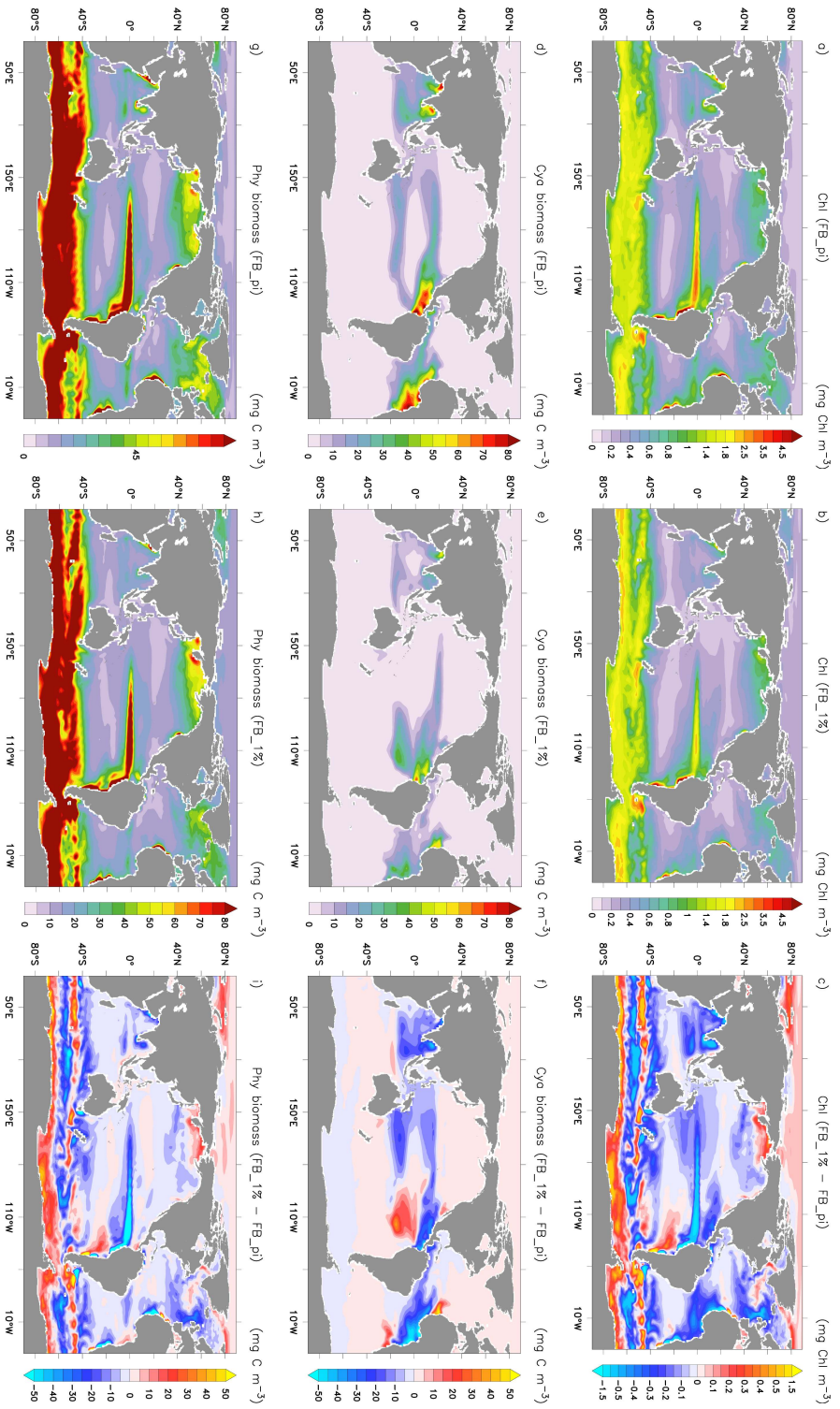


Figure 4.3: **Top:** Surface (0–22 m) chlorophyll [mg C m⁻³] in FB_pi (100 year mean) (a), in FB_1% (last 20 year ensemble mean) (b), and the difference between FB_1% and FB_pi (c). **Middle:** Surface (0–22 m) cyanobacteria biomass [mg C m⁻³] in FB_pi (100 year mean) (d), in FB_1% (last 20 year ensemble mean) (e), and the difference between FB_1% and FB_pi (f). **Bottom:** Surface (0–22 m) bulk phytoplankton biomass [mg C m⁻³] in FB_pi (100 year mean) (g), in FB_1% (last 20 year ensemble mean) (h), and the difference between FB_1% and FB_pi (i).

Table 4.2: Inventories of biogeochemical variables in the region 40°S to 40°N in experiment FB_pi (100 year mean), in FB_1% (last 20 year ensemble mean) and the respective change between FB_1% and FB_pi in percent.

parameter	FB_pi	FB_1%	change in %
standing stock phy and cya (Gt C)	498.6	430.3	13.7
standing stock phy (Gt C)	410.1	373.0	9.1
standing stock cya (Gt C)	88.5	57.3	35.3
NPP (Pg C yr ⁻¹)	38.3	31.1	18.3
mean surface (0–22 m) Chl concentration (mg C m ⁻³)	0.56	0.45	19.6
N ₂ fixation (Tg N yr ⁻¹)	114.9	70.1	39.9

cells (which is a robust feature of global warming scenarios (*Lu et al.*, 2007) and also seen in FB_1%, not shown), goes along with a poleward expansion of the low phytoplankton areas of the subtropical gyres. In some limited areas, on the other hand, nutrient limitation is alleviated, such as the equatorial eastern Atlantic, where phytoplankton concentrations increase over time. Here, the strong decline in cyanobacteria, as will be elucidated in the following, promotes growth of bulk phytoplankton.

The decline in cyanobacteria, which strongly contributes to the overall decline in total phytoplankton biomass in the tropical and subtropical ocean (~30%), is caused by a combination of temperature and phosphate limitation (Figure 4.5). In contrast to bulk phytoplankton, for cyanobacteria a distinct temperature curve with an optimum temperature of 28.0°C is prescribed (*Breitbarth et al.*, 2007; *Sonntag*, 2013). Increasing temperatures up to 28.0°C increase cyanobacteria's growth rate. This explains the slight expansion of their habitat polewards and the increasing concentrations in the eastern boundary upwelling regions (off Namibia, Peru, Northwest Africa and California). In particular, one hotspot of cyanobacteria abundance under high CO₂ is in the eastern southern tropical Pacific, where rising temperatures promote growth (Figure 4.5g-i). Temperatures above 28.0°C, on the contrary, limit growth. This is the case roughly between 15°S and 15°N. Here, temperatures exceeding 28.0°C represent the primary limiting factor in the transient CO₂ scenario. With respect to nutrients, phosphate is the limiting factor in our simulations (Figure 4.5a-f). Phosphate limitation is getting stronger in the subtropical gyres due to increased stratification and reduced mixing, which explains the decline in cyanobacteria there. Consequently, less iron is used up. Yet, dust deposition stays the same, which leads to a slight easing of the iron limitation under rising CO₂ (Figure 4.14a-c).

Chlorophyll, used in this study as a measure of strength of light absorption, is derived linearly from the phytoplankton concentrations (Equation 4.4). The changes in the chlorophyll distribution hence reflect the changes in phytoplankton and cyanobacteria (Figure 4.3a-c). Except for some limited regions which experience

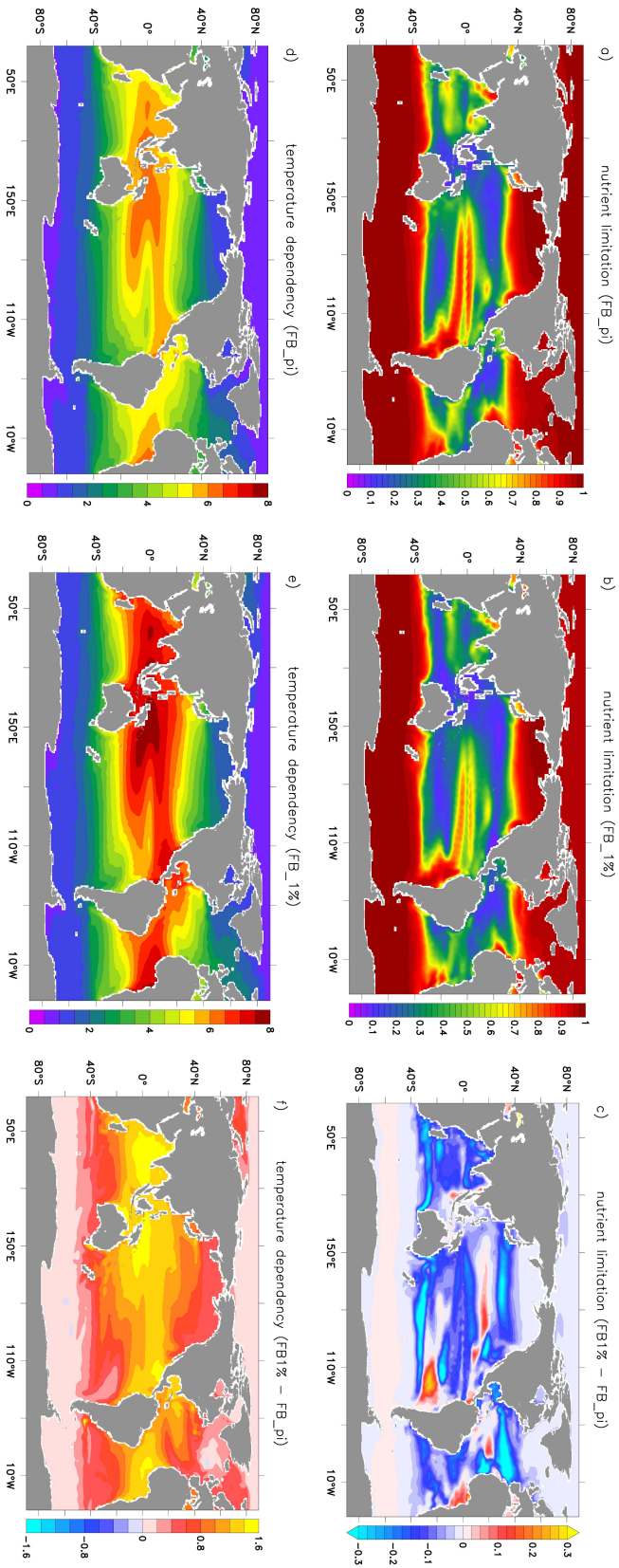


Figure 4.4: **Top:** Surface nutrient (nitrate) limitation of bulk phytoplankton in FB_pi (100 year mean) (a), in FB_1% (last 20 year ensemble mean) (b), and the difference between FB_1% and FB_pi (c). **Bottom:** Temperature dependency of growth in FB_pi (100 year mean) (d), in FB_1% (last 20 year ensemble mean) (e), and the difference between FB_1% and FB_pi (f), following the Eppley curve (1.066^T, *Iiyama et al.*, 2013).

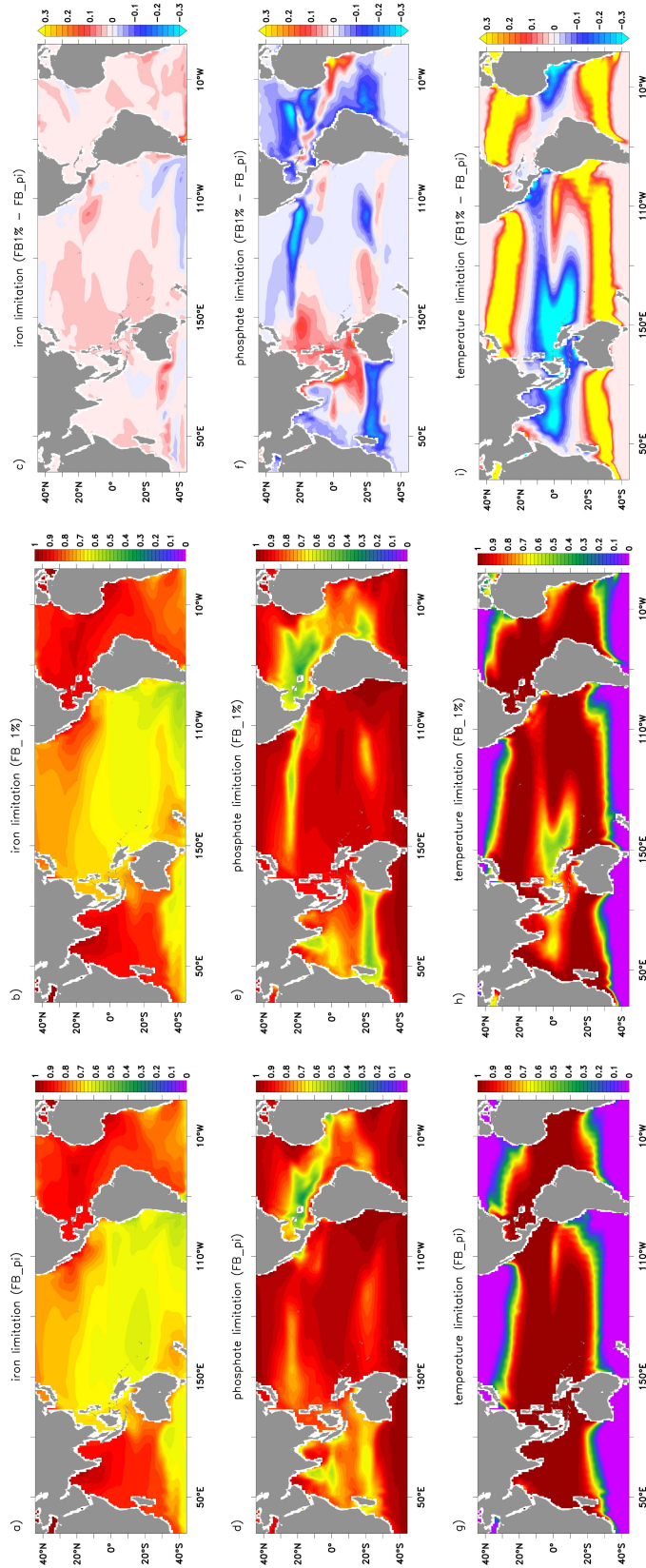


Figure 4.5: **Top:** Surface iron limitation of cyanobacteria in FB_pi (100 year mean) (a), in FB_1% (last 20 year ensemble mean) (b), and the difference between FB_1% and FB_pi (c). **Middle:** Surface phosphate limitation of cyanobacteria in FB_pi (100 year mean) (d), in FB_1% (last 20 year ensemble mean) (e), and the difference between FB_1% and FB_pi (f). **Bottom:** Surface temperature limitation of cyanobacteria in FB_pi (100 year mean) (g), in FB_1% (last 20 year ensemble mean) (h), and the difference between FB_1% and FB_pi (i).

an increase in chlorophyll, such as the eastern southern tropical Pacific, chlorophyll mostly declines under increasing CO₂ forcing. Largest changes in chlorophyll take place at the equator and the eastern boundary upwelling regions of up to 1.5 mg Chl m⁻³ (~50%). In the subtropical gyres the total change is smaller, however, the percentage change is similar (also ~50%). Overall, spatially averaged surface chlorophyll concentrations are reduced by ~20% in the area from 40°S to 40°N. Cyanobacteria contribute roughly 25% to the decrease in the mean concentration averaged over the area, in certain regions, however, up to 100%.

The patterns of change in phytoplankton distribution and concentrations in experiment NoFB_1% (relative to NoFB_pi) (not shown) are in general similar to FB_1% (relative to FB_pi) (Figure 4.3). The difference between the two setups, however, is, that in FB_1% these changes in marine biota feed back on the ocean temperature by dynamically influencing the light field. In the following, we describe the effects on climate which are arising from including this active biogeophysical feedback in projections with the Earth system model.

4.5 Impact of the light-absorption feedback on climate under increasing CO₂ forcing

In order to assess the impact of a changing phytoplankton distribution on climate's evolution, we compare the relative difference of the ensemble mean of the CO₂ increase projections (last 20 year ensemble means of FB_1% and NoFB_1%) to their respective control climate states (last 100 year means of FB_pi and NoFB_pi). We focus on the effects in the tropics and subtropics (effects on the global scale are shown in Appendix Ch4). We first elaborate on the effects on ocean temperature and mixed layer depth (and underlying mechanisms), followed by the resulting impacts on the atmospheric component of the Earth system (surface air temperature, wind patterns and precipitation). Finally, we describe changes in the ocean circulation and effects on phytoplankton growth itself.

4.5.1 Ocean temperature and mixed layer depth

Increasing atmospheric CO₂ concentrations cause a strong overall increase in SST in the tropical and subtropical ocean, regionally by more than 4 K, in both model setups (Figure 4.6a,b). The overall warming patterns are thereby consistent in FB and NoFB and generally in accordance with the CMIP5 transient 1% CO₂ increase scenario of the MPI-ESM LR (*Giorgetta et al., 2013*). Including the feedback, however, considerably enhances the warming in distinct regions of the tropical and subtropical ocean in FB compared to NoFB (Figure 4.6c). These regions largely reflect areas of

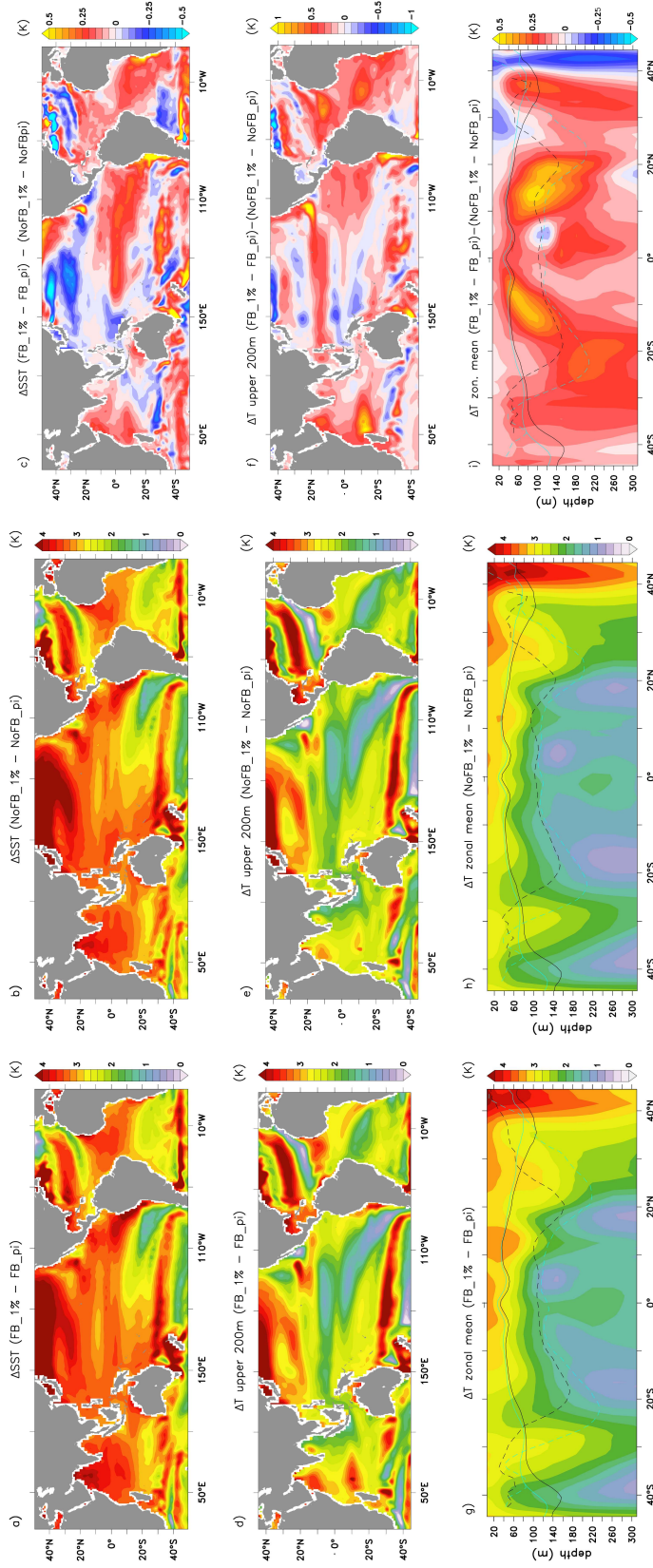


Figure 4.6: **Top:** Change in SST [K] in FB_1% (last 20 year ensemble mean) compared to FB_pi (100 year mean) (a), in NoFB_1% (last 20 year ensemble mean) compared to NoFB_pi (100 year mean) (b), and the difference between FB_1%-FB_pi and NoFB_1%-NoFB_pi (c). **Middle:** Change in the mean temperature of the upper 200 m [K] in FB_1% (last 20-yearmean) compared to FB_pi (100 year mean) (d), in NoFB_1% (last 20-yearmean) compared to NoFB_pi (100 year mean) (e), and the difference between FB_1%-FB_pi and NoFB_pi-NoFB_pi (f). **Bottom:** Change in the zonal mean temperature of the upper 300 m [K] in FB_1% (last 20 year ensemble mean) compared to FB_pi (100 year mean) (g), in NoFB_1% (last 20-yearmean) compared to NoFB_pi (100 year mean) (h), and the difference between FB_1%-FB_pi and NoFB_pi-NoFB_pi (i). The solid lines display the MLD in the respective pi-control experiments (black) and the 1% CO₂ increase scenarios (lightblue), and the dashed lines the thermocline depth in the respective pi-control experiments (black) and the 1% CO₂ increase scenarios (lightblue). In i) the respective lines of setup NoFB (as in h) are shown.

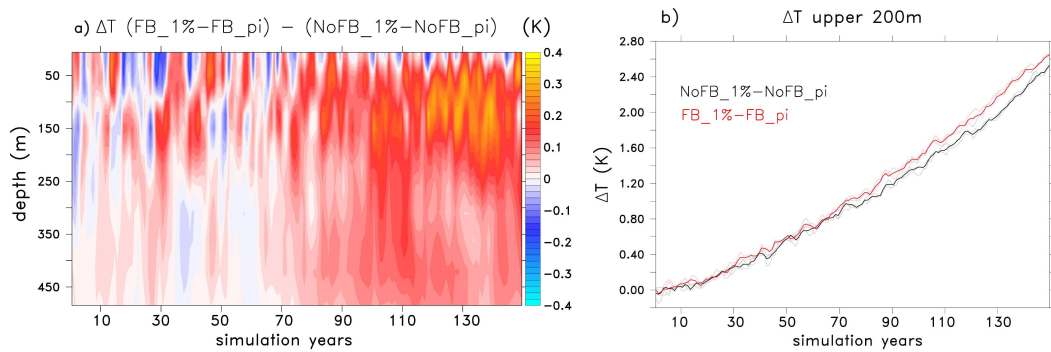


Figure 4.7: a) Hovmöller (time – depth) diagram of the upper 500 m of spatially averaged relative temperature change in the tropics (20°–20°N) between FB_1%-FB_pi and NoFB_1%-NoFB_pi. b) Timeseries of change in temperature averaged over the upper 200 m in the tropics (20°–20°N) between NoFB_1% and NoFB_pi (100 year mean) (black, thin lines: ensemble members, thick line: ensemble mean) and between FB_1% and FB_pi (100 year mean) (red, thin lines: ensemble members, thick line: ensemble mean).

upwelling: at the equator, in the eastern boundary upwelling regions off the South American and African continent, and in the western and northern parts of the Indian Ocean. The magnitudes of the additional warming thereby reach values of up to 0.7 K in the eastern boundary upwelling regions, representing an additional warming of more than 20%. In the equatorial Pacific, the Nino3.4 region (5°S–5°N, 170°W–120°W) exhibits a warming of 0.2 K, and the Indian ocean 0.25 K, which is roughly 10% of the warming signal of NoFB at the respective locations.

The additional regional surface warming effect can be explained as follows. The strong decline in phytoplankton and related chlorophyll throughout the tropical and subtropical ocean under global warming (Figure 4.3c) reduces the strength of light absorption at the surface. Light can thus penetrate deeper into the water column, leading to a warming of the subsurface layers below the mixed layer (Figure 4.6f,i). In the course of decreasing surface chlorophyll concentrations under rising CO₂, the subsurface warming signal is getting stronger with time (Figure 4.7a). Averaged over the tropical region (20°S to 20°N), the relatively warmer water reaches down to a depth of 200 m or even deeper with a maximum at about 100 m (Figure 4.7a). Strongest subsurface warming takes place between the mixed layer and the thermocline depth (Figure 4.6i). At the end of the simulation, the mean temperature of the upper 200 m spatially averaged over the tropical ocean is increased by 0.2 K in FB relative to NoFB (Figure 4.7b). This relatively warmer subsurface water from below the mixed layer feeds the upper part of the shallow overturning cells and is transported equatorward along isopycnals. In the equatorial and eastern boundary upwelling systems, this water is transported upwards and reaches the surface, leading to the enhanced surface warming signals here. Ekman transport and surface currents distribute the water away from the upwelling

hotspots, spreading the warming signal throughout large parts of the tropical and subtropical ocean.

In limited parts of the subtropical gyres, as well as in the Pacific warm pool, the direct effect of decreased surface radiative heating, and changes in the circulation, induce a cooling in FB compared to NoFB (Figure 4.6a-c). The warming signal is hereby regionally reduced by up to 10% in FB relative to NoFB. In largest parts of the tropical and subtropical ocean, however, the advective transport of warmer subsurface water to the surface in the upwelling regions as described above outweighs the local cooling effect one would expect from reduced surface light absorption. The origin of the warmer water is, in accordance with Chapter 3 of this thesis, located off-equator. Both in the subtropical gyres as well as the eastern margins of the gyres phytoplankton strongly decreases, and leads to deeper reaching light and additional heating below the mixed layer, from where the water feeds the upper part of the shallow overturning cells. The mixed layer depths get generally shallower under increasing CO₂ in both simulations (Figure 4.8a,b). The shoaling is, however, less pronounced in FB compared to NoFB (Figure 4.8c), especially in the tropical Atlantic, the Indian Ocean, and the eastern tropical Pacific. This is because the deeper reaching light, related to the phytoplankton decline, counteracts the effect of shoaling due to global warming. In some regions this results in a deepening of the mixed layer in FB_1% compared to FB_pi. Despite a relatively deeper MLD, still more light reaches below the mixed layer depth in FB_1% compared to FB_pi due to the decline in chlorophyll.

Cyanobacteria constitute an important fraction of the decrease in off-equatorial chlorophyll (~25% of the decrease in mean chlorophyll concentrations in the upper 20 m) and hence contribute to the amplified warming in the tropical and subtropical ocean. In the Pacific Ocean, cyanobacteria, however, increase their abundance in the eastern tropical region and hence rather damp the additional heating effect to some extent. Still, the overall decline in chlorophyll in largest parts of the tropical and subtropical Pacific prevails and results in the enhanced surface warming.

4.5.2 Surface air temperature, wind patterns and precipitation

The amplified regional warming of the surface ocean implies a warming of the overlying air masses (Figure 4.8d-f). The spatial pattern of change in surface (2 m) air temperature in the tropics and subtropics largely reflects the patterns of SST (Figure 4.6a-c). Strongest additional warming signals occur above the Benguela and Peruvian upwelling regions up to 0.6 K, which represents 20% of the overall warming here. Above the Pacific cold tongue, as well as above the western Indian Ocean and the tropical Atlantic an additional warming of roughly 0.2 K takes place, representing up to 10% of the overall warming. The SST induced warming of the tropo-

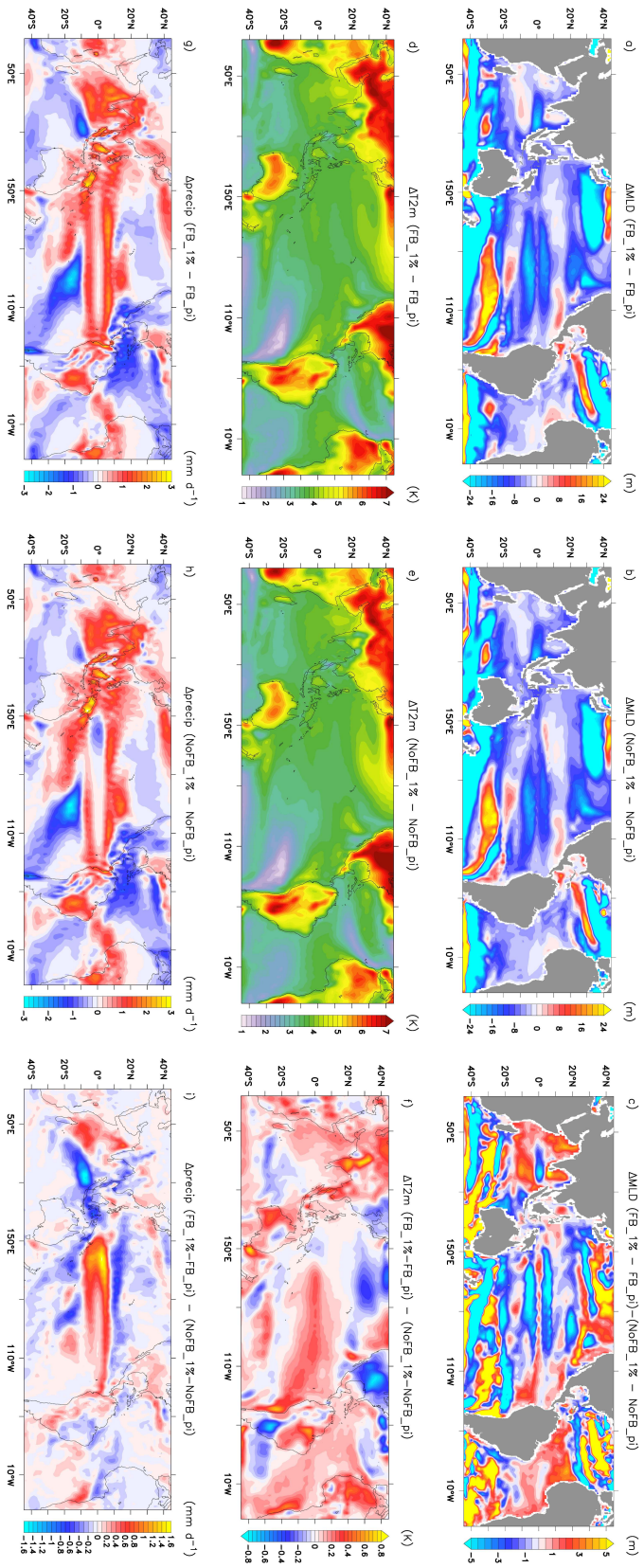


Figure 4.8: **Top:** Change in mixed layer depth [m] in FB_1% (last 20 year ensemble mean) compared to FB_pi (100 year mean) (a), in NoFB_1% (last 20 year ensemble mean) compared to NoFB_pi (100 year mean) (b), and the difference between FB_1%-FB_pi and NoFB_pi-NoFB_pi (last 20 year ensemble mean) compared to NoFB_pi (100 year mean) (c). **Middle:** Change in surface (2m) air temperature [K] in FB_1% (last 20 year ensemble mean) compared to FB_pi (100 year mean) (d), in NoFB_1% (last 20 year ensemble mean) compared to NoFB_pi (100 year mean) (e), and the difference between FB_1%-FB_pi and NoFB_pi-NoFB_pi (last 20 year ensemble mean) compared to NoFB_pi (100 year mean) (f). **Bottom:** Change in precipitation [mm d^{-1}] in FB_1% (last 20 year ensemble mean) compared to FB_pi (100 year mean) (g), in NoFB_1% (last 20 year ensemble mean) compared to NoFB_pi (100 year mean) (h), and the difference between FB_1%-FB_pi and NoFB_pi-NoFB_pi (last 20 year ensemble mean) compared to NoFB_pi (100 year mean) (i).

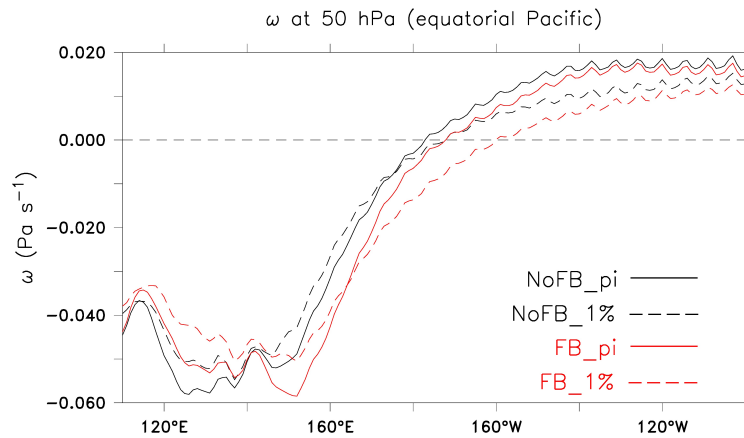


Figure 4.9: Vertical velocity ω [Pa s^{-1}] at 500 hPa above the equatorial Pacific (5°S – 5°N) in NoFB_pi (black solid, 100 year mean), NoFB_1% (black dashed, 20 year ensemble mean), FB_pi (red solid, 100 year mean), FB_1% (red dashed, last 20 year ensemble mean).

sphere also leads to warming above the continents, mainly over India (up to 20%), over North West Africa (8%), over the northern part of South America (10%) and over the western part of Australia (8%). A relative cooling of the air, on the contrary, is induced over North America and above colder SSTs in the poleward parts of the subtropical gyres, reducing the overall heating signal locally by 10% in these parts of the Earth.

The slowdown of the Walker circulation, which is in general a robust feature of CO₂ increase simulations with climate models (e.g. Vecchi and Soden, 2007) and also seen in both our model setups, is enhanced in FB compared to NoFB (Figure 4.9). Convection of air in the west and descent of air in the east are both more strongly reduced in FB compared to NoFB by roughly 30% (vertical velocity at 500 hPa above the equatorial Pacific averaged from 120 – 140°E and 120 – 160°W). Furthermore, the transition between rising and descending air is shifted more towards the east (by $\sim 15^{\circ}$ longitude in FB_1% instead of $\sim 5^{\circ}$ longitude in NoFB_1%). This comes about through the reduced zonal SST gradient caused by the enhanced warming of the cold tongue and cooling of the warm pool, respectively.

Implications for precipitation include a strong increase by up to 1.4 mm d^{-1} in the western tropical Pacific at 160°E (Figure 4.8g-i). This turns the negative trend in precipitation seen in NoFB into a positive trend (that means a net increase in precipitation) in FB at this location (Figure 4.8g,h). Over the warm pool and over Oceania, where among the largest changes in precipitation are projected in FB and NoFB, the increase in precipitation is, on the contrary, reduced in FB by roughly 10% compared to NoFB. Over the Indian Ocean, the pattern of a strong increase in precipitation extends further southward in the western part of the basin, associated with the

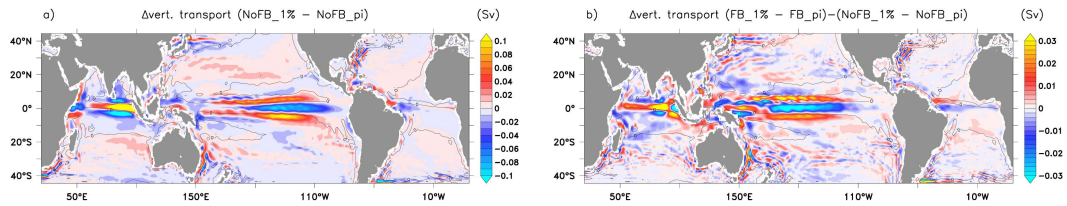


Figure 4.10: Change in mean vertical transport [Sv] of the upper 100 m in NoFB_1% (last 20 year ensemble mean) compared to NoFB_pi (100 year mean) (a), and the difference between FB_1%-FB_pi and NoFB_pi-NoFB_pi (b). The black lines displays the zero isoline of the vertical transport (mean of the upper 100 m), i.e. the transition between up- and downwelling, in experiment NoFB_pi.

enhanced surface warming in FB compared to NoFB. In the eastern part, on the contrary, the drier signal is enhanced and reaches further northward. Over the Atlantic Ocean, the simulated changes in precipitation are rather damped by including the feedback. The increase in precipitation above the equatorial region is reduced by up to 10%, and the decrease above the subtropical regions as well.

4.5.3 Ocean circulation and feedback on phytoplankton growth

The reduced shoaling of the mixed layer depth in FB due to deeper penetrating light (Figure 4.8) implies a weakening of the meridional mass transport via the shallow overturning cells (e.g., *Sweeney et al.*, 2005). This, together with the decrease of the trade winds due to wind anomalies directed towards the warm SST signals in the eastern coastal upwelling regions (not shown), results in a stronger decrease in the strength of equatorial upwelling in FB compared to NoFB by $\sim 30\%$ (Figure 4.10a,b). Hence, both the dynamical response of the ocean to changes in mixed layer depths, as well as the atmospheric feedback to the SST changes, amplify the surface warming effect at the equator, thus constituting positive feedbacks. The decreased upwelling strength, and associated reduced supply of nutrients to the surface, however, leads to a stronger decline in phytoplankton at the equator in setup FB compared to NoFB (Figure 4.11). This damps the local warming effect due to reduced surface light absorption (negative feedback). As seen in the resulting positive equatorial SST signal (Figure 4.6c), the overall warming effect due to the advection of warmer subsurface water originating off-equator dominates.

Phytoplankton growth located off-equator is probably also influenced by the reduced equatorial upwelling strength. The chlorophyll concentrations, however, do not show an overall stronger decrease in concentrations in FB compared to NoFB (Figure 4.11). Other factors, such as relative changes in temperature and stratification between the two setups, play a role. In the end, a complex pattern of regions with stronger, and regions with weaker decrease in chlorophyll occurs in FB com-

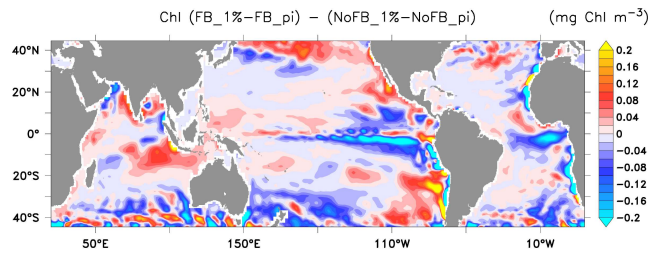


Figure 4.11: Relative difference in the change in surface chlorophyll [mg Chl m^{-3}] in the transient simulations (last 20 year ensemble mean) compared to the control states (100 year mean) between the two setups FB and NoFB ($(\text{FB}_{1\%} - \text{FB}_{\text{pi}}) - (\text{NoFB}_{1\%} - \text{NoFB}_{\text{pi}})$).

pared to NoFB. It is thus not possible to generally speak of a positive or negative feedback between phytoplankton changes and effects on climate. With respect to inventories of biogeochemical variables in the tropical and subtropical ocean, the relative percentage changes between FB_{1%} and NoFB_{1%} and their respective preindustrial control state are similar and hence only given for setup FB (Table 4.2).

4.6 Effects of potential physiological adaptation mechanisms of cyanobacteria in an increasing CO₂ ocean

As seen in Section 4.4, both bulk phytoplankton and cyanobacteria largely decline in the tropical and subtropical ocean as response to rising CO₂ in our model. Cyanobacteria thereby strongly contribute to the decrease in surface chlorophyll. Since a number of previous studies propose cyanobacteria to benefit in a warming climate, we repeat the simulations with one additional model setup. In the additional experimental setup, FB_{cya}, we provide cyanobacteria with a set of physiological advantages and adaptation mechanisms that have been proposed by previous studies to help this distinct phytoplankton group to cope with the climate stressors associated with global warming. The modifications include the adaptation to higher temperatures, a pH-dependent growth rate, and the ability to utilize DOP (DOM). This modified experimental setup serves two goals. First, it allows us to investigate the hypothesis that cyanobacteria might increase under rising CO₂ given the physiological advantages and adaptations. And second, we can test how sensitive the effects on climate are to a different evolution of marine biota and related biogeophysical feedback patterns.

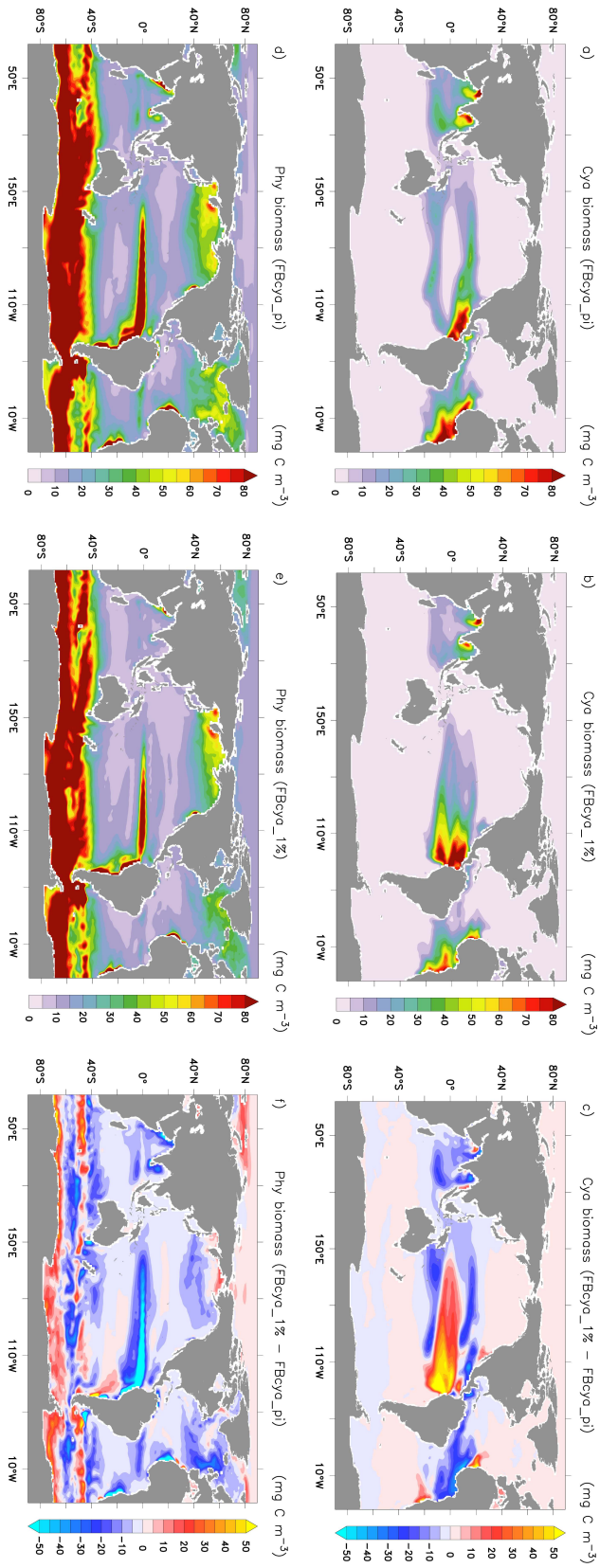


Figure 4.12: **Top:** Surface (0–22 m) cyanobacteria biomass [mg C m^{-3}] in FBcya_1% (last 20 year ensemble mean) (b), and the difference between FB_1% and FB_pi (c). **Bottom:** Surface (0–22 m) bulk phytoplankton biomass [mg C m^{-3}] in FBcya_pi (100 year mean) (d), in FBcya_1% (last 20 year ensemble mean) (e), and the difference between FBcya_1% and FBcya_pi (f).

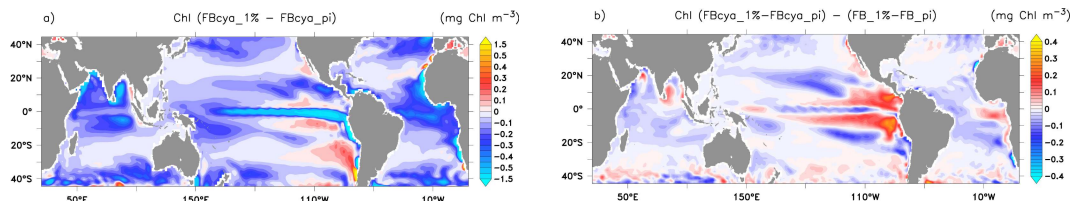


Figure 4.13: a) Change in surface (0–22 m) chlorophyll [mg C m^{-3}] in FBcya_1% (last 20 year ensemble mean) compared to FBcya_pi (100 year mean). b) Relative difference of the change in surface (0–22 m) chlorophyll [mg C m^{-3}] between FBcya_1% (last 20 year ensemble mean) compared to FB_pi (100 year mean) and FB_1% (last 20 year ensemble mean) compared to FB_pi (100 year mean).

4.6.1 Modified evolution of phytoplankton and chlorophyll

In the modified setup FBcya, cyanobacteria concentrations also largely decline under rising CO₂ in large parts of the tropical and subtropical ocean (Figure 4.12a-c). The decrease is, however, less strong than in FB (Figure 4.3d-f). Related to this, the reduction in N₂ fixation is less strong, namely 27.9% (from 120.5 Tg N yr⁻¹ in FBcya_pi to 86.8 Tg N yr⁻¹ at the end of FBcya_1%), compared to 39.9% in setup FB (see Table 4.2). One region that evolves as a hotspot of cyanobacteria abundance in FBcya_1% is the eastern tropical Pacific. The strong increase is, as already seen in FB_1%, mainly caused by the increasing temperatures in the upwelling region, which still stay below the optimum temperature. In FBcya_1%, the increase in cyanobacteria is stronger and extends into the central Pacific Ocean along the equator compared to FB_1%. Higher values of CO₂ (or lower values of pH) increase the growth rate (Figure 4.15a), and the additional growth on DOP (DOM), which is sufficiently available in the phytoplankton rich region, strongly promotes growth.

In the other parts of the tropical and subtropical ocean, as mentioned above, cyanobacteria decline due to temperature and phosphate limitation. Increasing the optimum temperature for growth with time indeed alleviates the temperature limitation of cyanobacteria under rising CO₂ in FBcya in comparison to FB (compare Figure 4.14i to Figure 4.5i). In the equatorial region, the optimum temperatures are however still slightly exceeded, leading to a decline of cyanobacteria concentrations within 10°S–10°N in the Atlantic and Indian Ocean, as well as in the western Pacific. The overall decrease is less pronounced in FBcya compared to FB (compare Figure 4.12c to Figure 4.3f).

With increasing CO₂ concentrations, seawater pH is lowered (Figure 4.15a). In the first two third of the simulation period, the evolving pH values stay above the applied optimum value for cyanobacteria growth of 7.77. Hence, overall, the pH-dependent growth rate is increased in largest parts of the tropical and subtropical ocean. In the last third of the simulation period, pH values fall below 7.77 and hence

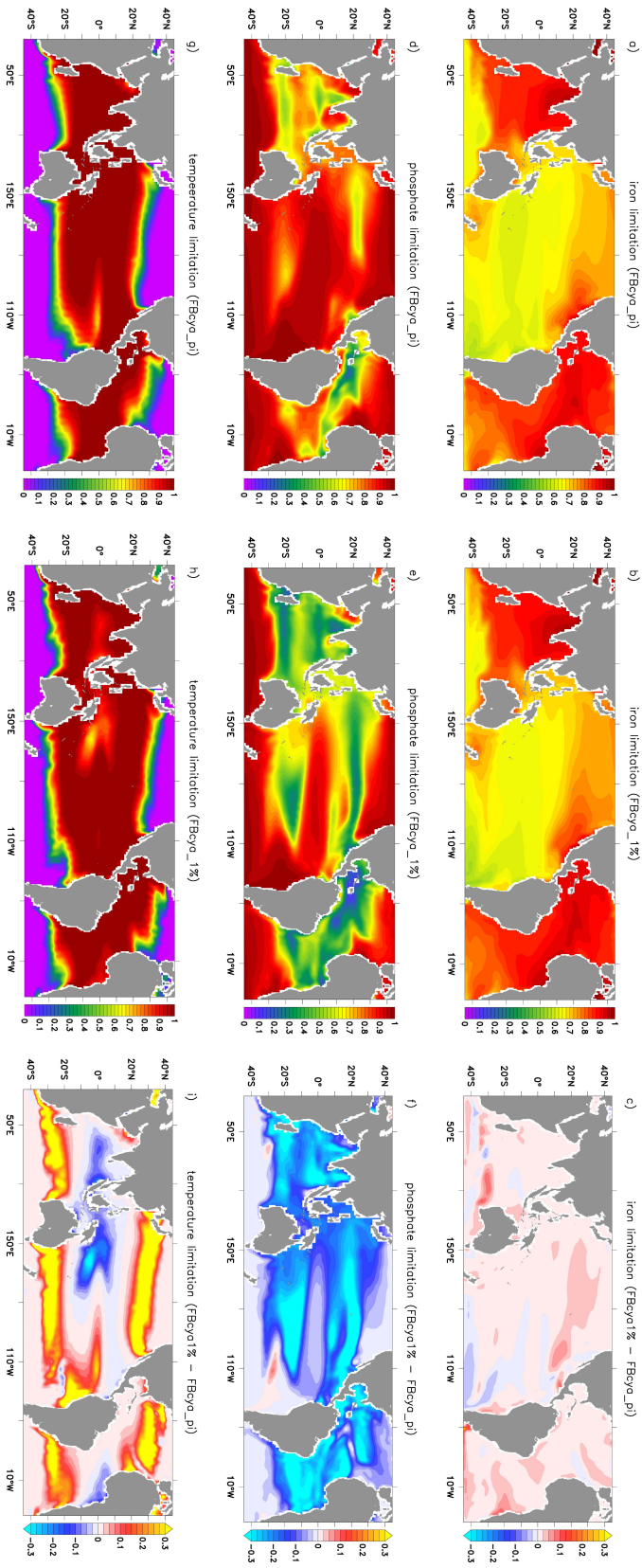


Figure 4.14: **Top:** Iron limitation of cyanobacteria in FBcya_pi (100 year mean) (a), in FBcya_1% (last 20 year ensemble mean) (b), and the difference between FBcya_1% and FBcya_pi (c). **Middle:** Phosphate limitation in FBcya_pi (100 year mean) (d), in FBcya_1% (last 20 year ensemble mean) (e), and the difference between FBcya_1% and FBcya_pi (f). **Bottom:** Temperature limitation in FBcya_pi (100 year mean) (g), in FBcya_1% (last 20 year ensemble mean) (h), and the difference between FBcya_1% and FBcya_pi (i).

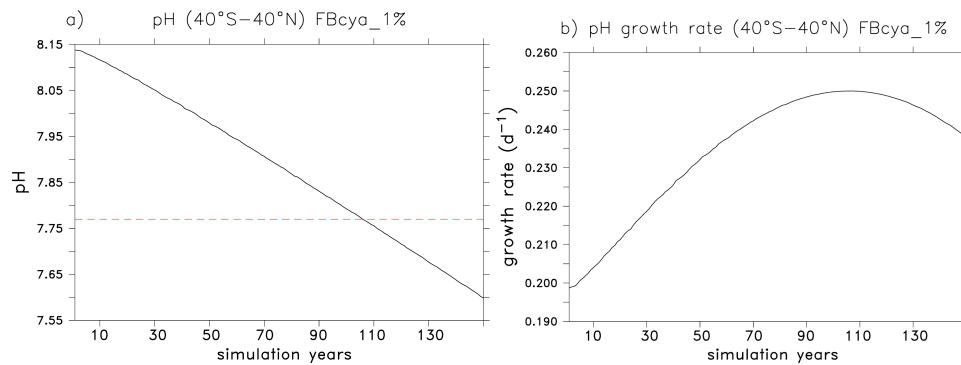


Figure 4.15: a) Timeseries of surface pH spatially averaged from 40°S to 40°N in FBcya_1% (black). The red dashed line indicates the optimum pH value (7.77) for cyanobacteria growth (see Equation 4.8). b) Timeseries of the growth rate of cyanobacteria according to the evolution of pH shown in a) (see Equation 4.8).

reduce the growth rate again. Still, the growth rate is higher than in the preindustrial control state FBcya_pi at the beginning of the simulation. Phosphate limitation, however, prevents cyanobacteria from increasing their concentrations (Figure 4.14f). The additional source of phosphorus from the DOP (DOM) pool in the model is apparently not large enough to overcome the phosphate deficit. Cyanobacteria, by growing on DOP (DOM), reduce the overall DOP (DOM) pool. Since only a certain fraction of decaying cyanobacteria feeds the DOP (DOM) pool (the rest goes into the sinking detritus pool), the fraction that is remineralized into phosphate at the surface is reduced, and so are the surface phosphate concentrations. Phosphate limitation hence gets stronger (Figure 4.14f), preventing cyanobacteria from increasing under rising CO₂. As already the case in FB_1%, iron limitation is not enhanced in the transient simulation and hence it is not the driving factor of the decline in cyanobacteria abundance in our model.

Changes in the cyanobacteria growth parameterization also affect bulk phytoplankton growth, on the one hand due to the competition with cyanobacteria for phosphate and light, and on the other hand due to changes in N₂ fixation. Overall, the patterns of change in bulk phytoplankton in FBcya_1% are, however, consistent with FB_1% (compare Figure 4.12d-f to 4.3g-i). In some parts, especially the subtropical gyres, phytoplankton concentrations are more strongly reduced in FBcya_1% compared to FB_1% due to the increased phosphate limitation (Figure 4.16).

The patterns of change in chlorophyll are similar in the two CO₂ increase scenarios, FBcya_1% and FB_% (compare Figure 4.13a to 4.3c). The difference is shown in Figure 4.13b. One region with a substantial difference is the eastern tropical Pacific due to the contribution of the strong rise in cyanobacteria abundance. In other regions, however, chlorophyll is even stronger declining in FBcya compared to FB. The

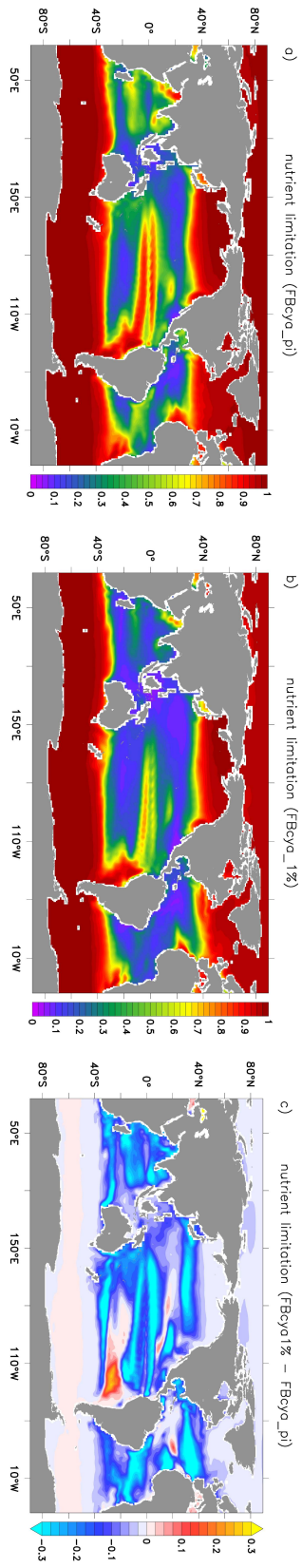


Figure 4.16: Nutrient (nitrate) limitation of bulk phytoplankton in FBcya_pi (100 year mean) (a), in FBcya_1% (last 20 year ensemble mean) (b), and the difference between FBcya_1% and FBcya_pi (c).

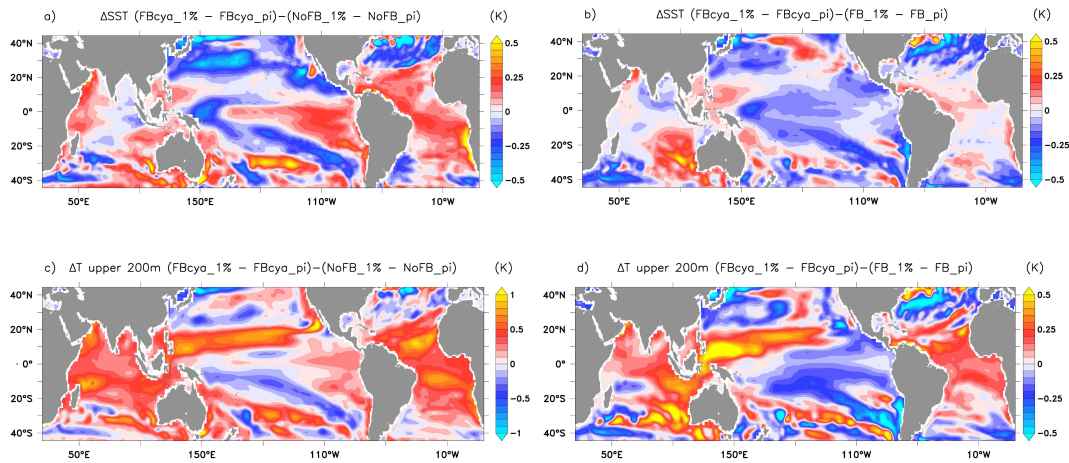


Figure 4.17: **Top:** Relative difference of the change in SST [K] between the setups FBcya and NoFB ((FBcya_1% - FBcya_pi) - (NoFB_1% - NoFB_pi)) (a), and between FBcya and FB ((FBcya_1% - FBcya_pi) - (FB_1% - FB_pi)) (b). **Bottom:** The same as upper row but for mean temperature [K] of the upper 200 m (c,d).

stronger decrease in bulk phytoplankton mentioned above lowers chlorophyll due to the higher chlorophyll content of bulk phytoplankton compared to cyanobacteria (see Section 4.2.2).

4.6.2 Impacts of the modified evolution of phytoplankton and chlorophyll on climate

Now, the question is if the differences in details in the evolution of phytoplankton and related chlorophyll in the simulation modifies the effects of the biogeophysical feedback on projected climate. We therefore compare the changes in the climate states between setup FBcya and FB (relative to NoFB).

The effects on the upper ocean temperature and SST as well as on other climate properties in scenario FBcya (compared to NoFB and their respective control states) are – as expected from a similar change in chlorophyll – overall similar as in FB (described in Section 4.5). The decline in chlorophyll leads to an addition of heat below the mixed layer, which is advected equatorwards via the shallow overturning cells and translates into a surface heating in the equatorial and eastern boundary upwelling areas (Figure 4.17a). The magnitudes of the additional warming is, however, regionally slightly different in FBcya than seen in FB (Figure 4.17b). In the equatorial Pacific, the increase in chlorophyll concentrations, which is due to the strong rise in cyanobacteria concentrations in FBcya_1%, traps more heat at the surface. Less radiation reaches below the mixed layer, leading to a weaker subsurface

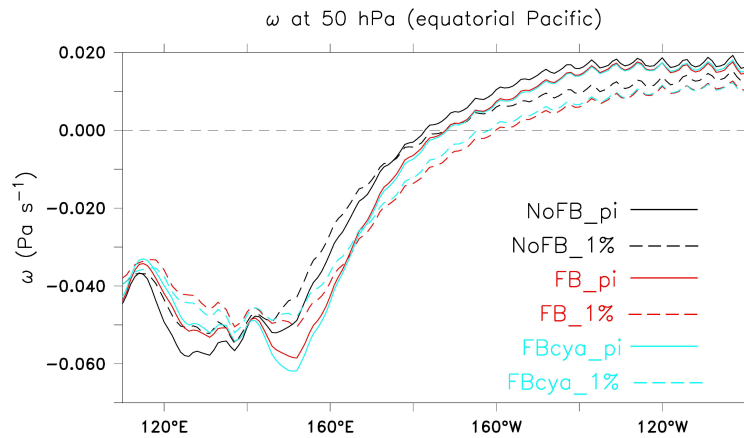


Figure 4.18: Vertical velocity ω [Pa s^{-1}] at 500 hPa above the equatorial Pacific (5°S – 5°N) in NoFB_pi (black solid, 100 year mean), NoFB_1% (black dashed, last 20 year ensemble mean), FB_pi (red solid, 100 year mean), FB_1% (red dashed, last 20 year ensemble mean), FBcya_pi (blue solid, 100 year mean), FBcya_1% (blue dashed, last 20 year ensemble mean). Analogous to Figure 4.9 but with added lines for setup FBcya.

warming of 0.1–0.25 K in FBcya compared to FB (Figure 4.17c,d). Associated with the weaker warming of the subsurface water, the upwelled water is also relatively cooler in FBcya compared to FB and results in a slightly less pronounced additional warming of the eastern South Pacific upwelling area (0.5 K) as well as of the cold tongue (0.1–0.3 K). The feature of a weaker warming in the equatorial Pacific is seen in both of the two realizations and hence indicates that the reduction of the warming effect due to higher surface chlorophyll is robust. Related to that, the water that spreads poleward from the upwelling region at the equator is relatively cooler in FBcya_1% than in FB_1%. This, together with the stronger local cooling effect due to the stronger decrease in surface chlorophyll in FBcya_1% (Figure 4.3b) results in a surface cooling in large parts of the subtropical gyres (Figure 4.17a).

A weaker warming of the cold tongue in FBcya implies a slightly weaker reduction in the strength of the Walker circulation in comparison to FB (Figure 4.18). Also the eastward shift between the transition of the ascending air in the east, and descending air in the west, is slightly less pronounced in the modified scenario FBcya (12 instead of 15° longitude). Related to that, the pattern of strong increase in precipitation in the tropical Pacific in FBcya relative to NoFB does not reach as far to the west as in FB relative to NoFB (compare Figure 4.19b and Figure 4.8i).

In contrast to the Pacific Ocean, in the Indian and Atlantic Ocean the slightly stronger decline in chlorophyll in FBcya compared to FB lead to a slightly stronger subsurface warming signal of 0.1–0.3 K in FBcya compared to FB (Figure 4.17d-f). Associated with that, the SST signal is slightly amplified by up to 0.2 K in the Ara-

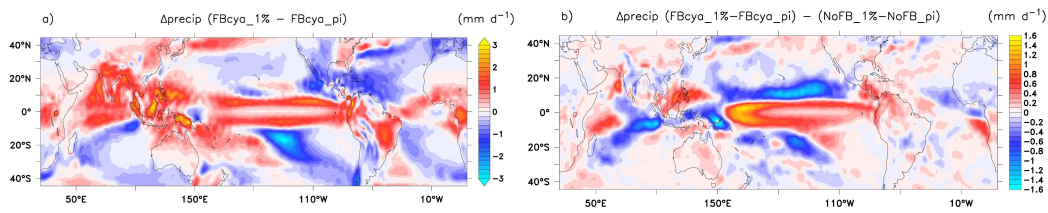


Figure 4.19: Change in precipitation in FBcya_1% (last 20 year ensemble mean) compared to FBcya_pi (100 year mean) (a), the difference between FB_1%-FB_pi and NoFB_pi-NoFB_pi (b).

bian Sea, in the Benguela Upwelling area and in the tropical Atlantic (Figure 4.17a-c).

In summary, the modified parameterization of cyanobacteria leads to a similar evolution of chlorophyll under rising CO_2 , and hence to similar effects on climate, that means to an additional tropical warming. Nevertheless, the magnitudes are altered. This shows that climate's response is indeed sensitive to details in the patterns of change in phytoplankton.

4.7 Summary and discussion

The effects of including the active biogeophysical feedback from phytoplankton light absorption on ocean temperature and climate have been investigated – and considered important – by many previous model studies under constant CO_2 forcing (e.g., Patara *et al.*, 2012, and references therein). As a logical extension, we conducted transient simulations with and without the active biogeophysical feedback in order to assess the impacts of a changing phytoplankton distribution on climate's evolution under rising CO_2 .

We find that changes in the phytoplankton distribution have indeed the potential to regionally amplify climate change. The projected reduction of the average surface chlorophyll concentrations by roughly 20% in the tropical and subtropical ocean under quadrupling CO_2 enhances warming in the tropics, regionally by up to 0.5 K, or 20%, respectively. The additional warming mostly takes place in the equatorial- as well as eastern boundary upwelling areas. Related implications for climate involve a stronger slowdown of the Walker circulation ($\sim 30\%$) and regionally enhanced changes in precipitation.

The additional surface warming caused by the decline in phytoplankton in the model is rather counterintuitive. Based on simulations with constant forcing, it was speculated that a surface cooling would take place in case of decreasing phytoplankton due to the decreased surface light absorption (Patara *et al.*, 2012). We,

however, see in our coupled model simulations that the advective process of upwelling of warmer subsurface water originating off-equator outweighs the local effect of declining chlorophyll, resulting in a surface warming instead. The important role of this non-local advective mechanism was already emphasized in Chapter 3 of this thesis, where an increase in surface light absorption strength due to including cyanobacteria as phytoplankton group, in turn, led to a cooling of the tropical and subtropical surface ocean. The changes in chlorophyll, and resulting changes in SST, taking place under quadrupling CO₂ are in the order of magnitude as including or not including cyanobacteria (Chapter 3 of this thesis). The consistent results in the constant climate state confirm the robustness of the mechanisms we see in the transient simulations. Other model studies also highlight the role of the non-local advective process induced by off-equatorial turbidity for equatorial SST in constant climate and hypothesized (based on simulations with a constant forcing) an additional warming to take place in case of a phytoplankton decline (*Sweeney et al.*, 2005; *Gnanadesikan and Anderson*, 2009; *Jochum et al.*, 2010) - a presumption which we confirm with our study.

The regions primarily responsible for the additional warming effect are the off-equatorial subtropical gyres and its eastern marginal areas. Cyanobacteria, as a dominant phytoplankton group in these areas, constitute an important fraction of the decline in water turbidity in the model. In contrast to bulk phytoplankton, which temporarily form deep chlorophyll maxima in the subtropical gyres, simulated positively buoyant cyanobacteria are concentrated at the surface (*Paulsen et al.*, 2017, Chapter 2 of this thesis). Any changes in concentrations and related light absorption strength have large impacts. The relevance of positively buoyant cyanobacteria for the light absorption feedback was already proposed based on one-dimensional and regional idealized model studies (*Hense*, 2007; *Sonntag and Hense*, 2011; *Sonntag*, 2013; *Hense et al.*, 2017). We affirm this hypothesis in the framework of a comprehensive Earth system model and show that the effects are in opposite to what one-dimensional considerations would let expect.

In the additional scenario, in which we provided cyanobacteria with a set of potential physiological advantages and adaptation mechanisms (pH-dependent growth, temperature adaptation and utilization of DOP (DOM)) to better cope with the stressors associated with climate change, cyanobacteria also decrease in large areas. The reason why cyanobacteria do not succeed to increase under rising CO₂ in these areas is mainly phosphate limitation. Although both the pH-dependent growth rate and adaptation to higher temperatures actually promote growth, the uptake of DOP (DOM) is not large enough to overcome the increasing phosphate depletion in the transient simulations. The respective studies which suggest an increase in cyanobacteria or N₂ fixation to take place, have often considered only individual factors, like pH-dependent growth (*Barcelos e Ramos et al.*, 2007; *Hutchins et al.*, 2007; *Levitan et al.*,

2007; *Hutchins et al.*, 2009) or increased nutrient (iron and nitrogen) deposition (e.g., *Krishnamurthy et al.*, 2009), but did not take into account the limiting effect of the declining phosphorus availability which concurrently takes place. Our results with the global model, on the contrary, account for the combination of diverse factors. Nevertheless, it has to be kept in mind that the respective underlying processes are only represented very simplified. In particular, the parameterization of cyanobacteria's growth on DOP (which is not represented prognostically in the model) is highly idealized through the uptake of DOM. The additional growth capacity of cyanobacteria gained by the growth on DOM is strongly dependent on model peculiarities, such as the fractionation of decaying phytoplankton into the dissolved and particulate organic matter pools as well as the respective remineralization rates. Furthermore, the constant, potentially underestimated N:P ratio applied for cyanobacteria in the model might lead to an overestimation of the requirement on phosphorus for their growth (*Paulsen et al.*, 2017, Chapter 2 of this thesis). With respect to the temperature adaptation of cyanobacteria, the linear increase of the optimum temperature with time which is applied in the additional scenario, has to be seen as a very idealized representation of the potential adaptation which could take place under greenhouse warming. Regarding the CO₂ forcing, it might be argued that our transient scenarios are quite extreme. The idealized 1% atmospheric CO₂ increase per year was applied for the purpose of process understanding. The respective CO₂ increase indeed exceeds the more realistic Representative Concentration Pathway (RCP) scenarios (*Moss et al.*, 2010) by far. However, also in the middle of our transient simulations, which roughly corresponds to a global warming of 2 K, already a decrease in cyanobacteria and bulk phytoplankton takes place in both setups (FB_1% and FBcya_1%).

One region, that, in contrast to the overall decline, evolves as hotspot of cyanobacteria abundance (especially in the modified scenario FBcya_1%), is the eastern tropical Pacific. Here, the increase in cyanobacteria due to alleviated temperature limitation and sufficiently available phosphate and DOP, to some extent counteracts the decline in chlorophyll. As a consequence, the additional warming signal due to the biogeophysical feedback is slightly – but detectably – reduced in the tropical Pacific in setup FBcya compared to FB. This shows that cyanobacteria, which might benefit in the real world even more than simulated in our simplistic scenario, might to some extent counteract the decline in chlorophyll, and hence the additional warming, in distinct regions, such as the tropical Pacific.

As already discussed, all conducted simulations have to be seen as idealized potential scenarios of the response of marine biota to rising CO₂. HAMOCC is not an ecosystem model but relies on rather simple assumptions of functional relationships between phytoplankton growth and environmental conditions. Especially for cyanobacteria, the physiological understanding is incomplete. Furthermore, exter-

nal factors like changes in iron and nitrogen deposition (e.g., *Krishnamurthy et al.*, 2010) which are not accounted for in our simulations, might additionally either fuel or impair N₂ fixers' growth and N₂ fixation. Besides uncertainties in the evolution and response to rising CO₂, the potential shortcomings in the distribution of cyanobacteria in the control states (*Paulsen et al.*, 2017, Chapter 2 of this thesis) have also to be kept in mind. The lack of observations in large parts of the ocean limits the model evaluation. Especially in the eastern tropical Pacific, which is a relevant area according to our model results, observational coverage is sparse. In addition, chlorophyll, which is used as a measure of light absorption strength in our feedback simulations, and which is prescribed as a linear function of the simulated phytoplankton concentrations, has to be seen as a first order estimate of the spatial distribution of light absorption. The magnitudes of the simulated effects are hence still subject to uncertainty. Nevertheless, acknowledging all uncertainties with respect to the magnitude of the effects, the results reveal the potential that phytoplankton changes have to regionally amplify climate change.

4.8 Conclusions

Based on simulations with the comprehensive Earth system model MPI-ESM we show that climate-change induced alterations in phytoplankton abundances have the potential, in turn, to alter climate change on the regional scale. Thereby, the projected decline in phytoplankton concentrations in the tropical and subtropical ocean amplifies tropical warming under rising CO₂. N₂-fixing cyanobacteria strongly contribute to the negative trend in phytoplankton concentrations. The tested potential adaptation mechanisms of cyanobacteria only regionally lead to an increase in their abundance, which slightly weakens the additional warming effect. The degree of additional warming is thus sensitive to details in the patterns of phytoplankton change. The uncertainty which prevails with respect to the phytoplankton evolution adds another source of uncertainty in climate projections which has been largely overlooked until now. More observations and research is needed to understand and simulate marine biota's response to changing environmental conditions, not only due to its role in the carbon-climate feedback, but also due to its role in the biogeophysical feedback of light absorption. In the tropical and subtropical ocean, positively buoyant, N₂-fixing cyanobacteria are a relevant candidate to be considered in the models.

Appendix Ch4: Effects on SST and surface air temperature on the global scale

The effects on SST and surface air temperature on the global scale of including the light absorption feedback in the transient simulations relative to the respective preindustrial reference state are shown in Figure 4.20a,b (analogous to Figure 4.6c and 4.8f, but globally).

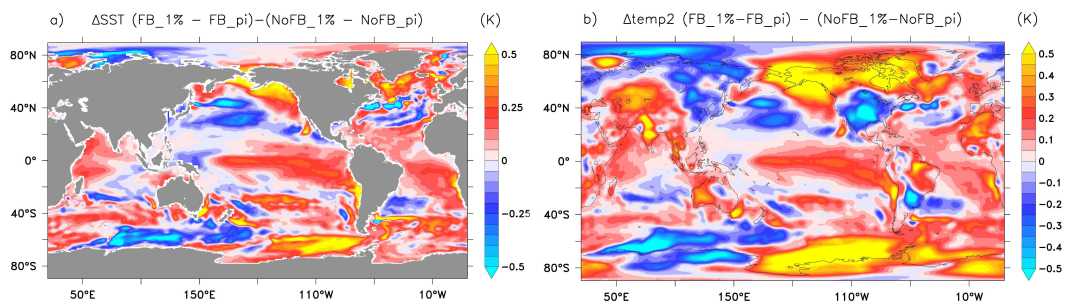


Figure 4.20: a) Relative difference of the change in SST [K] between FB_1% (last 20 year ensemble mean) and FB_pi (100 year mean) compared to NoFB_1% (last 20 year ensemble mean) and NoFB_pi (100 year mean). b) Relative difference of the change in surface (2 m) air temperature [K] between FB_1% (last 20 year ensemble mean) and FB_pi (100 year mean) compared to NoFB_1% (last 20 year ensemble mean) and NoFB_pi (100 year mean).

Chapter 5

Conclusions and outlook

5.1 Conclusions

In this thesis, I have investigated the role of marine N₂-fixing cyanobacteria in the Earth system. For this purpose, I have implemented cyanobacteria as a prognostic phytoplankton group in HAMOCC, the ocean biogeochemical component of the comprehensive Earth system model MPI-ESM. This enabled me to study the effects of cyanobacteria on ocean biogeochemistry, as well as the effects on climate due to the biogeophysical feedback from light absorption on the ocean heat budget. In a set of atmospheric CO₂ increase scenarios, I further investigated the response of cyanobacteria – and the related biogeophysical feedback – in a high CO₂ world. I conclude the thesis by revisiting the research questions posed in the introduction.

1. What are the effects of N₂-fixing cyanobacteria on ocean biogeochemistry?

The prognostic N₂-fixing cyanobacteria determine the spatial distribution and the temporal variability of the supply of bioavailable nitrogen into the ocean's euphotic zone. Both aspects are considerably improved by the prognostic representation of cyanobacteria compared to the diagnostic, geochemical approach of N₂ fixation which was applied before. The new model component is included in the standard model version of HAMOCC, which will be used for instance in CMIP6 simulations. The prognostic growth parameterization reproduces the large scale distribution of N₂ fixation rates, confined to the tropical and subtropical ocean between 40°S and 40°N, with a total value of ~135 Tg N yr⁻¹. In the diagnostic formulation the patterns were exclusively controlled by fixed nitrogen deficits. Now, the prognostic N₂ fixation is partially decoupled from the upwelling areas of nitrogen-depleted water masses due to the limiting factors of temperature, phosphate, and iron which

are additionally taken into account for cyanobacteria growth. Cyanobacteria, with a primary production of $\sim 3 \text{ Gt C yr}^{-1}$, contribute $\sim 7\%$ to the global primary production. The prognostic growth dynamics of cyanobacteria, responding to seasonal changes in physical conditions and acting on a variable standing stock, are able – and indeed required – to simulate a reasonable seasonal variability of N_2 fixation.

Along with a more realistic spatial distribution of the input of nitrate into the surface ocean, also the relative abundance of surface phosphate to nitrate is improved. Especially in high latitudes and in upwelling areas above denitrification sites, the absence of N_2 fixation increases the values of excess phosphate, which is in better agreement with climatological observations. Overall, the reorganization of nutrients in the upper ocean due to including N_2 -fixing cyanobacteria in the model results in a somewhat different biogeochemical mean state, which is expressed in small changes in net primary production and export production. The new values are still within the reported range of observed estimates.

The importance of treating N_2 fixation prognostically lies furthermore in its potential relevance for climate projections. Representing the ability of N_2 fixers to respond to changing environmental conditions is likely important to simulate related impacts on ocean's biological pump. Although current knowledge on the evolution of potentially relevant factors such as dust deposition is limited, the new model component of prognostic N_2 fixers is a mandatory first step to take these factors into account in projections of future climate.

2. What are the effects of light absorption by N_2 -fixing cyanobacteria on the climate system?

The simulations with the MPI-ESM indicate that light absorption by cyanobacteria influences the Earth system on climate relevant scales and magnitudes. Accounting for cyanobacteria in complement to bulk phytoplankton in the attenuation depth of light leads to a cooling of the mean surface ocean in the tropics, regionally by up to 0.5 K. This is because cyanobacteria shade and hence cool the subsurface water that enters the shallow meridional overturning cells and that is upwelled at the equator and in eastern boundary upwelling systems. This advective process of bringing cooler subsurface water to the surface, on the large scale, outweighs the direct heating effect that was indicated by observations and idealized one-dimensional studies on the local scale. Implications of the surface cooling for climate include a strengthening ($\sim 6\%$) and westward shift ($\sim 3^\circ$ longitude) of the Walker circulation and considerable changes in precipitation (up to 1.0 mm d^{-1}). Changes in temperature and in the supply of nutrients feed back on cyanobacteria growth itself, imposing a complex pattern of positive and negative feedback loops between cyanobacteria, and

ocean and atmosphere dynamics. The amplitude of the seasonal cycle of SST is increased in areas of cyanobacteria abundance by up to 20%, and tropical Pacific variability is enhanced by up to 30%.

Overall, including the dynamic feedback from phytoplankton (bulk phytoplankton and cyanobacteria) on the ocean heat budget in MPI-ESM reduces the SST bias and improves the variability in the tropical ocean in comparison to applying a globally constant attenuation depth (as done in the standard model configuration). The specific relevance of cyanobacteria in the biogeophysical feedback comes about through their traits of being able to fix N_2 and their positive buoyancy, which ensure cyanobacteria's abundance in areas of the ocean that have a regulative effect on tropical SST and climate.

3. How do changes in phytoplankton alter climate's response to rising CO_2 , and what is the role of cyanobacteria?

Both phytoplankton groups (bulk phytoplankton and cyanobacteria) are projected to decline in the tropical and subtropical region in the transient scenarios with 1% atmospheric CO_2 increase per year. For bulk phytoplankton, intensified nutrient limitation is responsible, and for cyanobacteria a combination of phosphate and temperature limitation, respectively. The related changes in radiative heating amplify tropical warming, regionally by up to 0.5 K, or $\sim 20\%$, under quadrupling atmospheric CO_2 concentrations. This is because the increased water clarity allows shortwave radiation to penetrate deeper into the water column, which leads to an enhanced heating of the subsurface water that is upwelled at the equator and in eastern boundary upwelling areas. Implications of the regionally enhanced surface warming include a stronger slowdown of the Walker circulation (30%) and regionally enhanced changes in precipitation.

The phytoplankton group of cyanobacteria strongly contribute to the decline in water turbidity under rising CO_2 . Implementing proposed physiological characteristics and adaptation mechanisms of cyanobacteria, such as a pH-dependent growth rate, temperature adaptation, and the uptake of dissolved organic phosphorus, only regionally leads to an increase in cyanobacteria abundance in the additional CO_2 increase scenario. The regional increase in the eastern equatorial Pacific slightly weakens the additional warming signal of the equatorial cold tongue, however, does not override the impact of the otherwise overall decline in phytoplankton.

The results show that climate-change induced alterations in phytoplankton abundance have the potential to regionally amplify tropical climate change – a feedback which has been largely overlooked in climate projections so far. According to the results of this thesis, cyanobacteria considerably contribute to changes in the phytoplankton distribution under rising CO_2 , and thus are relevant to be considered.

Concluding remark

The results of this thesis demonstrate two aspects why N_2 -fixing, positively buoyant cyanobacteria should be considered as a prognostic phytoplankton functional type in ocean biogeochemistry components of Earth system models. First, the prognostic growth dynamics of N_2 -fixing organisms are needed to represent the spatial and temporal supply of bioavailable nitrogen to the euphotic zone, as well as the response of N_2 fixation to changing environmental conditions. Second, cyanobacteria should be included in the biogeophysical feedback of phytoplankton radiative heating due to their regulative effect on tropical climate mean state and variability. Changes in cyanobacteria abundance have therefore the potential to feed back on future climate. On the basis of current knowledge, the implementation of cyanobacteria and the light absorption feedback presented in this study provides a reasonable representation of the respective processes, which allows further refinement in the course of expanding research.

5.2 Outlook

Constraining the effects The directions of action of the processes and mechanisms induced by cyanobacteria light absorption (that means the signs in the resulting effects on temperature and climate) seem to be robust. The magnitudes of the simulated effects are, however, subject to uncertainty. The sensitivity of the magnitudes to details in the distribution and light absorption strength of cyanobacteria, and at the same time the uncertainties which still herein persist, stress the need for more observations to further constrain the model results.

First of all, more observations of the distribution of cyanobacteria in the global ocean are needed to further test and evaluate the applied growth parameterization in the model. Especially for the eastern tropical Pacific, which is a cyanobacteria hotspot according to the model results, observational evidence is required for validation. Dust deposition is potentially an important factor to be considered.

Besides investigating the behaviour of cyanobacteria in present-day climate, a better understanding of their physiological response and adaptation strategies in changing environmental conditions is substantial for projecting future evolution of cyanobacteria under greenhouse warming. In particular, understanding the role of multiple determinant factors acting concurrently, including seawater pH, oxygen, temperature, irradiance and the availability of co-limiting nutrients is important. With respect to nutrients, phosphate seems to be a dominant limiting factor according to the results of this thesis. Extended research on the capacity to utilize other phosphorus sources, such as dissolved organic phosphorus, may help to estimate

cyanobacteria's potential of success.

In addition to expanding knowledge on the spatial distribution and future evolution of cyanobacteria, better knowledge about their characteristics of light absorption (that means their content of chlorophyll and other absorbing pigments) would allow to further constrain the strength of the feedback and the resulting magnitudes of the effects on ocean temperature and climate in the model.

Further feedback mechanisms Besides through absorbing light, the bloom forming behaviour of cyanobacteria affects ocean physics by two other feedback mechanisms. Cyanobacteria blooms increase the surface albedo (*Kahru et al.*, 1993) and reduce vertical mixing (*Jöhnk et al.*, 2008). The effects of these additional feedbacks have only been studied in an idealized one-dimensional and regional study so far (*Sonntag and Hense*, 2011; *Sonntag*, 2013). In order to assess the relevance of these feedbacks on the global scale and further to include the interactions with the atmosphere, a study with a global coupled model is necessary. Since the representation of phytoplankton in HAMOCC is now expanded by prognostic N₂-fixing, positively buoyant cyanobacteria, MPI-ESM could indeed be applied for this purpose. Still, for both feedbacks the observational evidence is sparse. More empirical data of the direct effects of cyanobacteria organisms on their physical environment is needed to reasonably parameterize the feedback mechanisms in the model.

References

- Ammerman, J. W., R. R. Hood, D. A. Case, and J. B. Cotner, Phosphorus deficiency in the Atlantic: An emerging paradigm in oceanography, *Eos, Transactions American Geophysical Union*, 84(18), 165–170, 2003.
- Anderson, W., A. Gnanadesikan, R. Hallberg, J. Dunne, and B. Samuels, Impact of ocean color on the maintenance of the pacific cold tongue, *Geophysical Research Letters*, 34(11), 2007.
- Anderson, W., A. Gnanadesikan, and A. Wittenberg, Regional impacts of ocean color on tropical pacific variability, *Ocean Science*, 5(3), 313, 2009.
- Andrews, O., N. Bindoff, P. Halloran, T. Ilyina, and C. Le Quéré, Detecting an external influence on recent changes in oceanic oxygen using an optimal fingerprinting method, *Biogeosciences*, 10(3), 1799–1813, 2013.
- Archer, D., and K. Johnson, A model of the iron cycle in the ocean, *Global Biogeochemical Cycles*, 14(1), 269–279, 2000.
- Ballabrera-Poy, J., R. Murtugudde, R. Zhang, and A. Busalacchi, Coupled ocean–atmosphere response to seasonal modulation of ocean color: Impact on interannual climate simulations in the tropical Pacific, *Journal of climate*, 20(2), 353–374, 2007.
- Bar-Zeev, E., I. Avishay, K. D. Bidle, and I. Berman-Frank, Programmed cell death in the marine cyanobacterium *Trichodesmium* mediates carbon and nitrogen export, *The ISME journal*, 7(12), 2340–2348, 2013.
- Barcelos e Ramos, J., H. Biswas, K. G. Schulz, J. LaRoche, and U. Riebesell, Effect of rising atmospheric carbon dioxide on the marine nitrogen fixer *Trichodesmium*, *Global biogeochemical cycles*, 21(2), 2007.
- Behrenfeld, M. J., R. T O'Malley, D. A. Siegel, C. R. McClain, J. L. Sarmiento, G. C. Feldman, A. J. Milligan, P. G. Falkowski, R. M. Letelier, and E. S. Boss, Climate-driven trends in contemporary ocean productivity, *Nature*, 444(7120), 752, 2006.

- Bergman, B., Nitrogen-fixing cyanobacteria in tropical oceans, with emphasis on the Western Indian Ocean, *South African journal of botany*, 67(3), 426–432, 2001.
- Berman-Frank, I., J. T. Cullen, Y. Shaked, R. M. Sherrell, and P. G. Falkowski, Iron availability, cellular iron quotas, and nitrogen fixation in *Trichodesmium*, *Limnology and Oceanography*, 46(6), 1249–1260, 2001.
- Bopp, L., L. Resplandy, J. C. Orr, S. C. Doney, J. P. Dunne, M. Gehlen, P. Halloran, C. Heinze, T. Ilyina, R. Seferian, et al., Multiple stressors of ocean ecosystems in the 21st century: projections with CMIP5 models, *Biogeosciences*, 10, 6225–6245, 2013.
- Boyce, D. G., M. R. Lewis, and B. Worm, Global phytoplankton decline over the past century, *Nature*, 466(7306), 591–596, 2010.
- Boyd, P. W., and S. C. Doney, Modelling regional responses by marine pelagic ecosystems to global climate change, *Geophysical Research Letters*, 29(16), 2002.
- Breitbarth, E., A. Oschlies, and J. LaRoche, Physiological constraints on the global distribution of *Trichodesmium* - effect of temperature on diazotrophy, *Biogeosciences*, 4(1), 53–61, 2007.
- Brodhagen, T., Effects of phytoplankton motility on upper ocean physics – Modelling biogeophysical feedback mechanisms, Master's thesis, Universität Hamburg, 2015.
- Capone, D. G., Marine nitrogen fixation: what's the fuss?, *Current opinion in microbiology*, 4(3), 341–348, 2001.
- Capone, D. G., J. P. Zehr, H. W. Paerl, B. Bergman, and E. J. Carpenter, *Trichodesmium*, a globally significant marine cyanobacterium, *Science*, 276(5316), 1221–1229, 1997.
- Capone, D. G., A. Subramaniam, J. P. Montoya, M. Voss, C. Humborg, A. M. Johansen, R. L. Siefert, and E. J. Carpenter, An extensive bloom of the diazotrophic cyanobacterium, *Trichodesmium*, in the Central Arabian Sea during the spring intermonsoon, *Mar. Ecol. Prog. Ser.*, 172, 281–292, 1998.
- Capone, D. G., J. A. Burns, J. P. Montoya, A. Subramaniam, C. Mahaffey, T. Gunderson, A. F. Michaels, and E. J. Carpenter, Nitrogen fixation by *Trichodesmium* spp.: An important source of new nitrogen to the tropical and subtropical North Atlantic Ocean, *Global Biogeochemical Cycles*, 19(2), 2005.
- Carpenter, E. J., and D. G. Capone, Nitrogen fixation in *Trichodesmium* blooms, in *Marine pelagic cyanobacteria: Trichodesmium and other diazotrophs*, pp. 211–217, Springer, 1992.

- Carpenter, E. J., and C. C. Price, Nitrogen fixation, distribution, and production of *Oscillatoria (Trichodesmium)* spp. in the western Sargasso and Caribbean Seas, *Limnology and Oceanography*, 22(1), 60–72, 1977.
- Carpenter, E. J., and K. Romans, Major role of the cyanobacterium *Trichodesmium* in nutrient cycling in the North Atlantic Ocean., *Science(Washington)*, 254(5036), 1356–1358, 1991.
- Carpenter, E. J., J. P. Montoya, J. Burns, M. R. Mulholland, A. Subramaniam, and D. G. Capone, Extensive bloom of a N₂-fixing diatom/cyanobacterial association in the tropical Atlantic Ocean, 1999.
- Carpenter, E. J., A. Subramaniam, and D. G. Capone, Biomass and primary productivity of the cyanobacterium *Trichodesmium* spp. in the tropical North Atlantic ocean, *Deep Sea Research Part I: Oceanographic Research Papers*, 51(2), 173–203, 2004.
- Carr, M.-E., M. A. Friedrichs, M. Schmeltz, M. N. Aita, D. Antoine, K. R. Arrigo, I. Asanuma, O. Aumont, R. Barber, M. Behrenfeld, et al., A comparison of global estimates of marine primary production from ocean color, *Deep Sea Research Part II: Topical Studies in Oceanography*, 53(5), 741–770, 2006.
- Church, M. J., C. Mahaffey, R. M. Letelier, R. Lukas, J. P. Zehr, and D. M. Karl, Physical forcing of nitrogen fixation and diazotroph community structure in the North Pacific subtropical gyre, *Global Biogeochemical Cycles*, 23(2), 2009.
- Cocco, V., F. Joos, M. Steinacker, T. Frölicher, L. Bopp, J. Dunne, M. Gehlen, C. Heinze, J. Orr, A. Oeschlies, et al., Oxygen and indicators of stress for marine life in multi-model global warming projections, *Biogeosciences*, 10, 1849–1868, 2013.
- Collins, M., S.-I. An, W. Cai, A. Ganachaud, E. Guilyardi, F.-F. Jin, M. Jochum, M. Lengaigne, S. Power, A. Timmermann, et al., The impact of global warming on the tropical Pacific Ocean and El Niño, *Nature Geoscience*, 3(6), 391–397, 2010.
- Collins, W., N. Bellouin, M. Doutriaux-Boucher, N. Gedney, P. Halloran, T. Hinton, J. Hughes, C. Jones, M. Joshi, S. Liddicoat, et al., Development and evaluation of an Earth-system model–HadGEM2, *Geoscientific Model Development*, 4(4), 1051–1075, 2011.
- Dabundo, R., M. F. Lehmann, L. Treibergs, C. R. Tobias, M. A. Altabet, P. H. Moisaner, and J. Granger, The contamination of commercial ¹⁵N₂ gas stocks with ¹⁵N-labeled nitrate and ammonium and consequences for nitrogen fixation measurements, *PLoS one*, 9(10), e110335, 2014.
- Davis, C. S., and D. J. McGillicuddy, Transatlantic abundance of the N₂-fixing colonial cyanobacterium *Trichodesmium*, *Science*, 312(5779), 1517–1520, 2006.

- Deutsch, C., J. L. Sarmiento, D. M. Sigman, N. Gruber, and J. P. Dunne, Spatial coupling of nitrogen inputs and losses in the ocean, *Nature*, 445(7124), 163–167, 2007.
- Devassy, V., and J. Goes, Phytoplankton community structure and succession in a tropical estuarine complex (central west coast of India), *Estuarine, Coastal and Shelf Science*, 27(6), 671–685, 1988.
- Doney, S. C., Oceanography: Plankton in a warmer world, *Nature*, 444(7120), 695–696, 2006.
- Dunne, J. P., J. G. John, E. Shevliakova, R. J. Stouffer, J. P. Krasting, S. L. Malyshch, P. Milly, L. T. Sentman, A. J. Adcroft, W. Cooke, et al., GFDL's ESM2 Global Coupled Climate–Carbon Earth System Models. Part II: Carbon System Formulation and Baseline Simulation Characteristics*, *Journal of Climate*, 26(7), 2247–2267, 2013.
- Dupouy, C., J. Neveux, A. Subramaniam, M. R. Mulholland, J. P. Montoya, L. Campbell, E. J. Carpenter, and D. G. Capone, Satellite captures *Trichodesmium* blooms in the southwestern tropical Pacific, *Eos, Transactions American Geophysical Union*, 81(2), 13–16, 2000.
- Dyrhman, S., P. Chappell, S. Haley, J. Moffett, E. Orchard, J. Waterbury, and E. Webb, Phosphonate utilization by the globally important marine diazotroph *Trichodesmium*, *Nature*, 439(7072), 68–71, 2006.
- Eichner, M., S. A. Kranz, and B. Rost, Combined effects of different CO₂ levels and N sources on the diazotrophic cyanobacterium *Trichodesmium*, *Physiologia plantarum*, 152(2), 316–330, 2014.
- Eppley, R. W., Temperature and phytoplankton growth in the sea, *Fish. Bull.*, 70(4), 1063–1085, 1972.
- Falcón, L. I., S. Pluvinage, and E. J. Carpenter, Growth kinetics of marine unicellular N₂-fixing cyanobacterial isolates in continuous culture in relation to phosphorus and temperature, *Marine Ecology Progress Series*, 285, 3–9, 2005.
- Falkowski, P. G., Evolution of the nitrogen cycle and its influence on the biological sequestration of CO₂ in the ocean, *Nature*, 387(6630), 272–275, 1997.
- Falkowski, P. G., and M. J. Oliver, Mix and match: how climate selects phytoplankton, *Nature reviews. Microbiology*, 5(10), 813, 2007.
- Falkowski, P. G., R. T. Barber, and V. Smetacek, Biogeochemical controls and feedbacks on ocean primary production, *Science*, 281(5374), 200–206, 1998.

- Fennel, K., Y. H. Spitz, R. M. Letelier, M. R. Abbott, and D. M. Karl, A deterministic model for N₂ fixation at stn. ALOHA in the subtropical North Pacific Ocean, *Deep Sea Research Part II: Topical Studies in Oceanography*, 49(1), 149–174, 2002.
- Foster, R. A., and J. P. Zehr, Characterization of diatom–cyanobacteria symbioses on the basis of *nifH*, *hetR* and 16S rRNA sequences, *Environmental Microbiology*, 8(11), 1913–1925, 2006.
- Galloway, J. N., F. J. Dentener, D. G. Capone, E. W. Boyer, R. W. Howarth, S. P. Seitzinger, G. P. Asner, C. Cleveland, P. Green, E. Holland, et al., Nitrogen cycles: past, present, and future, *Biogeochemistry*, 70(2), 153–226, 2004.
- Giorgetta, M. A., J. Jungclaus, C. H. Reick, S. Legutke, J. Bader, M. Böttinger, V. Brovkin, T. Crueger, M. Esch, K. Fieg, et al., Climate and carbon cycle changes from 1850 to 2100 in MPI-ESM simulations for the Coupled Model Intercomparison Project phase 5, *Journal of Advances in Modeling Earth Systems*, 5(3), 572–597, 2013.
- Gnanadesikan, A., and W. G. Anderson, Ocean water clarity and the ocean general circulation in a coupled climate model, *Journal of Physical Oceanography*, 39(2), 314–332, 2009.
- Gower, G. A. B. J. F., and E. J. Carpenter, Development of algorithms for remote sensing of *Trichodesmium* blooms, *Marine pelagic cyanobacteria: Trichodesmium and other diazotrophs*, 362, 193, 1992.
- Großkopf, T., W. Mohr, T. Baustian, H. Schunck, D. Gill, M. M. Kuypers, G. Lavik, R. A. Schmitz, D. W. Wallace, and J. LaRoche, Doubling of marine dinitrogen-fixation rates based on direct measurements, *Nature*, 488(7411), 361–364, 2012.
- Gruber, N., The dynamics of the marine nitrogen cycle and its influence on atmospheric CO₂ variations, in *The ocean carbon cycle and climate*, pp. 97–148, Springer, 2004.
- Gruber, N., and J. N. Galloway, An Earth-system perspective of the global nitrogen cycle, *Nature*, 451(7176), 293–296, 2008.
- Gruber, N., and J. L. Sarmiento, Global patterns of marine nitrogen fixation and denitrification, *Global Biogeochemical Cycles*, 11(2), 235–266, 1997.
- Guidi, L., P. H. Calil, S. Duhamel, K. M. Björkman, S. C. Doney, G. A. Jackson, B. Li, M. J. Church, S. Tozzi, Z. S. Kolber, et al., Does eddy-eddy interaction control surface phytoplankton distribution and carbon export in the North Pacific Subtropical Gyre?, *Journal of Geophysical Research: Biogeosciences*, 117(G2), 2012.

- Hense, I., Regulative feedback mechanisms in cyanobacteria-driven systems: a model study, *Marine Ecology Progress Series*, 339, 41–47, 2007.
- Hense, I., I. Stemmler, and S. Sonntag, Ideas and perspectives: climate-relevant marine biologically driven mechanisms in earth system models, *Biogeosciences*, 14(2), 403, 2017.
- Hewson, I., S. R. Govil, D. G. Capone, E. J. Carpenter, and J. A. Fuhrman, Evidence of *Trichodesmium* viral lysis and potential significance for biogeochemical cycling in the oligotrophic ocean, *Aquatic Microbial Ecology*, 36(1), 1–8, 2004.
- Hinners, J., Modeling the Effects of Ocean Acidification on N₂-fixing Cyanobacteria in the Baltic Sea, Master's thesis, Humboldt Universität zu Berlin, 2014.
- Holl, C. M., and J. P. Montoya, Interactions between nitrate uptake and nitrogen fixation in continuous cultures of the marine diazotroph *Trichodesmium* (Cyanobacteria), *Journal of Phycology*, 41(6), 1178–1183, 2005.
- Hood, R. R., N. R. Bates, D. G. Capone, and D. B. Olson, Modeling the effect of nitrogen fixation on carbon and nitrogen fluxes at BATS, *Deep Sea Research Part II: Topical Studies in Oceanography*, 48(8), 1609–1648, 2001.
- Hood, R. R., V. J. Coles, and D. G. Capone, Modeling the distribution of *Trichodesmium* and nitrogen fixation in the Atlantic Ocean, *Journal of Geophysical Research: Oceans*, 109(C6), 2004.
- Hutchins, D., F.-X. Fu, Y. Zhang, M. Warner, Y. Feng, K. Portune, P. Bernhardt, and M. Mulholland, CO₂ control of *Trichodesmium* N₂ fixation, photosynthesis, growth rates, and elemental ratios: Implications for past, present, and future ocean biogeochemistry, *Limnology and Oceanography*, 52(4), 1293, 2007.
- Hutchins, D. A., and F. Fu, Microorganisms and ocean global change., *Nature microbiology*, 2, 17,058, 2017.
- Hutchins, D. A., M. R. Mulholland, and F. Fu, Nutrient cycles and marine microbes in a CO₂-enriched ocean, *Oceanography*, 22(4), 128–145, 2009.
- Ilyina, T., K. D. Six, J. Segschneider, E. Maier-Reimer, H. Li, and I. Núñez-Riboni, Global ocean biogeochemistry model HAMOCC: Model architecture and performance as component of the MPI-Earth system model in different CMIP5 experimental realizations, *Journal of Advances in Modeling Earth Systems*, 5(2), 287–315, 2013.
- Jerlov, N., Optical water types, *Marine Optics. Elsevier Scientific, New York*, pp. 132–137, 1976.

- Jiao, N., G. J. Herndl, D. A. Hansell, R. Benner, G. Kattner, S. W. Wilhelm, D. L. Kirchman, M. G. Weinbauer, T. Luo, F. Chen, et al., Microbial production of recalcitrant dissolved organic matter: long-term carbon storage in the global ocean, *Nature Reviews Microbiology*, 8(8), 593–599, 2010.
- Jochum, M., S. Yeager, K. Lindsay, K. Moore, and R. Murtugudde, Quantification of the feedback between phytoplankton and ENSO in the Community Climate System Model, *Journal of Climate*, 23(11), 2916–2925, 2010.
- Jöhnk, K. D., J. Huisman, J. Sharples, B. Sommeijer, P. M. Visser, and J. M. Stroom, Summer heatwaves promote blooms of harmful cyanobacteria, *Global change biology*, 14(3), 495–512, 2008.
- Johnson, K. S., R. M. Gordon, and K. H. Coale, What controls dissolved iron concentrations in the world ocean? Authors' closing comments, *Marine Chemistry*, 57(3-4), 181–186, 1997.
- Jungclaus, J., N. Fischer, H. Haak, K. Lohmann, J. Marotzke, D. Matei, U. Mikolajewicz, D. Notz, and J. Storch, Characteristics of the ocean simulations in the Max Planck Institute Ocean Model (MPIOM) the ocean component of the MPI-Earth system model, *Journal of Advances in Modeling Earth Systems*, 5(2), 422–446, 2013.
- Kahru, M., J.-M. Leppäaenen, and O. Rud, Cyanobacterial blooms heating of the sea surface, *Marine ecology progress series. Oldendorf*, 101(1), 1–7, 1993.
- Kara, A. B., A. J. Wallcraft, and H. E. Hurlburt, A new solar radiation penetration scheme for use in ocean mixed layer studies: an application to the Black Sea using a fine-resolution Hybrid Coordinate Ocean Model (HYCOM), *Journal of physical oceanography*, 35(1), 13–32, 2005.
- Karl, D., A. Michaels, B. Bergman, D. Capone, E. Carpenter, R. Letelier, F. Lipschultz, H. Paerl, D. Sigman, and L. Stal, *Dinitrogen fixation in the worlds oceans*, Springer, 2002.
- Karl, D. M., and R. M. Letelier, Nitrogen fixation-enhanced carbon sequestration in low nitrate, low chlorophyll seascapes, *Marine Ecology Progress Series*, 364, 257–268, 2008.
- Karl, D. M., R. Letelier, D. V. Hebel, D. F. Bird, and C. D. Winn, *Trichodesmium* blooms and new nitrogen in the North Pacific gyre, in *Marine pelagic cyanobacteria: Trichodesmium and other diazotrophs*, pp. 219–237, Springer, 1992.
- Kranz, S. A., S. Dieter, K.-U. Richter, and B. Rost, Carbon acquisition by *Trichodesmium*: the effect of pCO₂ and diurnal changes, *Limnology and Oceanography*, 54(2), 548–559, 2009.

- Krauk, J. M., T. A. Villareal, J. A. Sohm, J. P. Montoya, and D. G. Capone, Plasticity of N:P ratios in laboratory and field populations of *Trichodesmium* spp., *Aquat. Microb. Ecol.*, 42, 243–253, 2006.
- Krishnamurthy, A., J. K. Moore, C. S. Zender, and C. Luo, Effects of atmospheric inorganic nitrogen deposition on ocean biogeochemistry, *Journal of Geophysical Research: Biogeosciences*, 112(G2), 2007.
- Krishnamurthy, A., J. K. Moore, N. Mahowald, C. Luo, S. C. Doney, K. Lindsay, and C. S. Zender, Impacts of increasing anthropogenic soluble iron and nitrogen deposition on ocean biogeochemistry, *Global Biogeochemical Cycles*, 23(3), 2009.
- Krishnamurthy, A., J. K. Moore, N. Mahowald, C. Luo, and C. S. Zender, Impacts of atmospheric nutrient inputs on marine biogeochemistry, *Journal of Geophysical Research: Biogeosciences*, 115(G1), 2010.
- Kustka, A. B., S. A. Sañudo-Wilhelmy, E. J. Carpenter, D. Capone, J. Burns, and W. G. Sunda, Iron requirements for dinitrogen- and ammonium-supported growth in cultures of *Trichodesmium* (IMS 101): Comparison with nitrogen fixation rates and iron: carbon ratios of field populations, *Limnology and Oceanography*, 48(5), 1869–1884, 2003.
- Landolfi, A., W. Koeve, H. Dietze, P. Kähler, and A. Oschlies, A new perspective on environmental controls of marine nitrogen fixation, *Geophysical Research Letters*, 42(11), 4482–4489, 2015.
- Langlois, R. J., J. LaRoche, and P. A. Raab, Diazotrophic diversity and distribution in the tropical and subtropical Atlantic Ocean, *Applied and Environmental Microbiology*, 71(12), 7910–7919, 2005.
- LaRoche, J., and E. Breitbarth, Importance of the diazotrophs as a source of new nitrogen in the ocean, *Journal of Sea Research*, 53(1), 67–91, 2005.
- Laufkötter, C., M. Vogt, N. Gruber, M. Aita-Noguchi, O. Aumont, L. Bopp, E. Buitenhuis, S. Doney, J. Dunne, T. Hashioka, et al., Drivers and uncertainties of future global marine primary production in marine ecosystem models, *Biogeosciences*, 12, 6955–6984, 2015.
- Letelier, R. M., and D. M. Karl, *Trichodesmium* spp. physiology and nutrient fluxes in the North Pacific subtropical gyre, 1998.
- Levitan, O., G. Rosenberg, I. Setlik, E. Setlikova, J. Grigel, J. Klepetar, O. Prasil, and I. Berman-Frank, Elevated CO₂ enhances nitrogen fixation and growth in the marine cyanobacterium *Trichodesmium*, *Global Change Biology*, 13(2), 531–538, 2007.

- Levitus, S., T. Boyer, M. Conkright, D. Johnson, T. J. Antonov, C. Stephens, and R. Gelfeld, World ocean database 1998, volume 2: Temporal distribution of mechanical bathythermograph profiles, *NOAA Atlas NESDIS*, 19, 1998.
- Lewis, M., J. Cullen, and T. Platt, Phytoplankton and thermal structure in the upper ocean: consequences of non-uniformity in chlorophyll profile, *Journal of Geophysical Research Oceans*, 88, 2565–2570, 1983.
- Lewis, M. R., M.-E. Carr, G. C. Feldman, W. Esaias, and C. McClain, Influence of penetrating solar radiation on the heat budget of the equatorial pacific ocean, *Nature*, 347(6293), 543, 1990.
- Lin, S., S. Henze, P. Lundgren, B. Bergman, and E. J. Carpenter, Whole-Cell Immunolocalization of Nitrogenase in Marine Diazotrophic Cyanobacteria, *Trichodesmium* spp., *Applied and Environmental Microbiology*, 64(8), 3052–3058, 1998.
- Löptien, U., C. Eden, A. Timmermann, and H. Dietze, Effects of biologically induced differential heating in an eddy-permitting coupled ocean-ecosystem model, *Journal of Geophysical Research: Oceans*, 114(C6), 2009.
- Lu, J., G. A. Vecchi, and T. Reichler, Expansion of the hadley cell under global warming, *Geophysical Research Letters*, 34(6), 2007.
- Lugomela, C., T. J. Lyimo, I. Bryceson, A. K. Semesi, and B. Bergman, *Trichodesmium* in coastal waters of Tanzania: diversity, seasonality, nitrogen and carbon fixation, *Hydrobiologia*, 477(1-3), 1–13, 2002.
- Luo, C., N. M. Mahowald, and J. Del Corral, Sensitivity study of meteorological parameters on mineral aerosol mobilization, transport, and distribution, *Journal of Geophysical Research: Atmospheres (1984–2012)*, 108(D15), 2003.
- Luo, Y.-W., S. Doney, L. Anderson, M. Benavides, I. Berman-Frank, A. Bode, S. Bonnet, K. Boström, D. Böttjer, D. Capone, et al., Database of diazotrophs in global ocean: abundance, biomass and nitrogen fixation rates, *Earth System Science Data*, 4(1), 47–73, 2012.
- Luo, Y.-W., I. D. Lima, D. M. Karl, C. A. Deutsch, and S. C. Doney, Data-based assessment of environmental controls on global marine nitrogen fixation, *Biogeosciences*, 11, 691–708, 2014.
- Mahaffey, C., A. F. Michaels, and D. G. Capone, The conundrum of marine N₂ fixation, *American Journal of Science*, 305(6-8), 546–595, 2005.
- Mahowald, N., C. Luo, J. Del Corral, and C. S. Zender, Interannual variability in atmospheric mineral aerosols from a 22-year model simulation and observational data, *Journal of Geophysical Research: Atmospheres (1984–2012)*, 108(D12), 2003.

- Mahowald, N. M., D. R. Muhs, S. Levis, P. J. Rasch, M. Yoshioka, C. S. Zender, and C. Luo, Change in atmospheric mineral aerosols in response to climate: Last glacial period, preindustrial, modern, and doubled carbon dioxide climates, *Journal of Geophysical Research: Atmospheres* (1984–2012), 111(D10), 2006.
- Maier-Reimer, E., I. Kriest, J. Segschneider, and P. Wetzel, The HAMBURG Ocean Carbon Cycle Model HAMOCC5.1 - Technical Description Release 1.1, *Reports on Earth System Science*, 14, 2005.
- Manizza, M., C. Le Quéré, A. J. Watson, and E. T. Buitenhuis, Ocean biogeochemical response to phytoplankton-light feedback in a global model, *Journal of Geophysical Research: Oceans*, 113(C10), 2008.
- Marsland, S. J., H. Haak, J. H. Jungclaus, M. Latif, and F. Röske, The Max-Planck-Institute global ocean/sea ice model with orthogonal curvilinear coordinates, *Ocean modelling*, 5(2), 91–127, 2003.
- Martin, J. H., G. A. Knauer, D. M. Karl, and W. W. Broenkow, VERTEX: carbon cycling in the northeast Pacific, *Deep Sea Research Part A. Oceanographic Research Papers*, 34(2), 267–285, 1987.
- Marzeion, B., A. Timmermann, R. Murtugudde, and F.-F. Jin, Biophysical feedbacks in the tropical pacific, *Journal of Climate*, 18(1), 58–70, 2005.
- McCarthy, J. J., and E. J. Carpenter, *Oscillatoria* (*Trichodesmium*) *Thiebautii* (*Cyanophyta*) in the Central North Atlantic Ocean, *Journal of Phycology*, 15(1), 75–82, 1979.
- Meehl, G., P. Gent, J. Arblaster, B. Otto-Bliesner, E. Brady, and A. Craig, Factors that affect the amplitude of El Nino in global coupled climate models, *Climate Dynamics*, 17(7), 515–526, 2001.
- Michaels, A. F., D. M. Karl, and D. G. Capone, Element stoichiometry, new production and nitrogen fixation, *OCEANOGRAPHY-WASHINGTON DC-OCEANOGRAPHY SOCIETY-*, 14(4), 68–77, 2001.
- Milinski, S., J. Bader, H. Haak, A. C. Siongco, and J. H. Jungclaus, High atmospheric horizontal resolution eliminates the wind-driven coastal warm bias in the southeastern tropical Atlantic, *Geophysical Research Letters*, 43(19), 2016.
- Mohanty, A., K. Satpathy, G. Sahu, K. Hussain, M. Prasad, and S. Sarkar, Bloom of *Trichodesmium erythraeum* (*Ehr.*) and its impact on water quality and plankton community structure in the coastal waters of southeast coast of India, 2010.
- Mohr, W., T. Grosskopf, D. W. Wallace, and J. LaRoche, Methodological underestimation of oceanic nitrogen fixation rates, *PLOS one*, 5(9), e12,583, 2010.

- Moisander, P. H., R. A. Beinart, I. Hewson, A. E. White, K. S. Johnson, C. A. Carlson, J. P. Montoya, and J. P. Zehr, Unicellular cyanobacterial distributions broaden the oceanic N₂ fixation domain, *Science*, 327(5972), 1512–1514, 2010.
- Monteiro, F., M. Follows, and S. Dutkiewicz, Distribution of diverse nitrogen fixers in the global ocean, *Global Biogeochemical Cycles*, 24(3), 2010.
- Monteiro, F., S. Dutkiewicz, and M. Follows, Biogeographical controls on the marine nitrogen fixers, *Global Biogeochemical Cycles*, 25(2), 2011.
- Moore, C., M. Mills, K. Arrigo, I. Berman-Frank, L. Bopp, P. Boyd, E. Galbraith, R. J. Geider, C. Guieu, S. Jaccard, et al., Processes and patterns of oceanic nutrient limitation, *Nature geoscience*, 6(9), 701, 2013.
- Moore, C. M., M. M. Mills, E. P. Achterberg, R. J. Geider, J. LaRoche, M. I. Lucas, E. L. McDonagh, X. Pan, A. J. Poulton, M. J. Rijkenberg, et al., Large-scale distribution of Atlantic nitrogen fixation controlled by iron availability, *Nature Geoscience*, 2(12), 867–871, 2009.
- Moore, J. K., and S. C. Doney, Iron availability limits the ocean nitrogen inventory stabilizing feedbacks between marine denitrification and nitrogen fixation, *Global Biogeochemical Cycles*, 21(2), 2007.
- Moore, J. K., S. C. Doney, and K. Lindsay, Upper ocean ecosystem dynamics and iron cycling in a global three-dimensional model, *Global Biogeochemical Cycles*, 18(4), 2004.
- Moss, R. H., J. A. Edmonds, K. A. Hibbard, M. R. Manning, S. K. Rose, D. P. Van Vuuren, T. R. Carter, S. Emori, M. Kainuma, T. Kram, et al., The next generation of scenarios for climate change research and assessment, *Nature*, 463(7282), 747, 2010.
- Mulholland, M. R., and D. G. Capone, The nitrogen physiology of the marine N₂-fixing cyanobacteria *Trichodesmium* spp., *Trends in plant science*, 5(4), 148–153, 2000.
- Murtugudde, R., J. Beauchamp, C. R. McClain, M. Lewis, and A. J. Busalacchi, Effects of penetrative radiation on the upper tropical ocean circulation, *Journal of Climate*, 15(5), 470–486, 2002.
- Najjar, R. G., X. Jin, F. Louanchi, O. Aumont, K. Caldeira, S. C. Doney, J.-C. Dutay, M. Follows, N. Gruber, F. Joos, et al., Impact of circulation on export production, dissolved organic matter, and dissolved oxygen in the ocean: Results from Phase II of the Ocean Carbon-cycle Model Intercomparison Project (OCMIP-2), *Global Biogeochemical Cycles*, 21(3), 2007.

- Nakamoto, S., S. P. Kumar, J. Oberhuber, J. Ishizaka, K. Muneyama, and R. Frouin, Response of the equatorial Pacific to chlorophyll pigment in a mixed layer isopycnal ocean general circulation model, *Geophysical Research Letters*, 28(10), 2021–2024, 2001.
- Navarro Rodriguez, A. J., Optical properties of photosynthetic pigments and abundance of the cyanobacterium *Trichodesmium* in the eastern Caribbean Basin, Ph.D. thesis, UNIVERSITY OF PUERTO RICO, MAYAGUEZ (PUERTO RICO), 1998.
- Needoba, J. A., R. A. Foster, C. Sakamoto, J. P. Zehr, and K. S. Johnson, Nitrogen fixation by unicellular diazotrophic cyanobacteria in the temperate oligotrophic North Pacific Ocean, *Limnology and Oceanography*, 52(4), 1317–1327, 2007.
- O’Neil, J., and M. Roman, Ingestion of the cyanobacterium *Trichodesmium* spp. by pelagic harpacticoid copepods *Macrosetella*, *Miracia* and *Oculosetella*, *Hydrobiologia*, 292(1), 235–240, 1994.
- Orcutt, K. M., F. Lipschultz, K. Gundersen, R. Arimoto, A. F. Michaels, A. H. Knap, and J. R. Gallon, A seasonal study of the significance of N₂ fixation by *Trichodesmium* spp. at the Bermuda Atlantic Time-series Study (BATS) site, *Deep Sea Research Part II: Topical Studies in Oceanography*, 48(8), 1583–1608, 2001.
- Padfield, D., G. Yvon-Durocher, A. Buckling, S. Jennings, and G. Yvon-Durocher, Rapid evolution of metabolic traits explains thermal adaptation in phytoplankton, *Ecology letters*, 19(2), 133–142, 2016.
- Paerl, H. W., and J. Huisman, Blooms like it hot, *Science*, 320(5872), 57, 2008.
- Palmer, J., and I. Totterdell, Production and export in a global ocean ecosystem model, *Deep Sea Research Part I: Oceanographic Research Papers*, 48(5), 1169–1198, 2001.
- Parekh, P., M. J. Follows, and E. A. Boyle, Decoupling of iron and phosphate in the global ocean, *Global Biogeochemical Cycles*, 19(2), 2005.
- Park, J.-Y., J.-S. Kug, H. Seo, and J. Bader, Impact of bio-physical feedbacks on the tropical climate in coupled and uncoupled GCMs, *Climate dynamics*, 43(7-8), 1811–1827, 2014.
- Park, J.-Y., J.-S. Kug, J. Bader, R. Rolph, and M. Kwon, Amplified arctic warming by phytoplankton under greenhouse warming, *Proceedings of the National Academy of Sciences*, 112(19), 5921–5926, 2015.
- Patara, L., M. Vichi, S. Masina, P. G. Fogli, and E. Manzini, Global response to solar radiation absorbed by phytoplankton in a coupled climate model, *Climate dynamics*, 39(7-8), 1951–1968, 2012.

- Paulsen, H., T. Ilyina, K. D. Six, and I. Stemmler, Incorporating a prognostic representation of marine nitrogen fixers into the global ocean biogeochemical model HAMOCC, *Journal of Advances in Modeling Earth Systems*, 9(1), 438–464, 2017.
- Paulson, C. A., and J. J. Simpson, Irradiance measurements in the upper ocean, *Journal of Physical Oceanography*, 7(6), 952–956, 1977.
- Polovina, J. J., E. A. Howell, and M. Abecassis, Ocean's least productive waters are expanding, *Geophysical Research Letters*, 35(3), 2008.
- Rayner, N., D. E. Parker, E. Horton, C. Folland, L. Alexander, D. Rowell, E. Kent, and A. Kaplan, Global analyses of sea surface temperature, sea ice, and night marine air temperature since the late nineteenth century, *Journal of Geophysical Research: Atmospheres*, 108(D14), 2003.
- Reick, C., T. Raddatz, V. Brovkin, and V. Gayler, Representation of natural and anthropogenic land cover change in mpi-esm, *Journal of Advances in Modeling Earth Systems*, 5(3), 459–482, 2013.
- Rodier, M., and R. Le Borgne, Population dynamics and environmental conditions affecting *Trichodesmium* spp. (filamentous cyanobacteria) blooms in the southwest lagoon of New Caledonia, *Journal of Experimental Marine Biology and Ecology*, 358(1), 20–32, 2008.
- Rodier, M., and R. Le Borgne, Population and trophic dynamics of *Trichodesmium thiebautii* in the SE lagoon of New Caledonia. Comparison with *T. erythraeum* in the SW lagoon, *Marine pollution bulletin*, 61(7), 349–359, 2010.
- Röske, F., Global oceanic heat and fresh water forcing datasets based on ERA-40 and ERA-15, *Tech. Rep. 13, Reports on Earth System Science*, 2005.
- Sañudo-Wilhelmy, S. A., A. B. Kustka, C. J. Gobler, D. A. Hutchins, M. Yang, K. Lwiza, J. Burns, D. G. Capone, J. A. Raven, and E. J. Carpenter, Phosphorus limitation of nitrogen fixation by *Trichodesmium* in the central Atlantic Ocean, *Nature*, 411(6833), 66–69, 2001.
- Sarang, R., P. Chauhan, S. Nayak, and U. Shreedhar, Cover: Remote sensing of *Trichodesmium* blooms in the coastal waters off Gujarat, India using IRS-P4 OCM, *International Journal of Remote Sensing*, 26(9), 1777–1780, 2005.
- Sarmiento, J. L., R. Slater, R. Barber, L. Bopp, S. C. Doney, A. Hirst, J. Kleypas, R. Matear, U. Mikolajewicz, P. Monfray, et al., Response of ocean ecosystems to climate warming, *Global Biogeochemical Cycles*, 18(3), 2004.
- Sathyendranath, S., A. D. Gouveia, S. R. Shetye, P. Ravindran, and T. Platt, Biological control of surface temperature in the arabian sea, 1991.

- Sathyendranath, S., V. Stuart, A. Nair, K. Oka, T. Nakane, H. Bouman, M.-H. Forget, H. Maass, and T. Platt, Carbon-to-chlorophyll ratio and growth rate of phytoplankton in the sea, *Marine Ecology Progress Series*, 2009.
- Schneck, R., C. H. Reick, and T. Raddatz, Land contribution to natural CO₂ variability on time scales of centuries, *Journal of Advances in Modeling Earth Systems*, 5(2), 354–365, 2013.
- SeaWiFS Project, Seawifs global monthly mapped 9 km chlorophyll a. ver. 1., PO.DAAC, CA, USA., 2003.
- Simmons, A., and J. Gibson, The ERA-40 Project Plan, ERA-40 Project Report Series No. 1, ECMWF, Reading, UK, p. 63, 2000.
- Six, K. D., and E. Maier-Reimer, Effects of plankton dynamics on seasonal carbon fluxes in an ocean general circulation model, *Global Biogeochemical Cycles*, 10(4), 559–583, 1996.
- Smith, E. L., Photosynthesis in relation to light and carbon dioxide, *Proceedings of the National Academy of Sciences of the United States of America*, 22(8), 504, 1936.
- Sohm, J. A., and D. G. Capone, Phosphorus dynamics of the tropical and subtropical North Atlantic: *Trichodesmium* spp. versus bulk plankton, *Marine Ecology-Progress Series*, 317, 21, 2006.
- Sohm, J. A., E. A. Webb, and D. G. Capone, Emerging patterns of marine nitrogen fixation, *Nature Reviews Microbiology*, 9(7), 499–508, 2011.
- Somes, C. J., and A. Oschlies, On the influence of "non-Redfield" dissolved organic nutrient dynamics on the spatial distribution of N₂ fixation and the size of the marine fixed nitrogen inventory, *Global Biogeochemical Cycles*, 29(7), 973–993, 2015.
- Somes, C. J., A. Schmittner, and M. A. Altabet, Nitrogen isotope simulations show the importance of atmospheric iron deposition for nitrogen fixation across the Pacific Ocean, *Geophysical Research Letters*, 37(23), 2010.
- Sonntag, S., Modeling biological-physical feedback mechanisms in marine systems, Ph.D. thesis, Universität Hamburg, 2013.
- Sonntag, S., and I. Hense, Phytoplankton behavior affects ocean mixed layer dynamics through biological-physical feedback mechanisms, *Geophysical Research Letters*, 38(15), 2011.
- Speich, S., B. Blanke, and W. Cai, Atlantic meridional overturning circulation and the southern hemisphere supergyre, *Geophysical Research Letters*, 34(23), 2007.

- Steele, M., R. Morley, and W. Ermold, PHC: A global ocean hydrography with a high-quality Arctic Ocean, *Journal of Climate*, 14(9), 2079–2087, 2001.
- Stevens, B., M. Giorgetta, M. Esch, T. Mauritsen, T. Crueger, S. Rast, M. Salzmann, H. Schmidt, J. Bader, K. Block, et al., Atmospheric component of the MPI-M Earth System Model: ECHAM6, *Journal of Advances in Modeling Earth Systems*, 5(2), 146–172, 2013.
- Strutton, P. G., and F. P. Chavez, Biological heating in the equatorial Pacific: Observed variability and potential for real-time calculation, *Journal of climate*, 17(5), 1097–1109, 2004.
- Subramaniam, A., C. W. Brown, R. R. Hood, E. J. Carpenter, and D. G. Capone, Detecting *Trichodesmium* blooms in SeaWiFS imagery, *Deep Sea Research Part II: Topical Studies in Oceanography*, 49(1), 107–121, 2001.
- Sweeney, C., A. Gnanadesikan, S. M. Griffies, M. J. Harrison, A. J. Rosati, and B. L. Samuels, Impacts of shortwave penetration depth on large-scale ocean circulation and heat transport, *Journal of Physical Oceanography*, 35(6), 1103–1119, 2005.
- Takahashi, T., W. S. Broecker, and S. Langer, Redfield ratio based on chemical data from isopycnal surfaces, *Journal of Geophysical Research: Oceans (1978–2012)*, 90(C4), 6907–6924, 1985.
- Taylor, A. H., R. J. Geider, and F. J. Gilbert, Seasonal and latitudinal dependencies of phytoplankton carbon-to-chlorophyll a ratios: results of a modelling study, *Marine Ecology Progress Series*, pp. 51–66, 1997.
- Taylor, K., Summarizing in a single diagram multiple aspects of model performance, *J. Geophys. Res.*, 10(6), 7183–7192, 2001.
- Thomas, M. K., C. T. Kremer, C. A. Klausmeier, and E. Litchman, A global pattern of thermal adaptation in marine phytoplankton, *Science*, 338(6110), 1085–1088, 2012.
- Timmermann, A., and F.-F. Jin, Phytoplankton influences on tropical climate, *Geophysical research letters*, 29(23), 2002.
- Vichi, M., N. Pinardi, and S. Masina, A generalized model of pelagic biogeochemistry for the global ocean ecosystem. Part I: Theory, *Journal of Marine Systems*, 64(1), 89–109, 2007.
- Villareal, T., and E. Carpenter, Buoyancy regulation and the potential for vertical migration in the oceanic cyanobacterium *Trichodesmium*, *Microbial Ecology*, 45(1), 1–10, 2003.

- Voss, M., H. W. Bange, J. W. Dippner, J. J. Middelburg, J. P. Montoya, and B. Ward, The marine nitrogen cycle: recent discoveries, uncertainties and the potential relevance of climate change, *Philosophical Transactions of the Royal Society of London B: Biological Sciences*, 368(1621), 20130,121, 2013.
- Walsby, A., The properties and buoyancy-providing role of gas vacuoles in *Trichodesmium* Ehrenberg, *British Phycological Journal*, 13(2), 103–116, 1978.
- Ward, B. A., S. Dutkiewicz, C. M. Moore, and M. J. Follows, Iron, phosphorus, and nitrogen supply ratios define the biogeography of nitrogen fixation, *Limnol. Oceanogr*, 58(6), 2059–2075, 2013.
- Watanabe, S., T. Hajima, K. Sudo, T. Nagashima, T. Takemura, H. Okajima, T. Nozawa, H. Kawase, M. Abe, T. Yokohata, et al., MIROC-ESM 2010: model description and basic results of CMIP5-20c3m experiments, *Geoscientific Model Development*, 4(4), 845–872, 2011.
- Weber, T., and C. Deutsch, Local versus basin-scale limitation of marine nitrogen fixation, *Proceedings of the National Academy of Sciences*, 111(24), 8741–8746, 2014.
- Westberry, T., M. Behrenfeld, D. Siegel, and E. Boss, Carbon-based primary productivity modeling with vertically resolved photoacclimation, *Global Biogeochemical Cycles*, 22(2), 2008.
- Westberry, T. K., and D. A. Siegel, Spatial and temporal distribution of *Trichodesmium* blooms in the world's oceans, *Global Biogeochemical Cycles*, 20(4), 2006.
- Wetzel, P., E. Maier-Reimer, M. Botzet, J. Jungclaus, N. Keenlyside, and M. Latif, Effects of ocean biology on the penetrative radiation in a coupled climate model, *Journal of Climate*, 19(16), 3973–3987, 2006.
- White, A. E., Y. H. Spitz, D. M. Karl, and R. M. Letelier, Flexible elemental stoichiometry in *Trichodesmium* spp. and its ecological implications, *Limnology and Oceanography*, 51(4), 1777–1790, 2006.
- Wolf-Gladrow, D. A., R. E. Zeebe, C. Klaas, A. Körtzinger, and A. G. Dickson, Total alkalinity: The explicit conservative expression and its application to biogeochemical processes, *Marine Chemistry*, 106(1), 287–300, 2007.
- Zehr, J. P., J. B. Waterbury, P. J. Turner, J. P. Montoya, E. Omoregie, G. F. Steward, A. Hansen, and D. M. Karl, Unicellular cyanobacteria fix N₂ in the subtropical North Pacific Ocean, *Nature*, 412(6847), 635–638, 2001.
- Zielinski, O., O. Llinás, A. Oschlies, and R. Reuter, Underwater light field and its effect on a one-dimensional ecosystem model at station ESTOC, north of the Canary Islands, *Deep Sea Research Part II: Topical Studies in Oceanography*, 49(17), 3529–3542, 2002.

Acknowledgements

First I would like to thank my supervisor Tatiana Ilyina for her continuous support and guidance during my PhD, for giving me the freedom and time to explore on my own and at the same time always helping if needed. I am looking forward to staying a while longer in the ocean biogeochemistry group.

I also thank my co-advisor Johann Jungclaus for his support with respect to the physical aspects of the thesis as well as his help on revising manuscripts, conference abstracts and posters. I thank Inga Hense for the discussions and helpful advice with regard to biological questions, and furthermore for stepping in as a supervisor and evaluator of the thesis from the university side. I thank Jochem Marotzke for being my panel chair and for giving advice on the chosen path of research during this thesis.

I thank Sebastian Sonntag for sharing experience and knowledge about the topic of cyanobacteria. I thank Jana Hinners for one of the parameterizations I used in one simulation.

Special thanks go to Irene Stemmler and Katharina Six for sharing their expertise on HAMOCC, their programming support, their discussions on scientific issues, their support in writing the first paper, their helpful comments on the thesis, conference talks and posters, and questions regarding Ferret. I thank the whole HAMOCC group for the nice working atmosphere, for the helpful discussions in the Tuesday meetings, for group lunches, and the nice company at conferences.

I thank Marlene for her help on Latex and Matlab issues, for proof reading parts of the thesis, and – primarily – for the great company in the office! I also thank the MPI Squash Team (Irene, Hongmei, Aaron, Fabrice, Veit, Leo) for the sportive challenge once a week. Moreover, I thank all students, colleagues and friends at MPI and IMPRS for a relaxed atmosphere and enjoyable lunch breaks.

I thank the International Max Planck Research School on Earth System Modelling (IMPRS-ESM) for funding. In particular I thank Antje Weitz, Cornelia Kampmann, and Wiebke Böhm for their help in case of non-scientific issues.

I want to thank my family for their support and the relaxing weekends at home. Thanks also to my friends for the great time besides work. Special thanks belong to Jannes for always being there for me, for always having a plan what to do after work, and for planning the next holidays – which will start now!

Used software and data

All simulations for this thesis were performed at the German Climate Computing Center (DKRZ). For the analysis of the model output, I used CDO, Ferret, and Matlab. For graphics in this thesis, I used Ferret and Matlab.

I used the database of *Luo et al.* (2012) of cyanobacterial diazotrophic biomass and N₂ fixation rates stored in the information system PANGAEA, doi:10.1594/PANGAEA.774851. I used data of nitrate and phosphate concentrations from the World Ocean Atlas (WOA) 2013 (<https://www.nodc.noaa.gov/OC5/woa13/>). I used SST data from HadISST1 (*Rayner et al.*, 2003) and from the PHC3 climatology (a blend of the *Levitus et al.* (1998) data with an updated data set for the Arctic from *Steele et al.* (2001)).

Aus dieser Dissertation hervorgegangene Vorver- öffentlichungen

List of Publications

Paulsen H., T. Ilyina, K.D. Six, and I. Stemmler (2017): Incorporating a prognostic representation of marine nitrogen fixers into the global ocean biogeochemical model HAMOCC. *Journal of Advances in Modeling Earth Systems.*, **9(1)**, 438–464.

Eidesstattliche Versicherung *Declaration on Oath*

Hiermit erkläre ich an Eides statt, dass ich die vorliegende Dissertationsschrift selbst verfasst und keine anderen als die angegebenen Quellen und Hilfsmittel benutzt habe.

I hereby declare, on oath, that I have written the present dissertation by myself and have not used other than the acknowledged resources and aids.

Hamburg, den 24. September 2017

